Supporting Information for:

Experimental and Computational Studies of High-Valent Nickel and Palladium Complexes

Nicole M. Camasso,[†] Allan J. Canty,*[‡] Alireza Ariafard,[‡] and Melanie S. Sanford*[†]

[†]Department of Chemistry, University of Michigan, 930 N University Ave, Ann Arbor, MI 48109

[‡]School of Physical Sciences, University of Tasmania, Private Bag 75, Hobart, Tasmania 7001, Australia

Table of Contents

I.	General Procedures and Materials and Methods	p. S2
II.	Synthesis of M^{II} Precursors	p. S3
III.	Synthesis of High-Valent Complexes	p. S5
IV.	Synthesis of M^{II} Reductive Elimination Products	p. S9
V.	Oxidation Studies	p. S16
VI.	Reductive Elimination Studies	p. S19
VII.	Cyclic Voltammetry Studies	p. S31
VIII.	Computational Details	p. S33
IX.	References	p. S40
X.	Spectral Data	p. S41
XI.	X-Ray Crystallography Experimental Data	p. S76

I. General Procedures and Materials and Methods

General Procedures

All experiments and manipulations were carried out under an inert nitrogen atmosphere using standard glovebox or Schlenk techniques unless otherwise indicated. NMR spectra were obtained on a Varian VNMR 700 (699.76 MHz for ^{1}H; 175.95 MHz for ^{13}C), a Varian VNMR 500 (500.09 MHz for ^{1}H; 470.56 MHz for ^{19}F) or a Varian VNMR 400 spectrometer (399.54 MHz for ^{1}H; 128.187 for ^{11}B). ^{1}H and ^{13}C chemical shifts are reported in parts per million (ppm) relative to TMS, with the residual solvent peak as an internal reference. ^{19}F chemical shifts and ^{11}B chemical shifts are reported in ppm and are referenced on a unified scale, where the single primary reference is the frequency of the residual solvent peak in the ^{1}H NMR spectrum. Abbreviations used in the NMR data: s, singlet; d, doublet; dd, doublet of doublets; t, triplet; td, triplet of doublets; m, multiplet; br, broad signal; bq, broad quartet. Cyclic voltammetry was performed using a CHI600C potentiostat from CH instruments. The electrodes were obtained from BASi. Mass spectral data were obtained on a Micromass magnetic sector mass spectrometer in electrospray ionization mode. X-ray crystallographic data were collected on a Rigaku AFC10K Saturn 944+ CCD-based X-ray diffractometer. Flash chromatography was conducted using a Biotage Isolera One system with cartridges containing high performance silica gel.

Materials and Methods

The following compounds were prepared via literature procedures: $[(PMe_3)_2Ni^{II}(CH_2CMe_2\text{-}o\text{-}C_6H_4)$,[1] $(COD)Pd^{II}(CH_2CMe_2\text{-}o\text{-}C_6H_4)$,[2] NMe_4SPh,[3] NMe_4OPh,[4] NMe_4Tp,[5] and acetylferrocenium tetrafluoroborate ($AcFcBF_4$).[6] The spectra of complex **3-Pd** matched that reported in the literature.[7] $AgBF_4$ was purchased from Strem Chemicals. NBu_4N_3, NMe_4OAc, and *S*-(trifluoromethyl) dibenzothiophenium triflate were purchased from Aldrich. 4,4'-difluorobiphenyl was purchased from Oakwood Chemicals. Potassium trispyrazolyl borate (KTp) was purchased from Alfa Aesar. Electrochemical studies were performed with electrochemical grade NBu_4BF_4 or NBu_4PF_6, which were purchased from Aldrich and used without further purification. Pentane (Fisher), diethyl ether (EMD), and tetrahydrofuran (Fisher) were deaerated via a N_2 sparge and dried by Inert Technologies solvent purification system. Acetonitrile (Acros) was sparged and used without further purification. Pyridine-d_5 and CD_3CN were obtained from Cambridge Isotopes Laboratories and were stored over activated 4 Å molecular sieves (EMD Millipore). Basic alumina (Aldrich) was dried for 48 h under vacuum at 210 °C. Celite was dried for 12 h under vacuum at 100 °C. Unless otherwise noted, all glassware was dried overnight in an oven at 150 °C and cooled under an inert atmosphere before use. All commercial reagents were used without further purification/drying unless explicitly stated in the experimental section.

II. Synthesis of M^{II} Precursors

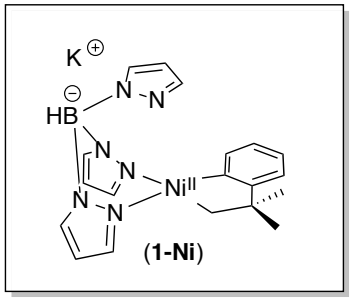

(**1-Ni**)

Synthesis of [(K)(Tp)Ni^{II}(CH$_2$CMe$_2$-*o*-C$_6$H$_4$)] (1-Ni).[3] In the glovebox, a 20 mL vial was charged with [(PMe$_3$)$_2$Ni^{II}(CH$_2$CMe$_2$-*o*-C$_6$H$_4$)] (250 mg, 0.73 mmol, 1.0 equiv). The solid was dissolved in acetonitrile (8 mL). Potassium trispyrazolylborate (202 mg, 0.80 mmol, 1.1 equiv) was added at room temperature, and the dark orange solution was stirred at rt for 30 min. Solvent and free PMe$_3$ were removed *in vacuo*. Diethyl ether (10 mL) was added to the brown residue, the suspension triturated, and the insoluble material collected. Complex **1-Ni** was dried under vacuum and isolated as a yellow solid (301 mg, 93% yield).

^{1}H NMR (700 MHz, CD$_3$CN, 23 ºC) δ 8.13 (br, 3H), 7.57 (br, 3H), 6.74 (d, J_{HH} = 7.3 Hz, 1H), 6.69 (t, J_{HH} = 7.3 Hz, 1H), 6.56 (d, J_{HH} = 7.3 Hz, 1H), 6.52 (t, J_{HH} = 7.3 Hz, 1H), 6.13 (br, 3H), 4.71 (bq, B-***H***), 1.31 (s, 6 H), 1.14 (s, 2H).

^{13}C NMR (128 MHz, CD$_3$CN, 23 ºC) δ 170.14, 164.49, 140.79, 138.19, 134.75, 121.85, 120.77, 119.73, 103.60, 47.16, 40.62, 33.61.

^{11}B NMR (128 MHz, CD$_3$CN, 23 ºC) δ –2.40 (d, J_{BH} = 112.0 Hz, ***B***-H).

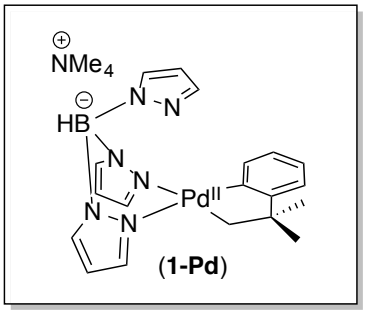

(**1-Pd**)

Synthesis of NMe_4[(Tp)Pd^{II}(CH_2CMe_2-*o*-C_6H_4)] (1-Pd): A 250 mL round bottom flask was charged with (COD)Pd(CH_2CMe_2-*o*-C_6H_4)[2] (300 mg, 0.864 mmol, 1.0 equiv). The yellow solid was dissolved in dichloromethane (50 mL) and NMe_4Tp (260 mg, 0.907 mmol, 1.1 equiv) was added at room temperature. The light tan solution was allowed to stir for 2 h. The crude reaction mixture was then concentrated to a tan solid, washed several times with ether (3 x 10 mL), and dried under vacuum to afford **1-Pd** as a white solid (404 mg; 89 % yield).

^{1}H NMR (700 MHz, CD_3CN, 23 ºC) δ 7.90 (br, 3H), 7.63 (br, 3H), 7.27 (d, J_{HH} = 7.2 Hz, 1H), 6.80 (t, J_{HH} = 7.2 Hz, 1H), 6.72 (t, J_{HH} = 7.2 Hz, 1H), 6.69 (d, J_{HH} = 7.2 Hz, 1H), 6.17 (br, 3H), 4.73 (bq, B-***H***), 3.04 (s, 12H), 1.96 (s, 2H), 1.33 (s, 6H).

^{13}C NMR (176 MHz, CD_3CN, 23 ºC) δ 168.40, 161.91, 140.44, 135.95, 134.72, 122.92, 121.46, 121.10, 103.62, 55.1, 47.31, 40.72, 33.59.

^{11}B NMR (225 MHz, CD_3CN, 23 ºC) δ –1.83 (d, J_{BH} = 112 Hz, ***B***-H).

HRMS-electrospray (m/z): $[M–NMe_4]^-$ calcd. for $C_{19}H_{22}BN_6Pd$, 451.1034; found, 451.1067

III. Synthesis of High-Valent Complexes

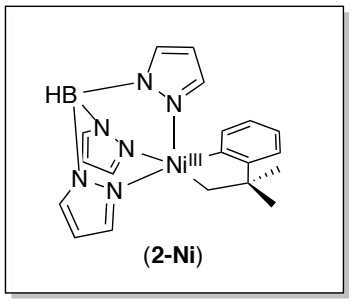

(**2-Ni**)

Synthesis of [(Tp)Ni^{III}(CH$_2$CMe$_2$-*o*-C$_6$H$_4$)] (2-Ni).[8] In the glovebox, a 20 mL vial was charged with K[(Tp)Ni^{II}(CH$_2$CMe$_2$-*o*-C$_6$H$_4$)] (180 mg, 0.41 mmol, 1.0 equiv). The yellow solid was dissolved in acetonitrile (10 mL), and a solution of $AgBF_4$ (78 mg, 0.41 mmol, 1.0 equiv) in acetonitrile (5 mL) was added at –35 ºC. The orange solution immediately turned dark red, with concomitant precipitation of a Ag^0. The crude reaction mixture was then filtered through a celite plug. The plug was washed with acetonitrile (5 mL), and the filtrates were combined and concentrated to approximately 3 mL. Orange crystals precipitated from the solution over the course of 10 min. These crystals were collected, washed with acetonitrile (5 mL), and dried under vacuum to afford **2-Ni** as an orange solid (98 mg, 60% yield). Samples for elemental analysis were obtained by cooling a saturated solution of **2-Ni** in acetonitrile to –35 ºC to obtain orange-red crystals of **2-Ni**.

^{11}B NMR (225 MHz, CD_3CN, 23 ºC) δ –3.07 (br, ***B***-H).

Elemental Analysis calcd. for $C_{19}H_{22}BN_6Ni$, C: 56.50, H: 5.49, N: 20.81; found, C: 56.63, H: 5.52, N: 20.83.

μ_{eff}(CH_3CN, 23 ºC): = 1.88

HRMS-electrospray (m/z) $[M]^+$ calcd. for $C_{19}H_{22}BN_6Ni$, 403.1352; found, 403.1352.

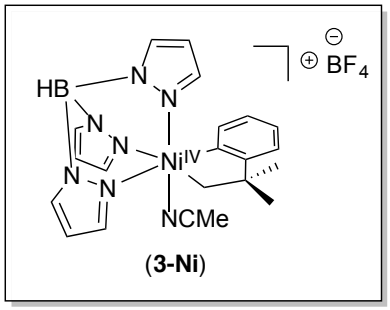

(**3-Ni**)

Synthesis of [(Tp)Ni^{IV}(CH$_2$CMe$_2$-*o*-C$_6$H$_4$)(MeCN)]BF$_4$ (3-Ni): In the glovebox, a 20 mL vial was charged with K[(Tp)Ni^{II}(CH$_2$CMe$_2$-*o*-C$_6$H$_4$)] (150 mg, 0.34 mmol, 1.0 equiv). The yellow solid was dissolved in acetonitrile (10 mL), and a solution of $AgBF_4$ (134 mg, 0.69 mmol, 1.0 equiv) in acetonitrile (5 mL) was added at –35 ºC. The orange solution immediately turned dark red, with concomitant precipitation of Ag^0. The crude reaction mixture was then filtered through a celite plug. The plug was washed with acetonitrile (5 mL), and the filtrates were combined and concentrated to approximately 2 mL. Red-orange crystals precipitated from the solution over the course of 15 min. These crystals were collected, washed with acetonitrile (5 mL), and dried under vacuum to afford **3-Ni** as a red-orange solid (91 mg, 51% yield).

^{1}H NMR (700 MHz, CD_3CN, 23 ºC) δ 8.18 (d, J_{HH} = 2.0 Hz, 1H), 8.13 (d, J_{HH} = 2.0 Hz, 1H), 7.99 (d, J_{HH} = 2.3 Hz, 1H), 7.97 (d, J_{HH} = 2.3 Hz, 1H), 7.86 (d, J_{HH} = 2.3 Hz, 1H), 7.26 (t, J_{HH} = 7.7 Hz, 1H), 7.19 (d, J_{HH} = 7.7 Hz, 1H), 6.94 (t, J_{HH} = 7.7 Hz, 1H), 6.77 (d, J_{HH} = 2.3 Hz, 1H), 6.74 (d, J_{HH} = 7.7 Hz, 1H), 6.55 (d, J_{HH} = 2.3 Hz, 1H), 6.49 (s, 1H), 6.22 (s, 1H), 6.09 (d, J_{HH} = 3.8 Hz, 1H), 6.00 (d, J_{HH} = 3.8 Hz, 1H), 4.61 (bq, B-***H***) 2.36 (s, 3H), 1.68 (s, 3H), 1.59 (s, 3H).

^{13}C NMR (176 MHz, CD_3CN, 0 ºC) δ 154.20, 151.08, 143.77, 141.80, 141.62, 138.08, 136.50, 136.07, 132.52, 128.97, 127.94, 127.49, 107.86, 107.15, 106.96, 87.40, 48.24, 31.38, 28.50.

^{11}B NMR (225 MHz, CD_3CN, 23 ºC) δ –1.18 (s, ***B***F$_4$), –4.38 (d, J_{BH} = 98 Hz, ***B***-H).

^{19}F NMR (471 MHz, CD_3CN, 23 ºC) δ –151.95.

HRMS-electrospray (m/z): [M]$^+$ calcd. for $C_{21}H_{25}BN_7Ni$, 444.1612; found, 444.1613.

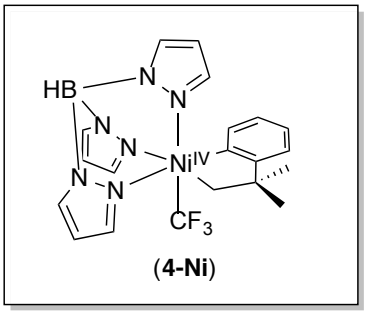

(**4-Ni**)

Synthesis of [(Tp)Ni^{IV}(CH_2CMe_2-*o*-C_6H_4)(CF_3)] (4-Ni): Following a modified procedure from the literature,[3] a 20 mL vial was charged with K[(Tp)Ni^{II}(CH_2CMe_2-*o*-C_6H_4)] (**1-Ni**) (210 mg, 0.47 mmol, 1.0 equiv) in the glovebox. The solid was dissolved in acetonitrile (15 mL). *S*-(Trifluoromethyl) dibenzothiophenium triflate (247 mg, 0.61 mmol, 1.3 equiv) was added at room temperature and the yellow-orange solution immediately turned yellow-brown. The reaction mixture was taken out of the glovebox and the solvent was removed by rotary evaporation. The crude yellow-brown solid was purified by flash chromatography on silica gel (mobile phase: ethyl acetate/hexanes with a gradient from 90:10 to 80:20). Compound **4-Ni** was isolated as a yellow solid (204 mg, 92% yield).

^{1}H NMR (700 MHz, CD_3CN, 23 ºC) δ 8.13 (d, J_{HH} = 1.9 Hz, 1H), 7.96 (d, J_{HH} = 1.9 Hz, 1H), 7.88 (d, J_{HH} = 2.3 Hz, 1H), 7.85 (d, J_{HH} = 2.3 Hz, 1H), 7.74 (d, J_{HH} = 2.2 Hz, 1H), 7.15 (multiple peaks, 2H), 7.04 (d, J_{HH} = 7.5 Hz, 1H), 6.88 (t, J_{HH} = 7.5 Hz, 1H), 6.68 (d, J_{HH} = 2.1 Hz, 1H), 6.40 (multiple peaks, 2H), 6.08 (t, J_{HH} = 2.1 Hz, 1H), 4.93 (d, J_{HH} = 5.5 Hz, 1H), 4.81 (dd, J_{HH} = 5.5 Hz, J_{HF} = 2.4 Hz, 1H), 4.52 (bq, B-***H***), 1.53 (s, 3H), 1.44 (s, 3H).

^{13}C NMR (128 MHz, CD_3CN, 23 ºC) δ 160.51, 156.03, 142.68, 141.64, 141.51, 135.56, 135.48, 135.17, 132.68, 126.65, 125.96, 125.59, 120.55 (Ni-***C***F_3, shift for CF_3 group extracted from ^{19}F–^{13}C HMBC NMR spectrum), 105.94, 105.88, 105.64, 77.67, 46.98, 31.01, 30.25.

^{19}F NMR (471 MHz, CD_3CN, 23 ºC) δ –16.11 (s, Ni-C***F***$_3$).

^{11}B NMR (128 MHz, CD_3CN, 23 ºC) δ –4.37 (d, J_{BH} = 115.9 Hz).

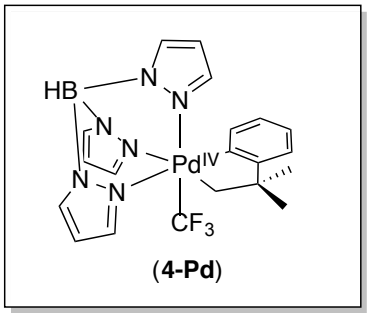

(**4-Pd**)

Synthesis of [(Tp)Pd^{IV}(CH_2CMe_2-*o*-C_6H_4)(CF_3)] (4-Pd): A 20 mL vial was charged with NMe_4[(Tp)Pd^{II}(CH_2CMe_2-*o*-C_6H_4)] (**1-Pd**) (290 mg, 0.55 mmol, 1.0 equiv). The solid was dissolved in acetonitrile (15 mL). *S*-(Trifluoromethyl) dibenzothiophenium triflate (288 mg, 0.72 mmol, 1.3 equiv) was added at room temperature and the light tan solution immediately turned orange-brown. The solvent was removed by rotary evaporation. The crude brown solid was purified by flash chromatography on silica gel (mobile phase: ethyl acetate/hexanes with a gradient from 90:10 to 70:30). Compound **4-Pd** was isolated as a light tan solid (245 mg, 86% yield).

^{1}H NMR (700 MHz, CD_3CN, 23 ºC): δ 8.04 (d, J_{HH} = 1.9 Hz, 1H), 7.89 (d, J_{HH} = 2.3 Hz, 1H), 7.87 (d, J_{HH} = 2.3 Hz, 1H), 7.83 (d, J_{HH} = 1.9 Hz, 1H), 7.79 (d, J_{HH} = 2.3 Hz, 1H), 7.26 (m, 1H), 7.18 (m, 1H), 7.10 (dd, J_{HH} = 7.7, 1.7 Hz, 1H), 6.93 (td, J_{HH} = 7.7, 1.7 Hz, 1H), 6.86 (d, J_{HH} = 2.2 Hz, 1H), 6.42 (t, J_{HH} = 2.2 Hz, 1H), 6.38 (t, J_{HH} = 2.2 Hz, 1H), 6.14 (d, J_{HH} = 2.2 Hz, 1H), 4.63 (bq, B-***H***), 4.19–4.13 (multiple peaks, 2H), 1.51 (s, 3H), 1.50 (s, 3H).

^{13}C NMR (176 MHz, CD_3CN, 23 ºC): δ 161.23, 154.38, 141.48, 140.93, 140.40, 136.09, 136.05, 135.62, 130.95, 126.71, 126.11, 126.08, 125.85 (Pd-***C***F_3, shift for CF_3 group extracted from ^{19}F–^{13}C HMBC NMR spectrum), 105.96, 105.88, 105.72, 67.02, 45.94, 31.63, 31.53.

^{19}F NMR (377 MHz, CD_3CN, 23 ºC): δ –18.39.

^{11}B NMR (225 MHz, CD_3CN, 23 ºC): δ –3.54 (d, J_{BH} = 102 Hz, ***B***-H).

IV. Synthesis of M^{II} Reductive Elimination Products

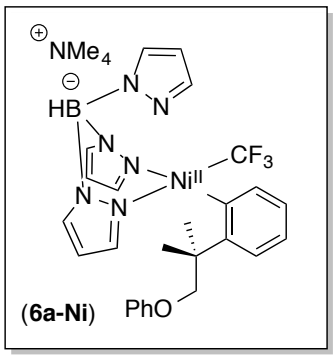

Synthesis of [(NMe_4)(Tp)Ni^{II}(C_6H_4-*o*-CMe_2CH_2OPh)(CF_3)] (6a-Ni).[3] A 20 mL vial was charged with [(Tp)Ni^{IV}(CH_2CMe_2-*o*-C_6H_4)(CF_3)] (**4-Ni**) (30 mg, 0.063 mmol, 1.0 equiv). The solid was dissolved in acetonitrile (5 mL). NMe_4OPh (13 mg, 0.075 mmol, 1.2 equiv) was added and the resulting solution was stirred at room temperature for 8 h. The solvent was removed *in vacuo* and the resulting yellow residue was washed with diethyl ether (3 x 10 mL). The solids were dried under vacuum to afford complex **6a-Ni** as a yellow solid (31 mg, 78% yield).

^{1}H NMR (700 MHz, CD_3CN, 23 ºC) δ 8.13 (d, J_{HH} = 7.9 Hz, 1H), 8.02 (d, J_{HH} = 2.3 Hz, 1H), 7.80 (d, J_{HH} = 1.8 Hz, 1H), 7.72 (d, J_{HH} = 1.8 Hz, 1H), 7.48 (d, J_{HH} = 2.3 Hz, 1H), 7.34 (d, J_{HH} = 2.3 Hz, 1H), 7.21 (t, J_{HH} = 7.9 Hz, 2H), 7.08 (d, J_{HH} = 7.9 Hz, 1H), 6.87 (multiple peaks, 3H), 6.71 (t, J_{HH} = 7.9, 1H), 6.63 (t, J_{HH} = 7.2 Hz, 1H), 6.40 (d, J_{HH} = 2.0 Hz, 1H), 6.31 (d, J_{HH} = 2.0 Hz, 1H), 6.18 (s, 1H), 5.80 (t, J_{HH} = 2.2 Hz, 1H), 4.81 (br, B-***H***), 4.39 (d, J_{HH} = 8.7 Hz, 1H), 4.36 (d, J_{HH} = 8.7 Hz, 1H), 3.07 (s, 12H), 2.30 (s, 3H), 1.85 (s, 3H).

^{13}C NMR (176 MHz, CD_3CN, 23 ºC) δ 159.84, 159.54, 151.22, 142.50, 142.18, 140.77, 138.57 (Ni-***C***F_3, shift for CF_3 group extracted from ^{19}F–^{13}C HMBC NMR spectrum), 136.13, 135.39, 134.67, 134.37, 129.22, 125.05, 121.22, 120.80, 119.89, 114.50, 104.03, 103.81, 103.44, 77.96, 55.72, 40.00, 27.19, 27.15.

^{19}F NMR (471 MHz, CD_3CN, 23 ºC) δ –20.52 (s, Ni-C***F***$_3$).

^{11}B NMR (128 MHz, CD_3CN, 23 ºC) δ –2.57 (d, J_{BH} = 115.7 Hz).

HRMS-electrospray (m/z): $[M–NMe_4]^-$ calcd. for $C_{26}H_{27}BF_3N_6NiO$, 565.1645; Found, 565.1640.

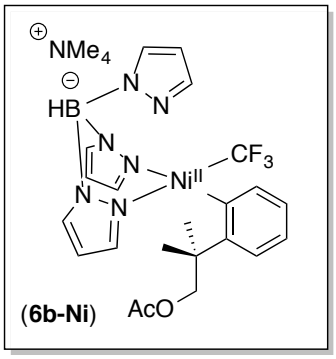

(**6b-Ni**)

[NMe_4(Tp)Ni^{II}(C_6H_4-*o*-CMe_2CH_2OAc)(CF_3)] (6b-Ni).[3] A 20 mL vial was charged with [(Tp)Ni^{IV}(CH_2CMe_2-*o*-C_6H_4)(CF_3)] (**4-Ni**) (30 mg, 0.063 mmol, 1.0 equiv). The solid was dissolved in acetonitrile (5 mL). NMe_4OAc (10 mg, 0.075 mmol, 1.2 equiv) was added, and the resulting solution was stirred at 40 ºC for 3 days. The reaction mixture was cooled to room temperature and solvent was removed *in vacuo*. The resulting yellow residue was washed with diethyl ether (3 x 10 mL). The solids were dried under vacuum to afford complex **6b-Ni** as a yellow solid (33 mg, 88% yield).

^{1}H NMR (700 MHz, CD_3CN, 23 ºC) δ 8.12 (d, J_{HH} = 2.3 Hz, 1H), 8.07 (d, J_{HH} = 7.4 Hz, 1H), 7.81 (d, J_{HH} = 1.8 Hz, 1H), 7.72 (d, J_{HH} = 1.8 Hz, 1H), 7.49 (d, J_{HH} = 2.3 Hz, 1H), 7.38 (d, J_{HH} = 2.3 Hz, 1H), 7.00 (d, J_{HH} = 7.4 Hz, 1H), 6.73 (m, 1H), 6.61 (t, J_{HH} = 7.4 Hz, 1H), 6.28 (d, J_{HH} = 2.0 Hz, 1H), 6.25 (d, J_{HH} = 2.0 Hz, 1H), 6.20 (d, J_{HH} = 2.2 Hz, 1H), 5.80 (d, J_{HH} = 2.2 Hz, 1H), 4.83 (br, B-***H***), 4.48 (d, J_{HH} = 10.7 Hz, 1H), 4.35 (d, J_{HH} = 10.7 Hz, 1H), 3.12 (s, 12H), 2.15 (s, 3H), 1.94 (s, 3H), 1.86 (s, 3H).

^{13}C NMR (176 MHz, CD_3CN, 23 ºC) δ 170.79, 159.57, 150.58, 142.40, 142.18, 140.75, 138.14 (Ni-***C***F_3, shift for CF_3 group extracted from ^{19}F–^{13}C HMBC NMR spectrum), 136.35, 135.49, 134.76, 134.19, 124.95, 121.24, 120.81, 104.05, 103.84, 103.46, 73.96, 56.23, 39.38, 27.25, 27.02, 20.17.

^{19}F NMR (471 MHz, CD_3CN, 23 ºC) δ –20.62 (s, Ni-C***F***$_3$).

^{11}B NMR (128 MHz, CD_3CN, 23 ºC) δ –2.54 (d, J_{BH} = 116.9 Hz).

HRMS-electrospray (m/z): $[M–NMe_4]^-$ calcd. for $C_{22}H_{25}BF_3N_6NiO_2$, 531.1438; found, 531.1442.

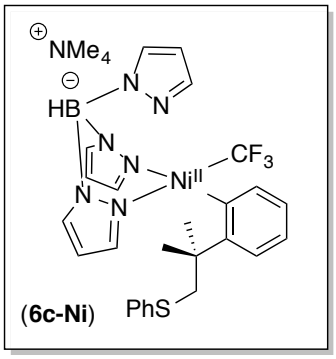

(**6c-Ni**)

Synthesis of [(NMe$_4$)(Tp)Ni^{II}(C$_6$H$_4$-*o*-CMe$_2$CH$_2$SPh)(CF$_3$)] (6c-Ni).[3] A 20 mL vial was charged with [(Tp)Ni^{IV}(CH$_2$CMe$_2$-*o*-C$_6$H$_4$)(CF$_3$)] (**4-Ni**) (50 mg, 0.11 mmol, 1.0 equiv). The solid was dissolved in acetonitrile (5 mL). NMe$_4$SPh (23 mg, 0.13 mmol, 1.2 equiv) was added and the resulting solution was stirred at room temperature for 10 min. The solvent was removed *in vacuo* and the resulting yellow residue was washed with diethyl ether (3 x 10 mL). The solids were dried under vacuum to afford complex **6c-Ni** as a yellow solid (68 mg, 94% yield).

^{1}H NMR (700 MHz, CD$_3$CN, 23 ºC) δ 8.20 (d, J_{HH} = 7.4 Hz, 1H), 8.04 (d, J_{HH} = 2.2 Hz, 1H), 7.77 (d, J_{HH} = 1.9 Hz, 1H), 7.73 (d, J_{HH} = 1.9 Hz, 1H), 7.40 (d, J_{HH} = 2.2 Hz, 1H), 7.31–7.24 (multiple peaks, 3H), 7.18 (t, J_{HH} = 7.6 Hz, 2H), 7.09 (t, J_{HH} = 7.8 Hz, 1H), 7.04 (d, J_{HH} = 7.8 Hz, 1H), 6.72 (t, J_{HH} = 7.2 Hz, 1H), 6.66 (t, J_{HH} = 7.2 Hz, 1H), 6.32 (br, 1H), 6.28 (br, 1H), 6.17 (br, 1H), 5.77 (br, 1H), 4.83 (br, B-***H***), 3.68 (d, J_{HH} = 12.9 Hz, 1H), 3.67 (d, J_{HH} = 12.9 Hz, 1H), 3.08 (s, 12H), 2.19 (s, 3H), 1.95 (s, 3H).

^{13}C NMR (176 MHz, CD$_3$CN, 23 ºC) δ 159.24, 152.73, 142.37, 142.06, 140.90, 139.31, 138.99 (Ni-***C***F$_3$, shift for CF$_3$ group extracted from ^{19}F–^{13}C HMBC NMR spectrum), 136.03, 135.34, 134.70, 134.38, 128.60, 127.85, 124.95, 124.68, 121.26, 120.87, 103.99, 103.89, 103.43, 55.16, 47.94, 40.21, 29.29, 29.28.

^{19}F NMR (471 MHz, CD$_3$CN, 23 ºC) δ –20.50 (s, Ni-C***F***$_3$).

^{11}B NMR (128 MHz, CD$_3$CN, 23 ºC) δ –2.57 (d, J_{BH} = 113.4 Hz).

HRMS-electrospray (m/z): [M–NMe$_4$]$^-$ calcd. for C$_{26}$H$_{27}$BF$_3$N$_6$NiS, 581.1417; found, 581.1430.

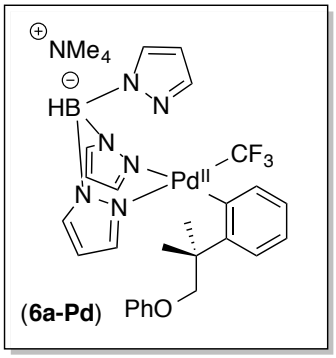

(**6a-Pd**)

Synthesis of $NMe_4[(Tp)Pd^{II}(C_6H_4$-*o*-$CMe_2CH_2OPh)(CF_3)]$ (6a-Pd): A 20 mL vial equipped with a magnetic stir bar was charged with $[(Tp)Pd^{IV}(CH_2CMe_2$-*o*-$C_6H_4)(CF_3)]$ (**4-Pd**) (50 mg, 0.094 mmol, 1.0 equiv) and dissolved in acetonitrile (8 mL). NMe_4OPh (17 mg, 0.10 mmol, 1.1 equiv) was added and the resulting solution was stirred at 70 ºC for 32 h. The reaction mixture was cooled to room temperature, and solvent was removed by rotary evaporation. The resulting yellow residue was washed with diethyl ether (3 x 10 mL). The solids were dried under vacuum to afford complex **6a-Pd** as a yellow solid (35 mg, 56% yield).

^{1}H NMR (700 MHz, CD_3CN, 23 ºC): δ 7.89 (d, J_{HH} = 7.4 Hz, 1H), 7.77–7.66 (multiple peaks, 3H), 7.49 (d, J_{HH} = 2.3 Hz, 1H), 7.41 (s, 1H), 7.24 (d, J_{HH} = 7.9 Hz, 1H), 7.15 (t, J_{HH} = 7.9 Hz, 2H), 6.87 (t, J_{HH} = 7.5 Hz, 1H), 6.83 (t, J_{HH} = 7.5 Hz, 1H), 6.76 (d, J_{HH} = 7.8 Hz, 3H), 6.60 (s, 1H), 6.28 (s, 1H), 6.16 (s, 1H), 5.85 (s, 1H), 4.75 (bq, B-***H***) 4.35 (d, J_{HH} = 8.6 Hz, 1H), 4.26 (br, 1H), 3.07 (s, 12H), 1.78 (s, 3H), 1.47 (s, 3H).

^{13}C NMR (176 MHz, CD_3CN, 23 ºC): δ 159.80, 154.43, 150.59, 141.25, 136.98, 136.83 (Pd-***C***F_3, shift for CF_3 group extracted from ^{19}F–^{13}C HMBC NMR spectrum), 135.52, 135.20, 134.06, 129.07, 126.12, 122.56, 121.79, 119.65, 114.48, 103.90, 103.88, 103.61, 77.53, 55.18, 39.64, 27.03, 27.02.

^{11}B NMR (225 MHz, CD_3CN, 23 ºC): δ –2.04 (d, J_{BH} = 113 Hz, ***B***-H). HRMS-electrospray (m/z): $[M - NMe_4]^-$ calcd. for $C_{26}H_{27}BF_3N_6PdO$, 613.1326; found, 613.1344.

^{19}F NMR (471 MHz, CD_3CN, 23 ºC) δ –18.75.

^{11}B NMR (225 MHz, CD_3CN, 23 ºC): δ –2.04 (d, J_{BH} = 113 Hz, ***B***-H).

HRMS-electrospray (m/z): $[M–NMe_4]^-$ calcd. for $C_{26}H_{27}BF_3N_6PdO$, 613.1326; found, 613.1344.

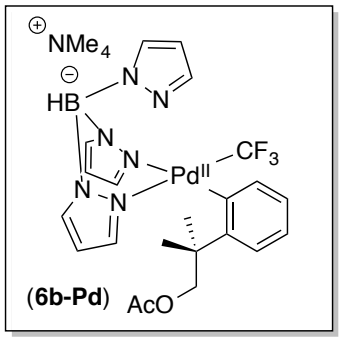

Crude Synthesis of NMe_4[(Tp)Pd^{II}(C_6H_4-*o*-CMe_2CH_2OAc) (CF_3)] (6b-Pd): A 20 mL vial equipped with a magnetic stir bar was charged with [(Tp)Pd^{IV}(CH_2CMe_2-*o*-C_6H_4)(CF_3)] (**4-Pd**) (20 mg, 0.037 mmol, 1.0 equiv) and dissolved in acetonitrile (4 mL). NMe_4OAc (24 mg, 0.19 mmol, 5 equiv) was added and the resulting solution was stirred at 70 ºC for 3 weeks. The reaction mixture was cooled to room temperature and solvent was removed by rotary evaporation. The resulting yellow residue was washed with diethyl ether (3 x 10 mL). Due to the extremely slow reactivity of NMe_4OAc and the Pd complex, this reaction required prolonged heating and excess acetate to reach only 95% conversion after the three-week time period. Complex **6b-Pd** was characterized without complete removal of excess tetramethylammonium acetate.

^{1}H NMR (700 MHz, CD_3CN, 23 ºC): δ 7.86 (d, J_{HH} = 7.2 Hz, 1H), 7.83 (d, J_{HH} = 2.3 Hz, 1H), 7.73 (s, 1H), 7.69 (s, 1H), 7.47 (m, 1H), 7.44 (d, J_{HH} = 2.3 Hz, 1H), 7.14 (d, J_{HH} = 7.9 Hz, 1H), 6.86 (m, 1H), 6.74 (t, J_{HH} = 7.2 Hz, 1H), 6.56 (s, 1H), 6.30 (t, J_{HH} = 2.0 Hz, 1H), 6.20 (t, J_{HH} = 2.0 Hz, 1H), 5.93 (t, J_{HH} = 2.0 Hz, 1H), 4.69 (bq, B-***H***), 4.44 (d, J_{HH} = 10.7 Hz, 1H), 4.32 (d, J_{HH} = 10.7 Hz, 1H), 3.15 (s, 12H), 1.88 (s, 3H), 1.62 (s, 3H), 1.41 (s, 3H).

^{13}C NMR (176 MHz, CD_3CN, 23 ºC): δ 170.61, 149.85, 141.28, 137.10, 136.81 (Pd-***C***F_3, shift for CF_3 group extracted from ^{19}F–^{13}C HMBC NMR spectrum), 135.51, 135.09, 134.89, 134.26, 125.94, 122.53, 121.75, 103.88, 103.86, 103.58, 73.68, 55.01, 39.02, 27.11, 25.12, 20.12.

^{19}F NMR (377 MHz, CD_3CN, 23 ºC): δ –18.78.

^{11}B NMR (225 MHz, CD_3CN, 23 ºC): δ –2.04 (d, J_{BH} = 117 Hz, ***B***-H).

HRMS-electrospray (m/z): $[M–NMe_4]^-$ calcd. for $C_{22}H_{25}BF_3N_6O_2Pd$, 579.1112; found, 579.1136

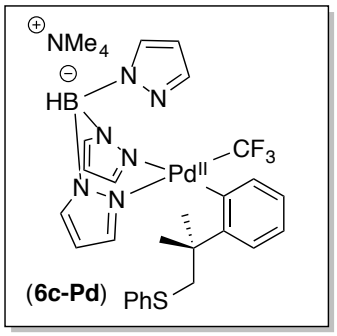

(**6c-Pd**)

Synthesis of NMe_4[(Tp)Pd^{II}(C_6H_4-*o*-CMe_2CH_2SPh)(CF_3)] (6c-Pd): A 20 mL vial equipped with a magnetic stir bar was charged with [(Tp)Pd^{IV}(CH_2CMe_2-*o*-C_6H_4)(CF_3)] (**4-Pd**) (50 mg, 0.094 mmol, 1.0 equiv) and dissolved in acetonitrile (8 mL). NMe_4SPh (19 mg, 0.10 mmol, 1.1 equiv) was added and the resulting solution was stirred at 70 ºC for 12 h. Solvent was removed by rotary evaporation. The resulting yellow residue was washed with diethyl ether (3 x 10 mL). The solids were dried under vacuum to afford complex **6c-Pd** as a yellow solid (55 mg, 84% yield).

^{1}H NMR (700 MHz, CD_3CN, 23 ºC): δ 7.93 (d, J_{HH} = 7.4 Hz, 1H), 7.77 (d, J_{HH} = 2.2 Hz, 1H), 7.75 (s, 1H), 7.70 (s, 1H), 7.42 (d, J_{HH} = 2.2 Hz, 1H), 7.38 (s, 1H), 7.18 (dd, J_{HH} = 7.9, 1.5 Hz, 1H), 7.16–7.09 (multiple peaks, 4H), 7.03 (m, 1H), 6.86 (t, J_{HH} = 7.2 Hz, 1H), 6.77 (t, J_{HH} = 7.2, 1H), 6.60 (s, 1H), 6.29 (d, J_{HH} = 2.2 Hz, 1H), 6.19 (d, J_{HH} = 2.2 Hz, 1H), 5.84 (t, J_{HH} = 2.2 Hz, 1H), 4.79 (bq, B-***H***), 3.59 (d, J_{HH} = 11.6 Hz, 1H), 3.44 (br, 1H), 3.09 (s, 12H) 1.85 (s, 3H), 1.56 (s, 3H).

^{13}C NMR (176 MHz, CD_3CN, 23 ºC): δ 154.49, 151.49, 141.31, 139.46, 137.03, 136.81 (Pd-***C***F_3, shift for CF_3 group extracted from ^{19}F–^{13}C HMBC NMR spectrum), 135.45, 133.84, 128.46, 127.42, 125.78, 124.31, 122.62, 121.68, 103.94, 103.88, 103.51, 55.17, 47.33, 39.77, 29.75, 29.12.

^{19}F NMR (471 MHz, CD_3CN, 23 ºC): δ –18.78.

^{11}B NMR (225 MHz, CD_3CN, 23 ºC): δ –2.04 (d, J_{BH} = 109 Hz, ***B***-H).

HRMS-electrospray (m/z): [M–NMe_4]$^-$ calcd. for $C_{26}H_{27}BF_3N_6PdS$, 629.1098; Found, 629.1116.

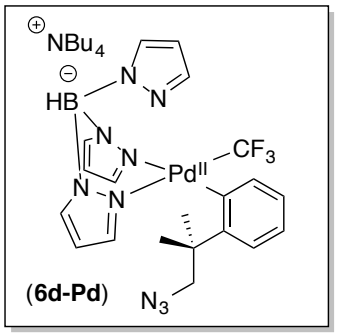

(**6d-Pd**)

Crude Synthesis of $NBu_4[(Tp)Pd^{II}(C_6H_4$-*o*-$CMe_2CH_2N_3)(CF_3)]$ (6d-Pd): A 20 mL vial equipped with a magnetic stir bar was charged with $[(Tp)Pd^{IV}(CH_2CMe_2$-*o*-$C_6H_4)(CF_3)]$ (**4-Pd**) (20 mg, 0.037 mmol, 1.0 equiv) and dissolved in acetonitrile (4 mL). NBu_4N_3 (54 mg, 0.19 mmol, 5 equiv) was added and the resulting solution was stirred at 70 ºC for one week. The reaction mixture was then cooled to room temperature, and solvent was removed by rotary evaporation. The resulting yellow residue was washed with diethyl ether (3 x 10 mL). Due to the extremely slow reactivity of NBu_4N_3 and the Pd^{IV} complex, this reaction required prolonged heating and excess azide to reach only 90% conversion after the one-week time period. Complex **6d-Pd** was characterized without complete removal of excess tetrabutylammonium azide.

^{1}H NMR (700 MHz, CD_3CN, 23 ºC): δ 7.97 (d, J_{HH} = 7.4 Hz, 1H), 7.84 (d, J_{HH} = 2.2 Hz, 1H), 7.81 (s, 1H), 7.66 (s, 1H), 7.49 (s, 1H), 7.35 (d, J_{HH} = 2.2 Hz, 1H), 7.11 (dd, J_{HH} = 7.9, 1.5 Hz, 1H), 6.85 (td, J_{HH} = 7.4, 1.5 Hz, 1H), 6.79 (td, J_{HH} = 7.9, 1.5 Hz, 1H), 6.52 (s, 1H), 6.33 (d, J_{HH} = 2.1 Hz, 1H), 6.19 (d, J_{HH} = 2.1 Hz, 1H), 5.94 (t, J_{HH} = 2.1 Hz, 1H), 4.77 (bq, B-***H***), 3.62 (d, J_{HH} = 11.7 Hz, 1H), 3.48 (d, J_{HH} = 11.7 Hz, 1H), 3.13–3.06 (m, 8H), 1.62 (multiple peaks, 14H), 1.37 (m, 8H), 0.99 (t, J_{HH} = 7.4 Hz, 12 H).

^{13}C NMR (176 MHz, CD_3CN, 23 ºC): δ 154.91, 149.98, 141.63, 141.08, 140.94, 136.90 (Pd-***C***F_3, shift for CF_3 group extracted from ^{19}F–^{13}C HMBC NMR spectrum), 136.84, 135.89, 135.64, 133.41, 125.91, 122.79, 121.74, 104.15, 103.80, 103.67, 62.88, 58.32, 40.06, 27.77, 27.39, 23.31, 19.32, 12.79.

^{19}F NMR (471 MHz, CD_3CN, 23 ºC): δ –19.03.

^{11}B NMR (225 MHz, CD_3CN, 23 ºC): δ –2.06 (d, J_{BH} = 113 Hz, ***B***-H).

HRMS-electrospray (m/z): $[M–NBu_4]^-$ calcd. for $C_{20}H_{22}BF_3N_9Pd$, 562.1078; found, 562.1093

V. Oxidation Studies

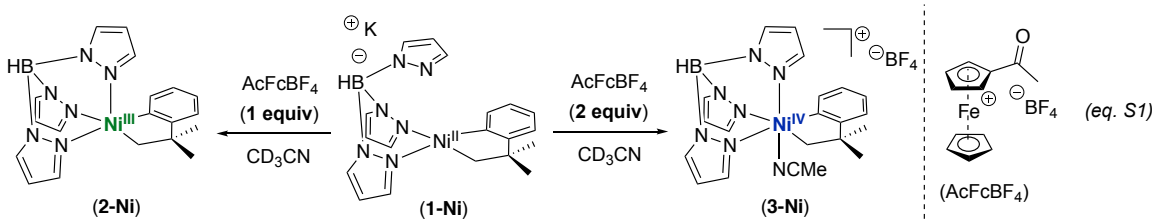

Experimental Procedure for the oxidation of 1-Ni: A 4 mL vial was charged with **1-Ni** (5.0 mg, 0.0096 mmol, 1.0 equiv) and CD_3CN (0.5 mL). This light tan solution was transferred to a screw cap NMR tube. A solution of the corresponding amount of acetylferrocenium tetrafluoroborate ($AcFcBF_4$; 3.0 mg, 0.0096 mmol, 1.0 equiv or 6.0 mg, 0.0192 mmol, 2 equiv) in CD_3CN was added. The tube was quickly capped, shaken vigorously, and was analyzed by ^1H NMR spectroscopy after <5 min at room temperature. In the presence of 2 equiv of $AcFcBF_4$, Ni^{IV} complex **3-Ni** was formed in 95% NMR yield. In the presence of 1 equiv of $AcFcBF_4$, analysis by ^1H NMR and ^{11}B NMR spectroscopy revealed the formation of a paramagnetic species that we previously characterized as Ni^{III} complex **2-Ni**.[8]

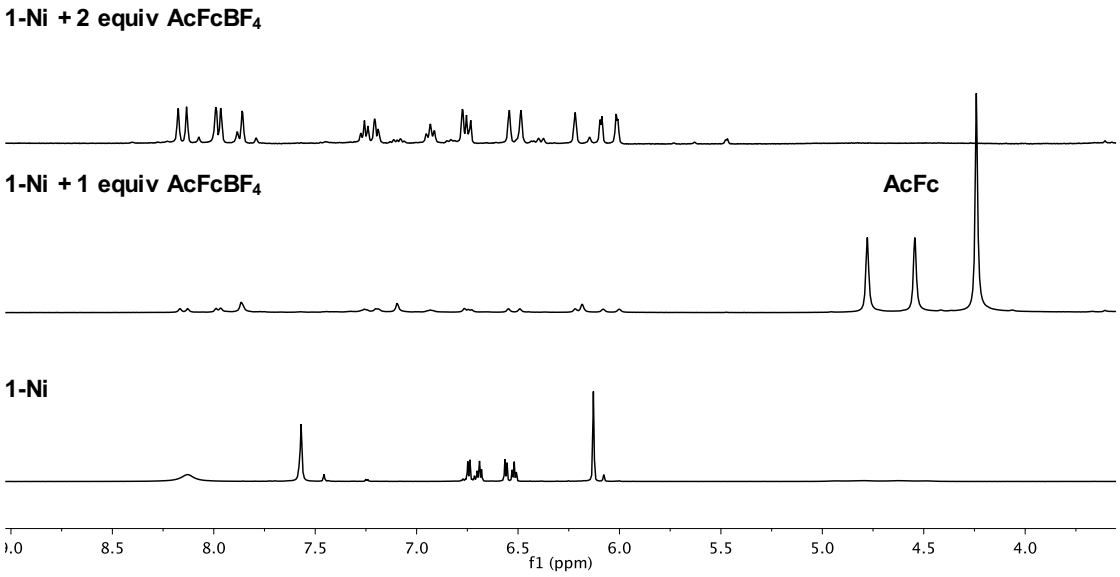

Figure S1. ^1H NMR spectra of **1-Ni** and the treatment of **1-Ni** with 1 or 2 equiv of $AcFcBF_4$

For Pd:

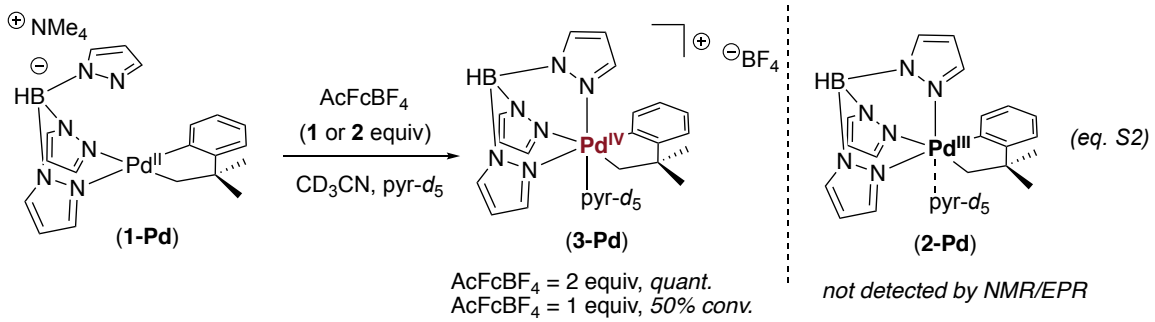

<u>Experimental Procedure for the oxidation of 1-Pd:</u> A 4 mL vial was charged with **1-Pd** (5.0 mg, 0.0096 mmol, 1.0 equiv), pyridine-d_5 (4 μL; 0.05 mmol; 5.2 equiv), and CD_3CN (0.5 mL). This light tan solution was transferred to a screw cap NMR tube. A solution of the corresponding amount of acetylferrocenium tetrafluoroborate ($AcFcBF_4$; 3.0 mg, 0.0096 mmol, 1.0 equiv or 6.0 mg, 0.0192 mmol, 2 equiv) in CD_3CN was added. The tube was quickly capped, shaken vigorously, and was analyzed by ^{1}H NMR spectroscopy after <5 min at room temperature. In the presence of 2 equiv of $AcFcBF_4$, Pd complex **3-Pd** was formed in approximately quantitative yield against acetylferrocene as the internal ^{1}H NMR standard. In the presence of 1 equiv of $AcFcBF_4$, Pd complex **3-Pd** was formed in approximately 50% yield against acetylferrocene as the internal ^{1}H NMR standard with 50% of unreacted **1-Pd** remaining.

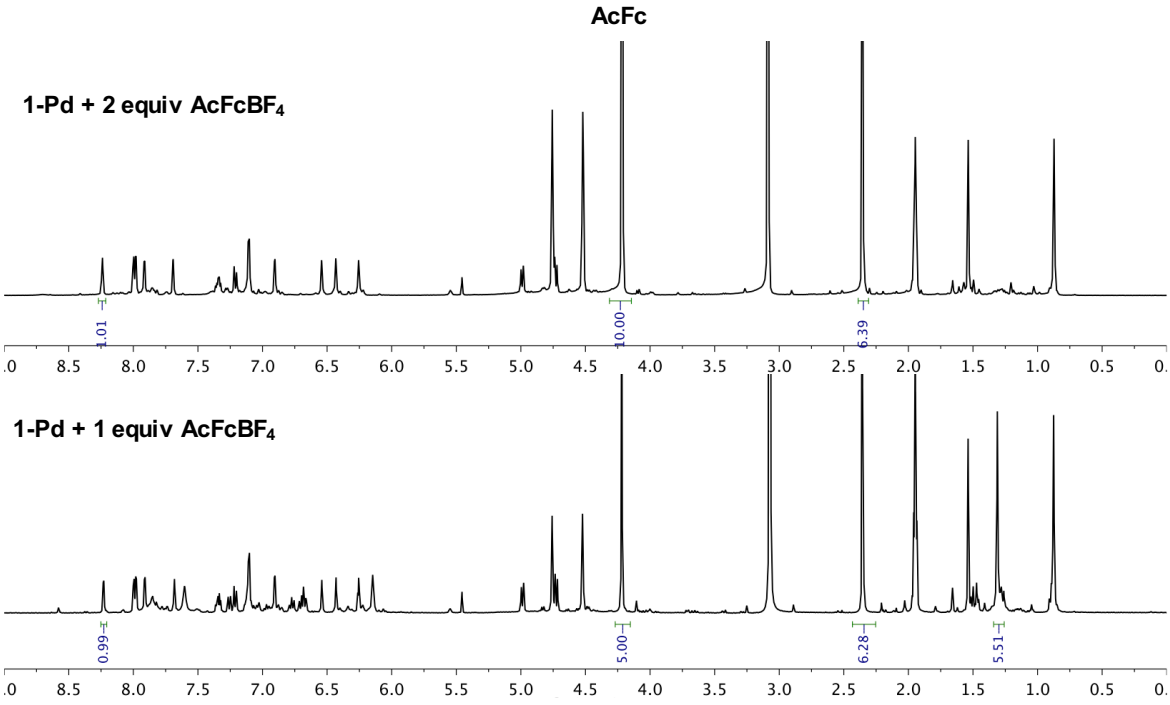

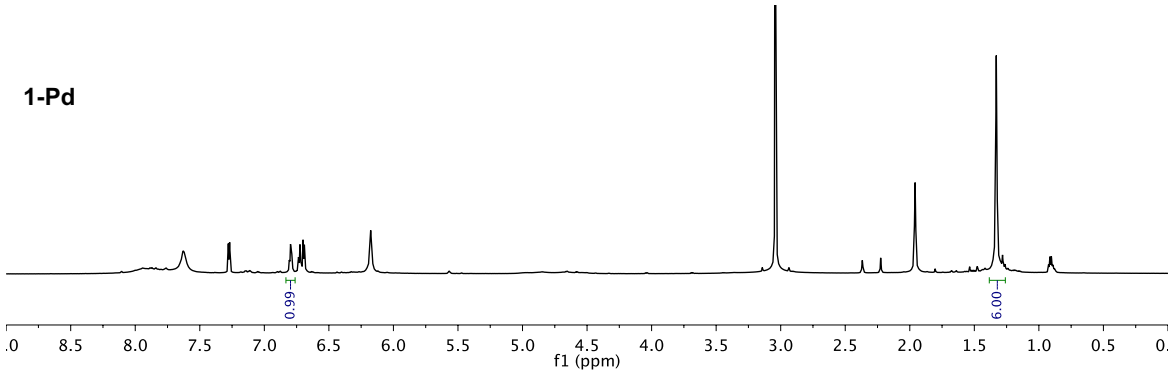

Figure S2. Full ^{1}H NMR Spectra of **1-Pd** and the treatment of **1-Pd** with 1 or 2 equiv of $AcFcBF_4$

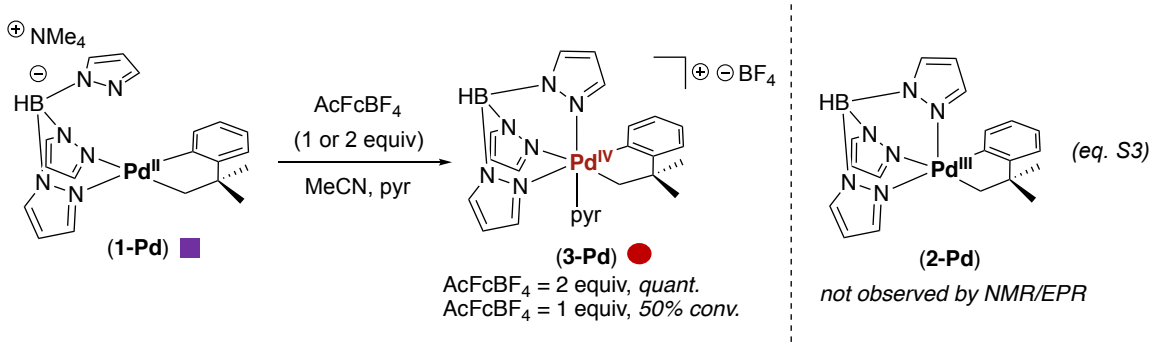

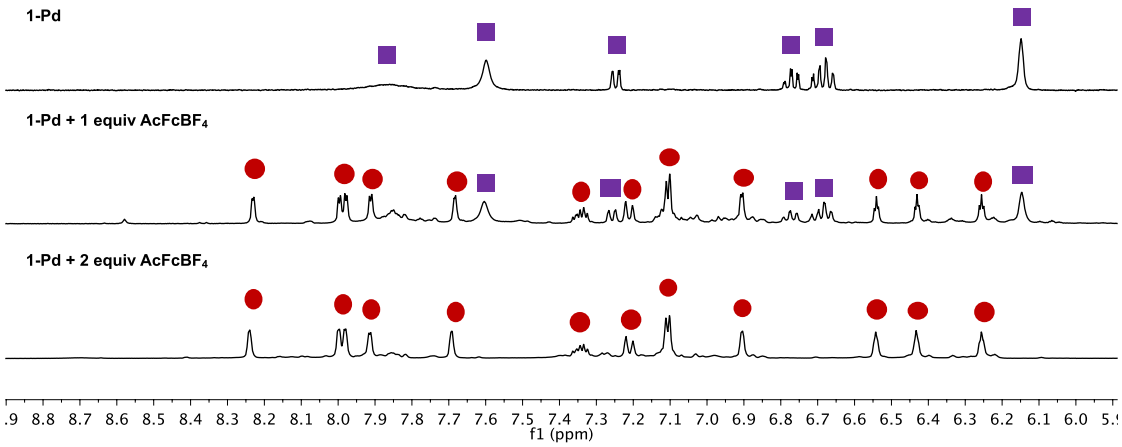

Figure S3. Zoomed in ^{1}H NMR spectra of **1-Pd** and the treatment of **1-Pd** with 1 or 2 equiv of $AcFcBF_4$, illustrating the corresponding resonances for the two complexes

VI. Reductive Elimination Studies

Determining Initial Rates for C–C Coupling: Cationic Ni^{IV}

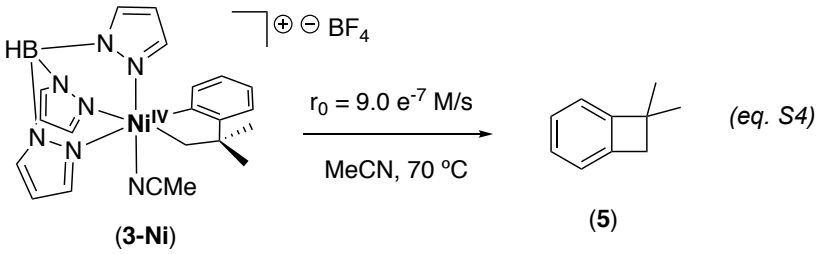

Experimental Procedure: In the glovebox, complex **3-Ni** (3.1 mg, 0.0059 mmol, 1.0 equiv) was added to a J-Young valve NMR tube equipped with an O-ring seal and then dissolved in CD_3CN (0.5 mL) at room temperature. DMSO (1.0 µL, 0.014 mmol, 2.4 equiv) was added as an internal proton standard. The NMR sample was taken out of the glovebox and immediately placed in liquid nitrogen/ethyl acetate bath (approximately –84 ºC). The frozen sample was then placed in the NMR spectrometer that was pre-heated to 70 ºC. Reductive elimination from **3-Ni** was monitored by ^1H NMR spectroscopy at this temperature. Concentration versus time data were acquired from the integration of the methylene proton signals of **5** and **3-Ni** with respect to the internal standard. Initial rate values were obtained from the slope of a linear-fit line corresponding to the growth of **5** (Figure S4).

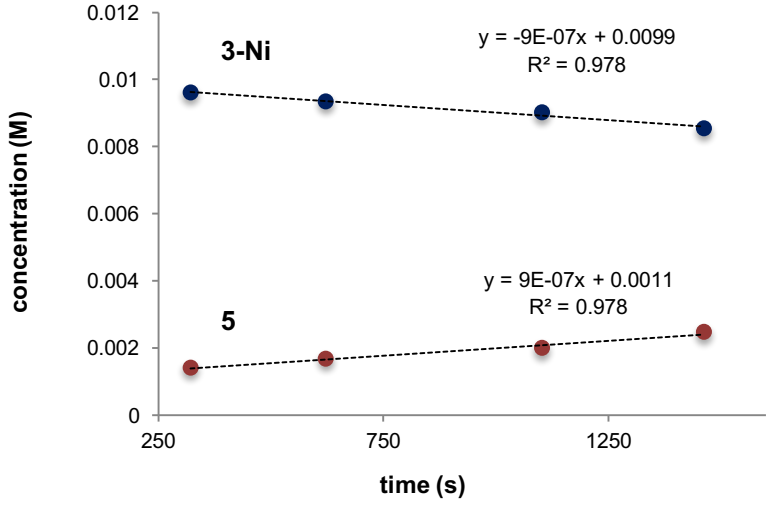

Figure S4. Concentration vs. Time Data for Reductive Elimination of **3-Ni** to Form **5**. Starting Conditions: [Ni] = 0.011 M, T = 70 ºC

Determining Initial Rates for C–C Coupling: Ni^{IV}-CF_3 vs. Pd^{IV}-CF_3

For Ni:

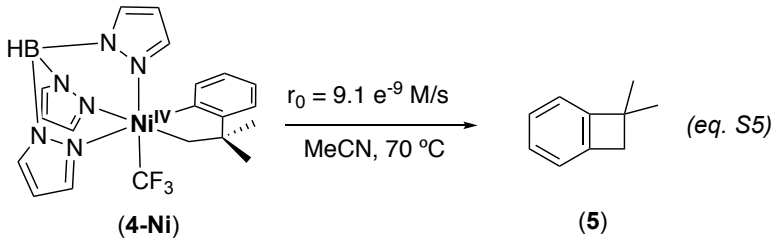

(**4-Ni**) (**5**)

Experimental Procedure: In the glovebox, complex **4-Ni** (2.8 mg, 0.0059 mmol, 1.0 equiv) was added to a J-Young valve NMR tube equipped with an O-ring seal and then dissolved in CD_3CN (0.5 mL) at room temperature. DMSO (1.0 µL, 0.014 mmol, 2.4 equiv) was added as an internal proton standard. The NMR sample was taken out of the glovebox and analyzed by ^1H NMR spectroscopy to obtain integrations for the internal standard and complex **4-Ni**. The sample was then placed in an oil bath at 70 ºC to induce reductive elimination. At various time points, the NMR sample was taken out of the oil bath and immediately cooled in an ice bath. Concentration versus time data were acquired from the integration of the methylene proton signals of **5** and **4-Ni** with respect to the internal standard. The initial rate of reductive elimination was determined by monitoring the first 10% of the reaction progress by ^1H NMR spectroscopy. Initial rate values were obtained from the slope of a linear-fit line corresponding to the growth of **5** (Figure S5).

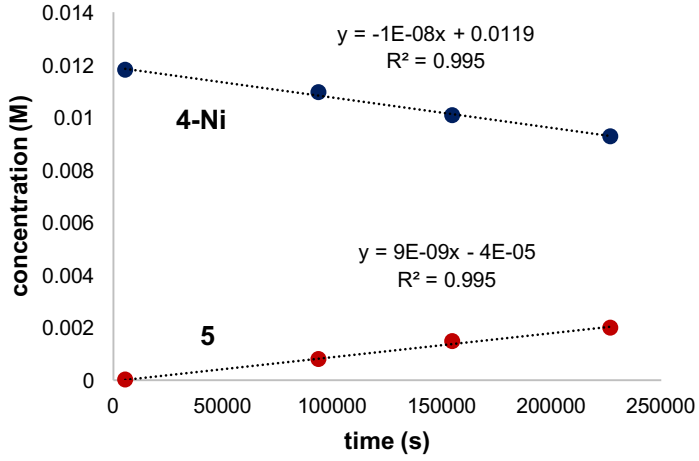

Figure S5. Concentration vs. Time Data for Reductive Elimination of **4-Ni** to Form **5**. Starting Conditions: [Ni] = 0.011 M, T = 70 ºC

For Pd:

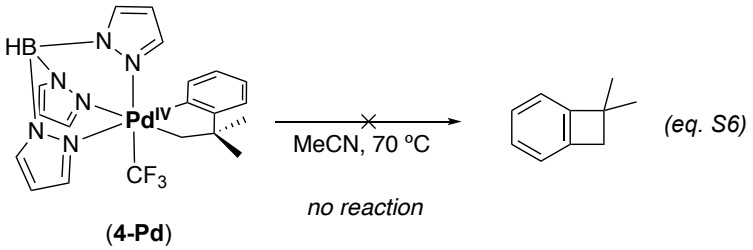

(**4-Pd**)

Experimental Procedure: In the glovebox, complex **4-Pd** (3.0 mg, 0.0059 mmol, 1.0 equiv) was added to a J-Young valve NMR tube equipped with an O-ring seal and then dissolved in CD_3CN (0.5 mL) at room temperature. DMSO (1.0 µL, 0.014 mmol, 2.4 equiv) was added as an internal proton standard. The NMR sample was placed in an oil bath at 70 ºC. However, no reactivity or decomposition of **4-Pd** was observed after monitoring the reaction by ^{1}H NMR spectroscopy for 3 weeks.

Determining Order in Reagents for C–X Bond Formation at Pd^{IV}

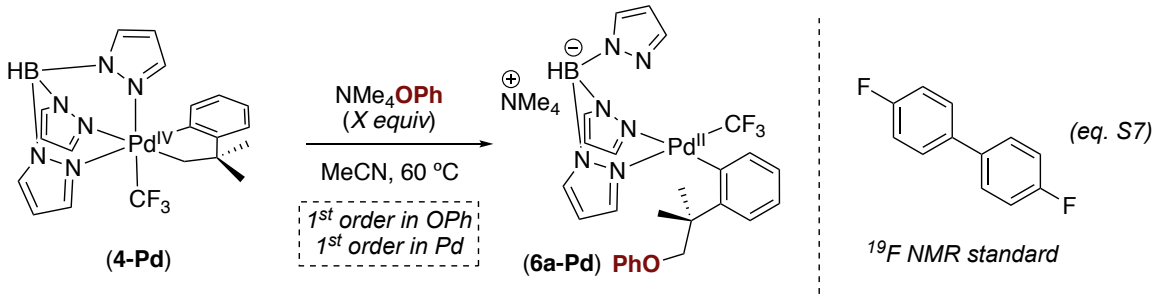

(**4-Pd**) (**6a-Pd**)

Experimental Procedure: Pd^{IV} Complex **4-Pd** (3.0 mg, 0.0057 mmol, 1.0 equiv) was weighed into a J-Young valve NMR tube equipped with an O-ring seal. Various amounts of NMe_4OPh (0.0068 mmol to 0.057 mmol) and the ^{19}F NMR standard 4,4'-difluorobiphenyl (~ 2 mg) were weighed into 4 mL vials, and the solids were dissolved in CD_3CN (0.5 mL). The resulting solution was added to the NMR tube at room temperature. The tube was then placed into an NMR spectrometer that had been pre-heated to 60 ºC. The rate of reductive elimination from **4-Pd** to form **6a-Pd** was monitored by ^{19}F NMR spectroscopy at 60 ºC. Concentration versus time data were acquired by integration of the CF_3 signals of **4-Pd** and **6a-Pd** with respect to the internal standard (Figure S6). Initial rates were obtained from the slope of a linear-fit line monitoring the first 5-20% of the reaction progress. A plot of $\ln(r_0)$ vs. $\ln([^-OPh])$ showed that the rate of coupling is first-order in $^-$OPh (Figure S7).

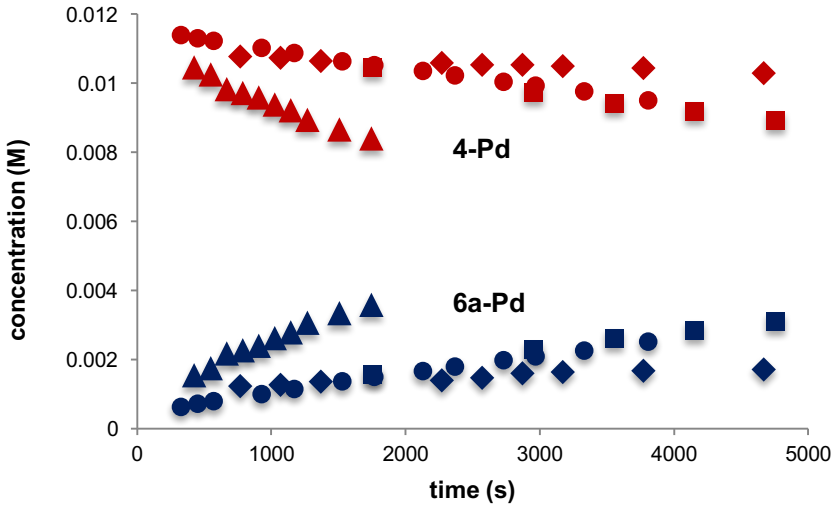

Figure S6. Concentration vs. Time Data for the Reductive Elimination of **4-Pd** to Form **6a-Pd** in the Presence of 1.2, 2.5, 5, and 10 equiv of NMe_4OPh.

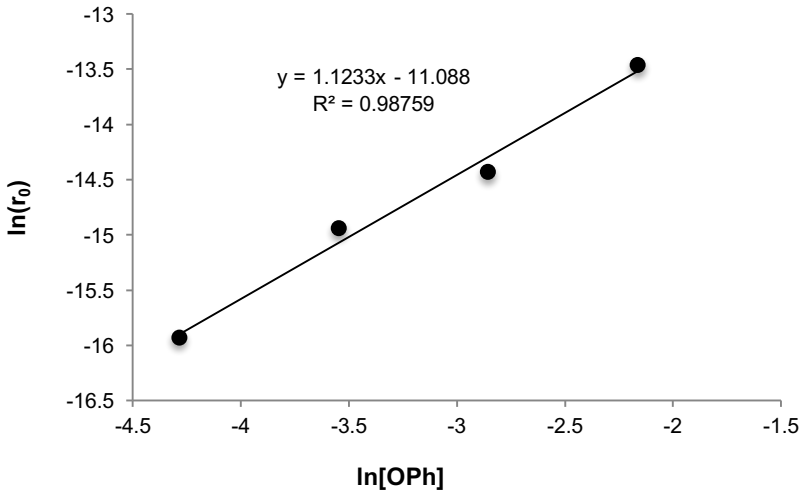

Figure S7. (ln[OPh]) vs (ln[r_0]) Plot. The slope of the line is approximately 1.

Determining Initial Rates for C–X Bond-Formation at 60 ºC

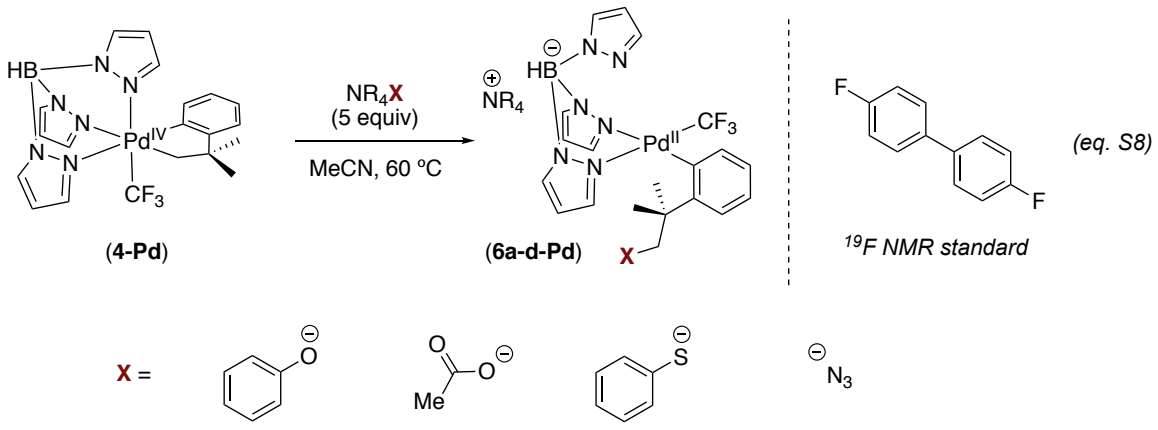

Experimental Procedure: In the glovebox Pd^{IV} complex **4-Pd** (3.0 mg, 0.0057 mmol, 1.0 equiv) was added to a J-Young valve NMR tube equipped with an O-ring seal. The respective nucleophile, NR_4X, where X = OPh, OAc, SPh, N_3 (0.0288 mmol, 5 equiv), along with the internal standard 4,4'-difluorobiphenyl (~ 2 mg) was weighed into a 4 mL vial and then dissolved in CD_3CN (0.5 mL). The resulting solutions were added to the NMR tube at room temperature and taken out of the glovebox. The tube was then placed into an NMR spectrometer that had been pre-heated to 60 ºC. The rates of reductive elimination were determined by monitoring the first 10-40% of the reaction progress by ^{19}F NMR spectroscopy at this temperature. Concentration versus time data were acquired from the integration of the CF_3 signals of **4-Pd** and **6-Pd** with respect to the internal standard. Initial rate values were obtained from the slope of a linear-fit line corresponding to the decay of **4-Pd** (Figures S8-S11).

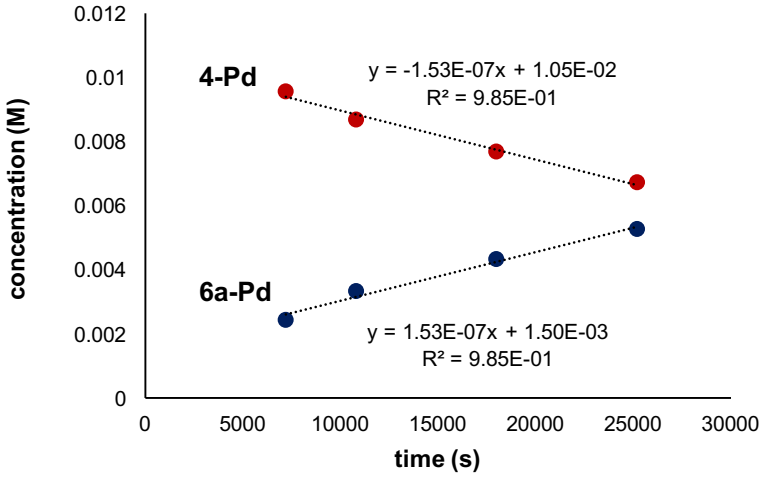

Figure S8. Concentration vs. Time Data for Reductive Elimination from **4-Pd** to Form **6a-Pd**. Starting Conditions: [Pd] = 0.011 M, [OPh] = 0.057 M, T = 60 ºC

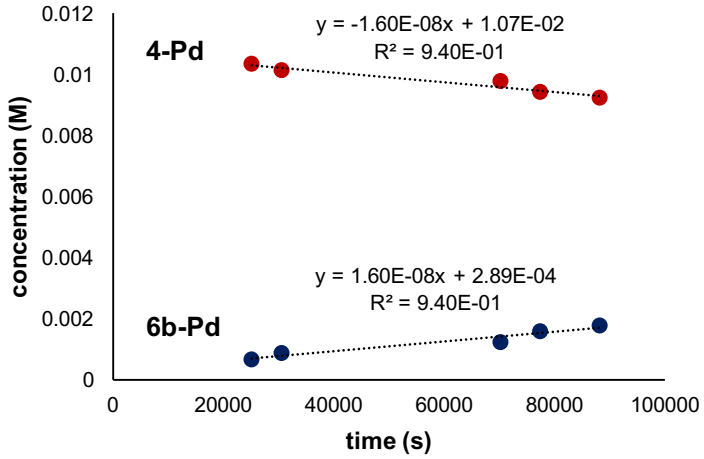

Figure S9. Concentration vs. Time Data for Reductive Elimination from **4-Pd** to Form **6b-Pd**. Starting Conditions: [Pd] = 0.011 M, [OAc] = 0.057 M, T = 60 ºC

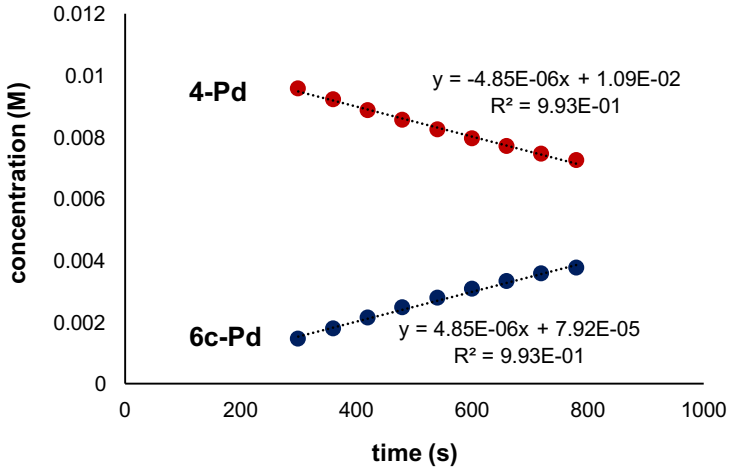

Figure S10. Concentration vs. Time Data for Reductive Elimination from **4-Pd** to Form **6c-Pd**. Starting Conditions: [Pd] = 0.011 M, [SPh] = 0.057 M, T = 60 ºC

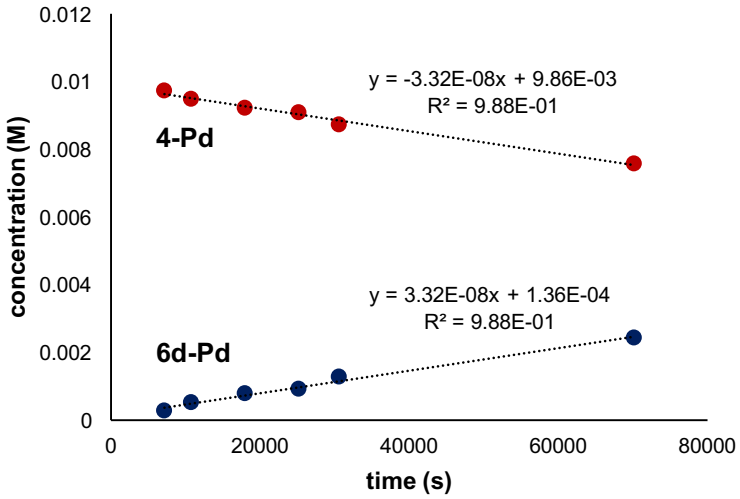

Figure S11. Concentration vs. Time Data for Reductive Elimination from **4-Pd** to Form **6d-Pd**. Starting Conditions: [Pd] = 0.011 M, [N_3] = 0.057 M, T = 60 ºC

Nucleophilicity Values

The Swain-Scott nucleophilicity parameters for the various nucleophiles (phenoxide [OPh], acetate [OAc], thiophenoxide [SPh], and azide [N_3]) were obtained from a report published by Pearson and co-workers.[9] The reported nucleophilicity parameters were plotted vs. experimental initial rates. The nucleophilicity table for complex **4-Ni** was previously reported by our group.[3] The results for **4-Pd** are displayed in Table S1 and Figure S12.

Table S1. Nucleophilicity parameters and initial rate values for C–X bond-formation reactions from complex **4-Pd** to form **6a-d-Pd** with 5 equiv of nucleophile

Nucleophile (X^-)	Nucleophilicity (n_X)	Initial Rate (r_0) (M/s)	log(r_0)
$^-$OPh	5.75	1.53e-7	–6.85
$^-$OAc	4.30	1.60e-8	–7.79
$^-$SPh	9.92	4.85e-6	–5.31
$^-N_3$	5.78	3.32-8	–7.45

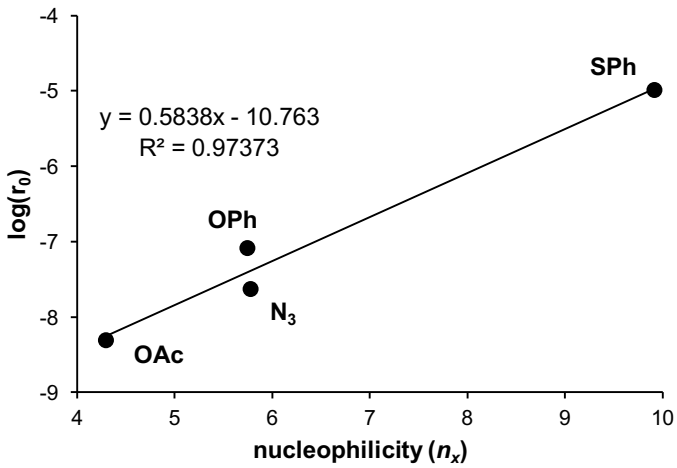

Figure S12. Plot of nucleophilicity parameters vs. initial rate of C–X coupling from **4-Pd** to form **6a-d-Pd**

Determining Activation Parameters for C–O Coupling at Ni^{IV} and Pd^{IV}

For Ni:

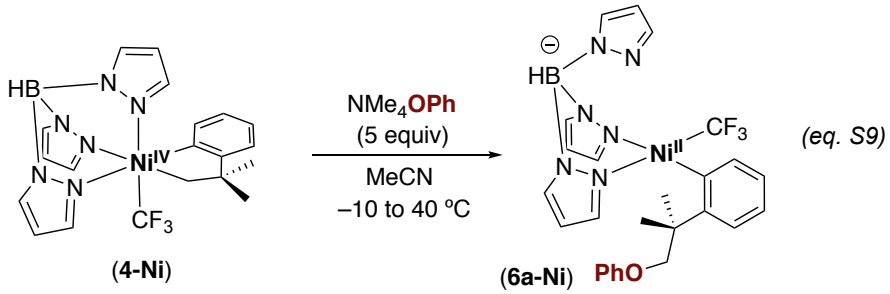

Experimental Procedure: The activation parameters for C–O coupling at Ni^{IV} were determined through an Eyring Plot in the temperature range of –10 to 40 ºC. In the glovebox, complex **4-Ni** (2.6 mg, 0.0055 mmol, 1.0 equiv), NMe_4OPh (4.4 mg, 0.027 mmol, 5.0 equiv), and the ^{19}F NMR standard 4,4-difluorobiphenyl (~2 mg) were weighed into a 4 mL vial. CD_3CN (0.5 mL) was added at –35 ºC and the resulting solution was transferred to a J-Young valve NMR tube equipped with an O-ring seal at this temperature. The NMR tube was taken out of the glovebox and immediately flash frozen in an ethyl acetate/liquid nitrogen bath (–84 ºC). The sample was placed into an NMR spectrometer where the probe had been pre-set to the respective temperature (–10 to 40 ºC). The rate of reductive elimination was determined by monitoring approximately the first 10% of the reaction by ^{19}F NMR spectroscopy at –10 ºC, 5 ºC, 25 ºC, 30 ºC, and 40 ºC. Concentration versus time data were acquired from the integration of the CF_3 signals of **4-Ni** and **6a-Ni** with respect to the internal standard. Initial rate values were obtained from the slope of a linear-fit line corresponding to the decay of **4-Ni**. The activation parameters for C–O coupling were extracted from the resulting Eyring Plot.

Temp (K)	Initial Rate (M s^{-1})	Rate Constant (*k*)	1/T (K^{-1})	ln(*k*/t)
263.2	1.91 x 10^{-8}	2.88 x 10^{-5}	0.0038	–16.02
278.2	1.22 x 10^{-7}	1.84 x 10^{-4}	0.0036	–14.23
298.2	1.21 x 10^{-6}	1.83 x 10^{-3}	0.0034	–12.00
303.2	2.01 x 10^{-6}	3.03 x 10^{-3}	0.0033	–11.55
313.2	4.73 x 10^{-6}	7.14 x 10^{-3}	0.0032	–10.69

Table S2. Eyring Plot Data for the Reductive Elimination of **4-Ni** to Form **6a-Ni**

For Pd:

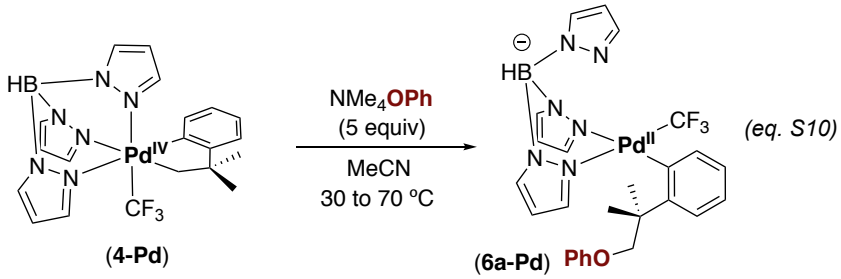

Experimental Procedure: The activation parameters for C–O coupling at Pd^{IV} were determined through an Eyring Plot in the temperature range of 30 to 70 ºC. In the glovebox, complex **4-Pd** (3 mg, 0.0055 mmol, 1.0 equiv), NMe_4OPh (4.4 mg, 0.027 mmol, 5.0 equiv), and the ^{19}F NMR standard 4,4-difluorobiphenyl (~2 mg) were weighed into a 4 mL vial. CD_3CN (0.5 mL) was added at –35 ºC and the resulting solution was transferred to a J-Young valve NMR tube equipped with an O-ring seal at this temperature. The NMR tube was taken out of the glovebox and immediately flash frozen in an ethyl acetate/liquid nitrogen bath (–84 ºC). The sample was placed into an NMR spectrometer where the probe had been pre-set to the respective temperature 30 to 70 ºC). The rate of reductive elimination was determined by monitoring approximately the first 10% of the reaction by ^{19}F NMR spectroscopy at the indicated temperature. Concentration versus time data were acquired from the integration of the CF_3 signals of **4-Pd** and **6a-Pd** with respect to the internal standard. Initial rate values were obtained from the slope of a linear-fit line corresponding to the decay of **4-Pd**. The activation parameters for C–O coupling were extracted from the resulting Eyring Plot.

Temp (K)	Initial Rate (M s^{-1})	Rate Constant (*k*)	1/T (K^{-1})	ln(*k*/t)
303.2	1.31 x 10^{-8}	1.98 x 10^{-5}	0.0033	–16.54
313.2	2.39 x 10^{-8}	3.61 x 10^{-5}	0.0032	–15.97
323.2	3.34 x 10^{-8}	1.11 x 10^{-4}	0.0031	–14.88
333.2	2.86 x 10^{-7}	4.32 x 10^{-4}	0.0030	–13.56

343.2	9.33×10^{-7}	1.41×10^{-3}	0.0029	–12.40

Table S3. Eyring Plot Data for the Reductive Elimination of **4-Pd** to Form **6a-Pd**

Azide Reactivity: Ni vs. Pd

For Ni:

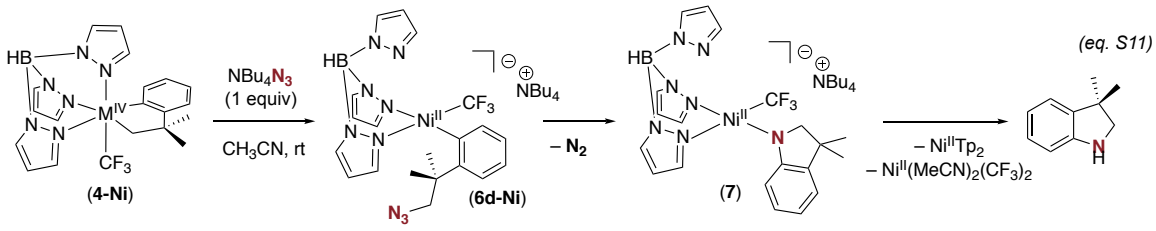

***in situ* Observation and Decomposition of [(NBu_4)(Tp)Ni^{II}(C_6H_4-*o*-$CMe_2CH_2N_3$)(CF_3)] (6d-Ni).**[3] A J. Young valve NMR tube equipped with an O-ring seal was charged with [(Tp)Ni^{IV}(CH_2CMe_2-*o*-C_6H_4)(CF_3)] (**4-Ni**) (10 mg, 0.021 mmol, 1.0 equiv). This solid was dissolved in acetonitrile (0.5 mL). NBu_4N_3 (6.0 mg, 0.021 mmol, 1.0 equiv) was added, and the resulting solution was monitored at room temperature by ^{1}H and ^{19}F NMR spectroscopy. Over the course of 1 h, the reaction mixture changed color from yellow to purple. Over an additional 15 h, the color changed again to orange.

Intermediate **6d-Ni** was observed *in situ* and characterized at approximately 20% conversion.

^{1}H NMR (700 MHz, CD_3CN, 23 ºC) δ 8.28 (d, J_{HH} = 7.2 Hz, 1H), 8.03 (d, J_{HH} = 2.0 Hz, 1H), 7.79 (m, 1H), 7.63 (br, 1H), 7.37 (br, 1H), 7.32 (br, 1H), 7.10 (m, 1H), 6.72 (t, J_{HH} = 7.4 Hz, 1H), 6.64 (t, J_{HH} = 7.4 Hz, 1H), 6.43 (d, J_{HH} = 6.9 Hz, 1H), 6.33 (br, 1H), 6.19 (overlapping peaks, 1H), 5.79 (br, 1H), 3.72 (d, J_{HH} = 11.9 Hz, 1H), 3.71 (d, J_{HH} = 11.9 Hz, 1H), 2.02 (s, 3H), 1.76 (s, 3H).

^{19}F NMR (471 MHz, CD_3CN, 23 ºC) δ –20.59 (s, Ni-C***F***$_3$).

After 15 h at room temperature, complex **4-Ni** and intermediate **6d-Ni** were fully consumed to generate 3,3'-dimethylindoline in quantitative conversion. Reaction conversion was determined by integration of the methylene protons of the indoline vs. an internal standard, 3-(trifluoromethyl)anisole via ^{1}H NMR spectroscopy. 3,3'-dimethylindoline was characterized by comparison of its ^{1}H NMR spectrum with that reported in the literature[10] and by mass spectrometry.

Monitoring Indoline Formation by ^{1}H and ^{19}F NMR Spectroscopy

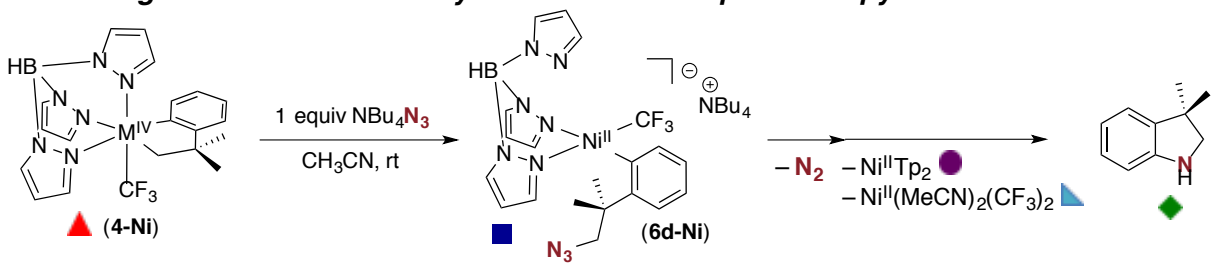

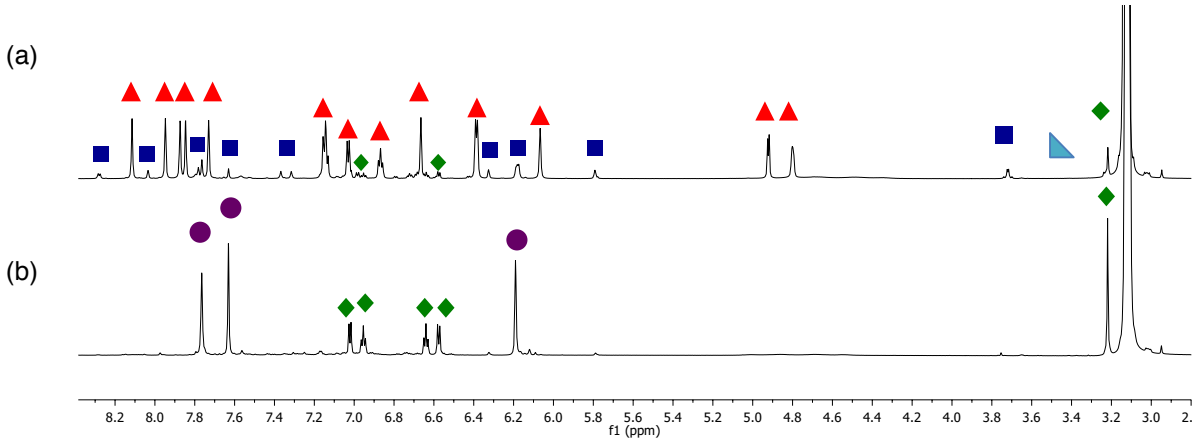

Figure S13. ^{1}H NMR spectra showing the reaction progress for the formation of 3,3,-dimethylindoline from complex **4-Ni** and azide intermediate **6d-Ni**. (a) 2 h, 23 ºC (b) 15 h, 23 ºC.

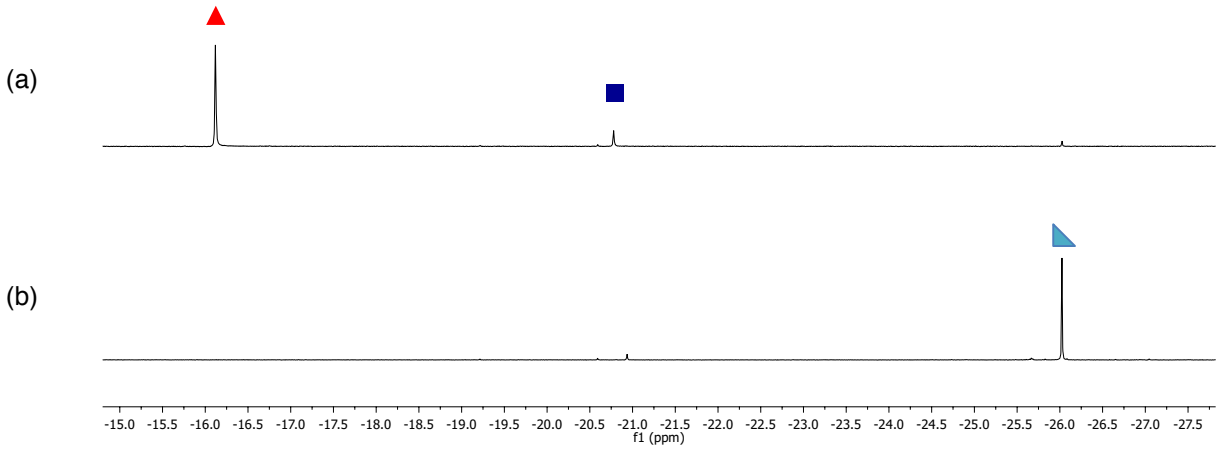

Figure S14. ^{19}F NMR spectra showing the reaction progress for the formation of $Ni^{II}(MeCN)_2(CF_3)_2$ from complex **4-Ni** and azide intermediate **6d-Ni**. (a) 2 h, 23 ºC (b) 15 h, 23 ºC.

For Pd:

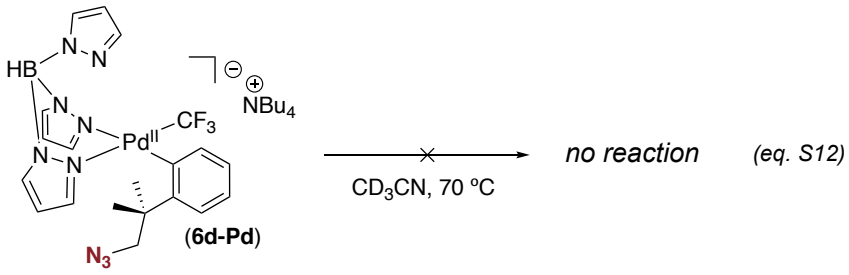

Thermolysis of 6d-Pd. A J. Young valve NMR tube equipped with an O-ring seal was charged with [(NBu_4)(Tp)Pd^{II}(C_6H_4-*o*-$CMe_2CH_2N_3$)(CF_3)] (**6d-Pd**) (10 mg, 0.012 mmol, 1.0 equiv). This solid was dissolved in acetonitrile (0.5 mL). NBu_4N_3 (17 mg, 0.060 mmol, 5.0 equiv) was added, and the resulting solution was monitored at 70 ºC by ^1H and ^{19}F NMR spectroscopy. Over the course of 1 week at this temperature complex **6d-Pd** was stable to any further reactivity.

VII. Cyclic Voltammetry Studies

Experimental Procedure: Cyclic voltammetry on complexes **1-Ni** and **1-Pd** were performed in a 3-electrode cell consisting of a 3 mm glassy carbon disc working electrode, a Ag/Ag^+ reference electrode with a Ag wire in a fritted chamber containing a solution of $AgBF_4$ (0.01 M) and NBu_4PF_6 (0.1 M) in acetonitrile, and a Pt wire counter electrode. A 2 mL solution of the complex (0.01 M) and NBu_4PF_6 (0.1 M) in acetonitrile was added to the electrochemical cell. Cyclic voltammetry scans were taken at 100 mV/s. After obtaining the CV for each complex, ferrocene was added as an internal reference.

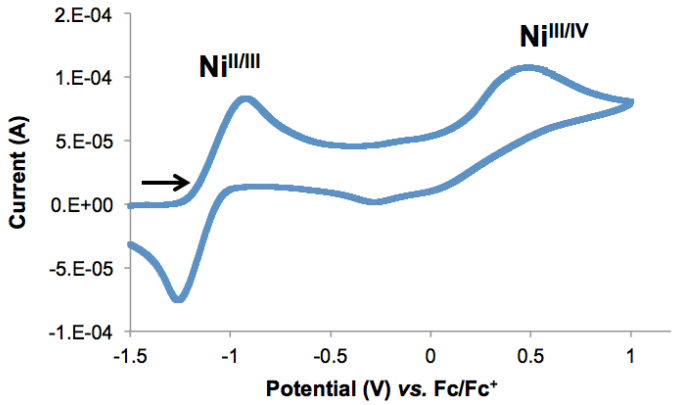

Figure S15. CV of **1-Ni** in MeCN. [Ni] = 0.01 M, [NBu_4PF_6] = 0.1 M, scan rate = 100 mV/s.

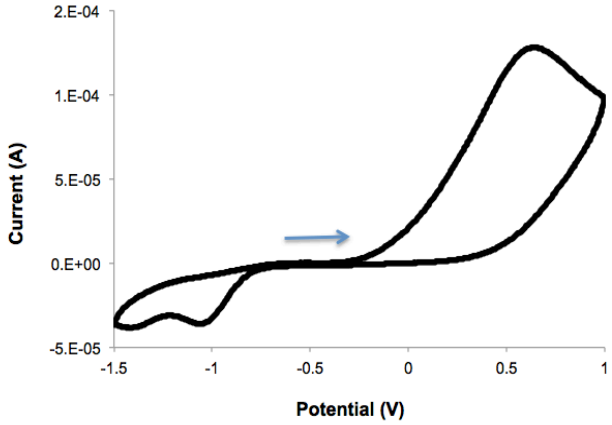

Figure S16. CV of **1-Pd** in the Absence of Added Pyridine. Conditions: [Pd] = 0.01 M in MeCN, [NBu_4PF_6] = 0.1 M in MeCN, Scan rate = 100 mV/s

We hypothesized that the irreversibility in the CV of complex **1-Pd** could be improved with the addition of a strong L-type ligand such as pyridine to stabilize the high-valent center. Cyclic voltammetry of complex **1-Pd** was therefore performed under the previous conditions with the addition of 2 mL of pyridine. [Pd] = 0.005 M in a 50/50 mixture of

acetonitrile/pyridine. As shown in Figure S17, the reversibility of the complex is improved with added pyridine.

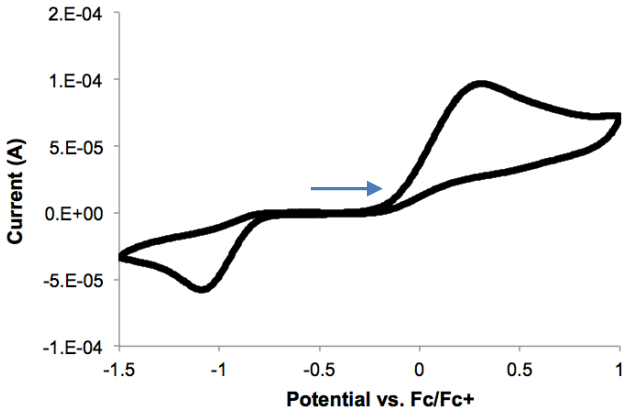

Figure S17. CV of **1-Pd** with Added Pyridine. Conditions: [Pd] = 0.005 M in MeCN/pyr, [NBu_4PF_6] = 0.1 M, Scan Rate = 100 mV/s

VIII. Computational Details

Gaussian 09[11] was used for DFT calculations at the B3LYP level for optimization, using the Stuttgart/Dresden ECP (SDD) basis set for Pd[12] and the 6-31G(d) basis set for other atoms (referred to as basis set BS1). Single point calculations were performed at the B3LYP-D3 level,[13] utilizing the quadruple-ξ valence polarised def2-QZVP[14] basis set on Ni and Pd along with the corresponding ECP and the 6-311+G(2d,p) basis set on other atoms (basis set BS2). All calculations were carried out for acetonitrile as solvent with the IEFPCM (SCRF) model. All thermodynamic data were calculated at the standard state (298.15 K and 1 atm) and entropy calculations were adjusted by the method proposed by Okuno.[15] This computational procedure has been benchmarked for palladium when applied to C···C coupling from a closely related 2,2'-bipyridine (bpy) cation $[Pd^{IV}(CH_2CMe_2\text{-}o\text{-}C_6H_4\text{-}C,C')(F)(bpy\text{-}N,N')]^+$ in acetonitrile.[16] The triflate (OTf) salt of this cation computes as $\Delta G^{\ddagger}$ 24.7 kcal/mol, compared with experimental ($\Delta G^{\ddagger}$ 23.8 kcal/mol) and different computation procedures ($\Delta G^{\ddagger}$ 23.3 kcal/mol) for a sulfonamide (Tf_2N) salt.[16] All transition structures contained one imaginary frequency, exhibiting atom displacements consistent with the anticipated reaction pathway. The nature of transition structures was confirmed by Intrinsic Reaction Coordinate (IRC) searches, vibrational frequency calculations, and potential energy surface scans. Natural bond order analyses[17] were performed in conjunction with BS1. For studies of formation of the indolinide complex, computation for geometry optimization and single-point employed the UCAM-B3LYP and UCAM-B3LYP-D3 functionals, respectively, within the broken-symmetry unrestricted methodology to facilitate calculations for triplet and open-shell singlet configurations.[18,19]

Wiberg Bond Indices (WBI) Calculations of 4-Ni and 4-Pd

Wiberg Bond Indices (WBI) were computed to compare the two M–N^1 and M–N^2 bonds (*trans* to CF_3 and Ph, respectively) with the M···N^3 interaction (Table S4). The data show shorter Pd–N^1 distances *trans* to CF_3 compared with trans to Ph (Pd–N^2). Consequently, larger Wiberg Bond Indices for the Pd–N^1 bonds *trans* to CF_3 were found, as anticipated for the stronger *trans* effect of the aryl group. In addition, the uniformly longer Pd–$N^{1/2}$ and Pd···N^3 distances compared to Ni are reflected in uniformly lower WBI's for Pd. Overall, pathway B can be considered a "five-coordinate-like" transition state in the Pd system.

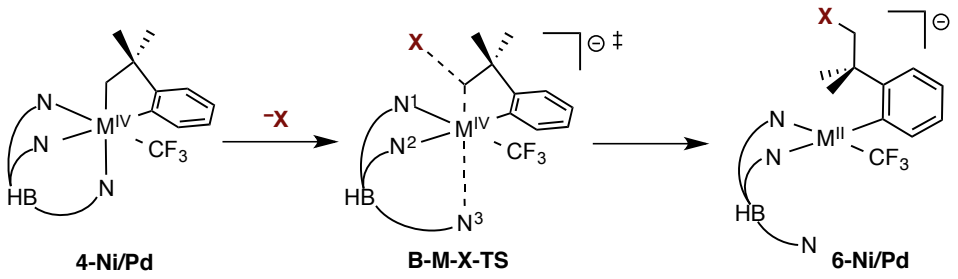

4-Ni/Pd **B-M-X-TS** **6-Ni/Pd**

Nuc (X)		M–N^1	WBI	M–N^2	WBI	M---N^3	WBI
Ni:	OPh	2.022	0.396	2.050	0.372	2.528	0.184
	SPh	2.019	0.392	2.047	0.368	2.603	0.165
Pd:	OPh	2.167	0.345	2.209	0.324	2.818	0.153
	SPh	2.165	0.345	2.047	0.368	2.937	0.132

Table S4. M-N and M···N distances together with Wiberg Bond Indices for these interactions in κ^3-Tp transition structures (**B-M-X-TS**) for the reactions of complexes **4-Ni/Pd** with anionic nucleophiles X = $^-$OPh and $^-$SPh.

Figure S18. Complete energy profiles for the reaction of phenoxide with **4-Ni** (abbreviated in Figure 9(a)) illustrating alternative pathways involving preliminary dissociation of a pyrazole donor (in blue), or direct interaction of [OPh]$^-$ with octahedral **4-Ni** (in black). Energies ΔG (ΔH) in kcal/mol.

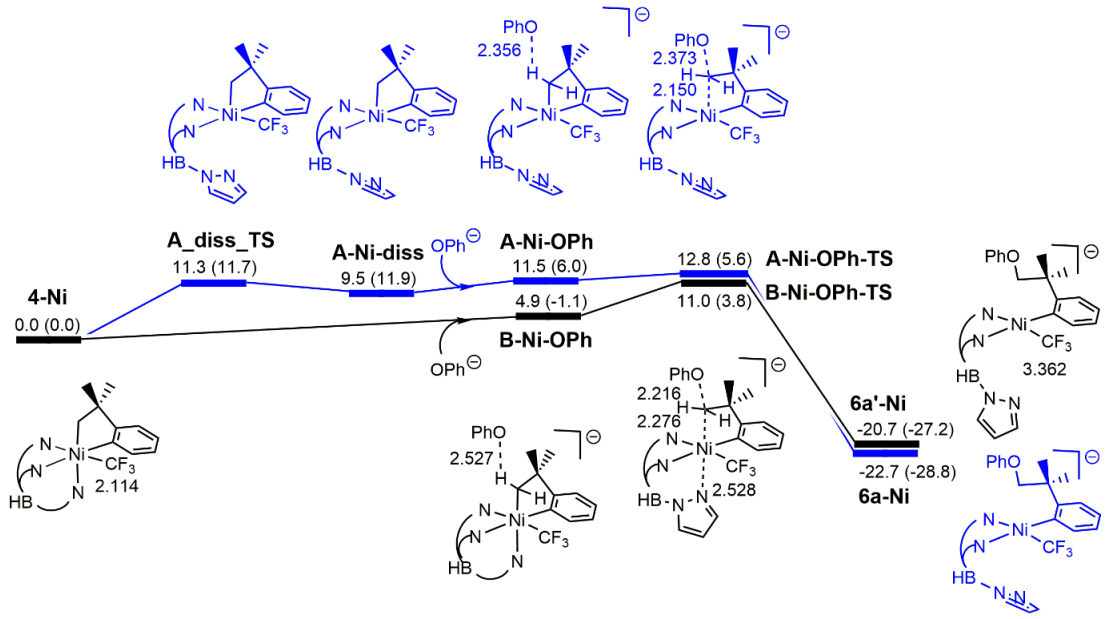

Figure S19. Complete energy profiles for the reaction of phenoxide with **4-Pd** (abbreviated in Figure 9b) illustrating alternative pathways involving preliminary dissociation of a pyrazole donor (in blue), or direct interaction of [OPh]$^-$ with octahedral **4-Ni** (in black). Energies ΔG (ΔH) in kcal/mol.

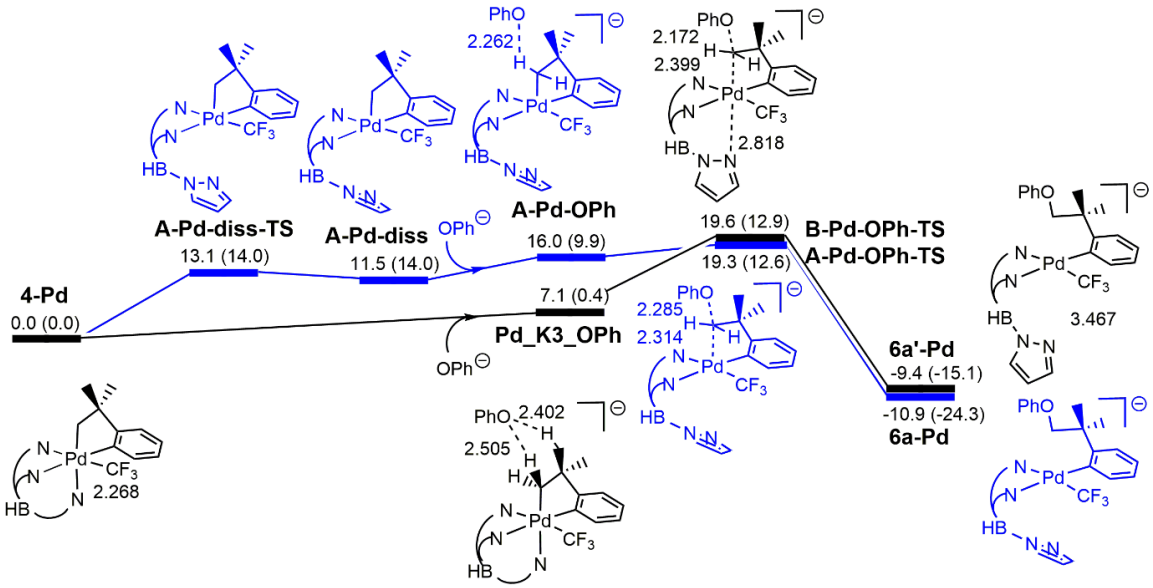

Figure S20. Energy profiles for the reaction of thiophenoxide with **4-Ni** (see Figure 10) illustrating alternative pathways involving preliminary dissociation of a pyrazole donor (in blue), or direct interaction of [SPh]$^-$ with octahedral **4-Ni** (in black). Energies ΔG (ΔH) in kcal/mol.

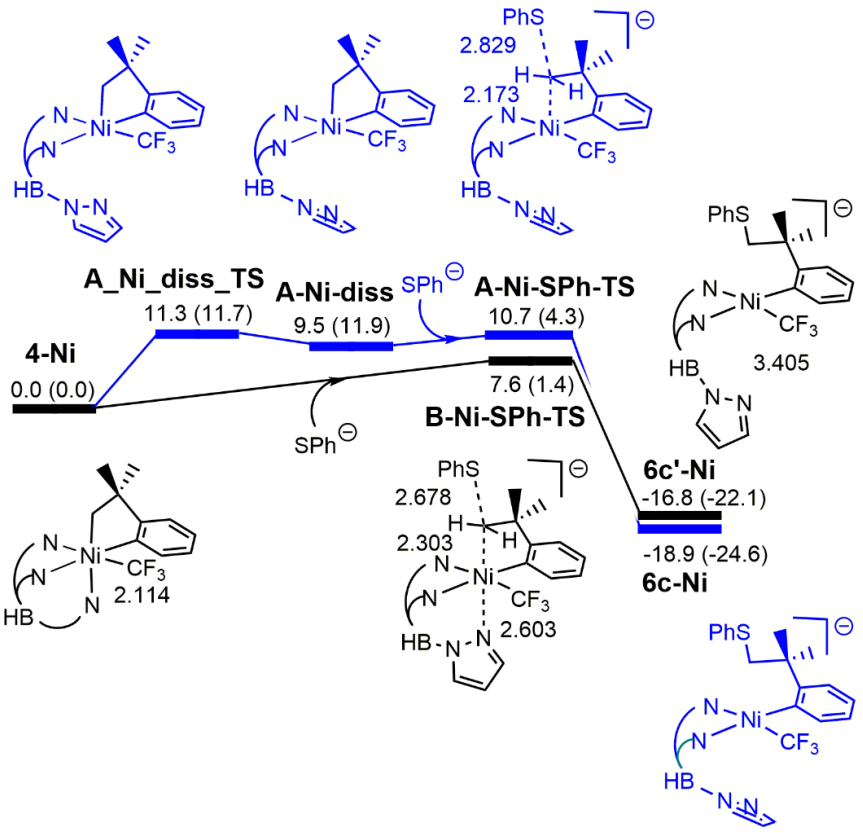

Figure S21. Energy profiles for the reaction of thiophenoxide with **4-Pd** (see Figure 10) illustrating alternative pathways involving preliminary dissociation of a pyrazole donor (in blue), or direct interaction of [SPh]$^-$ with octahedral **4-Pd** (in black). Energies ΔG (ΔH) in kcal/mol.

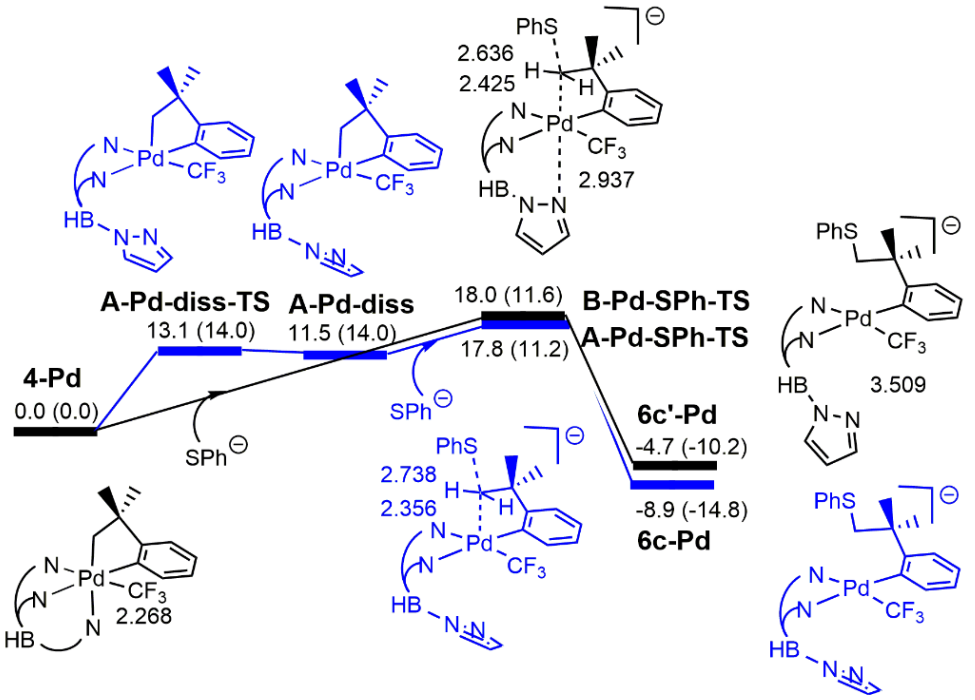

Figure S22. Energy profiles for the reaction of acetate with **4-Ni** illustrating alternative pathways involving preliminary dissociation of a pyrazole donor (in blue), or direct interaction of [OAc]$^-$ with octahedral **4-Ni** (in black). Energies ΔG (ΔH) in kcal/mol.

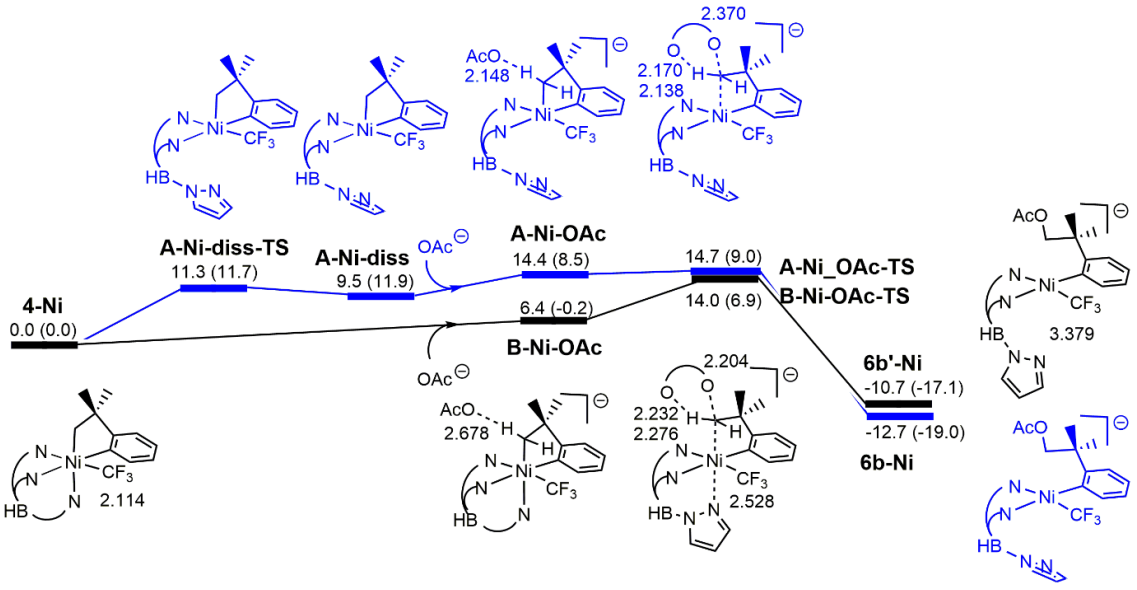

Figure S23. Energy profiles for the reaction of acetate with **4-Pd** illustrating alternative pathways involving preliminary dissociation of a pyrazole donor (in blue), or direct interaction of $[OAc]^-$ with octahedral 4-Pd (in black). Energies ΔG (ΔH) in kcal/mol.

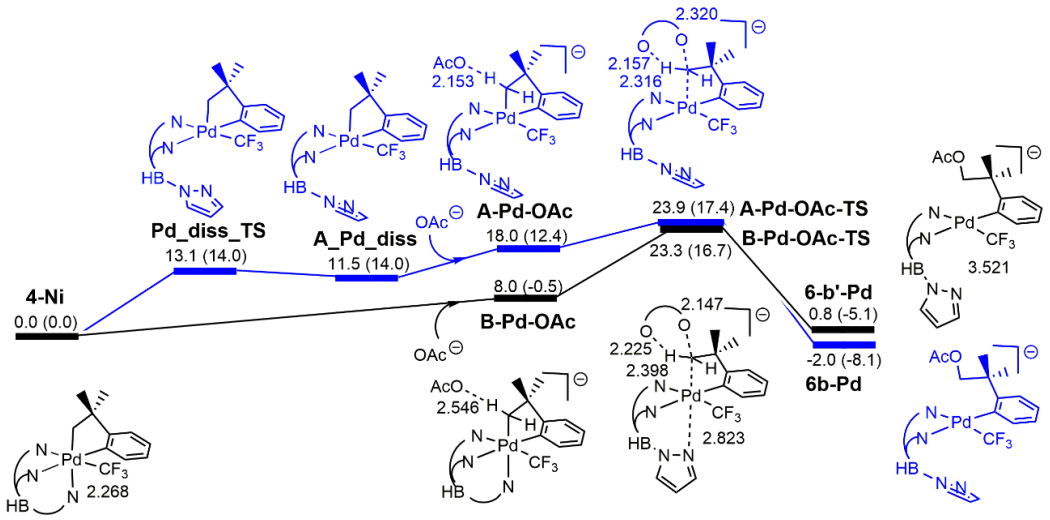

Figure S24. Energy profiles for the reaction of azide with **4-Ni** illustrating alternative pathways involving preliminary dissociation of a pyrazole donor (in blue), or direct interaction of $[N_3]^-$ with octahedral **4-Ni** (in black). Energies ΔG (ΔH) in kcal/mol.

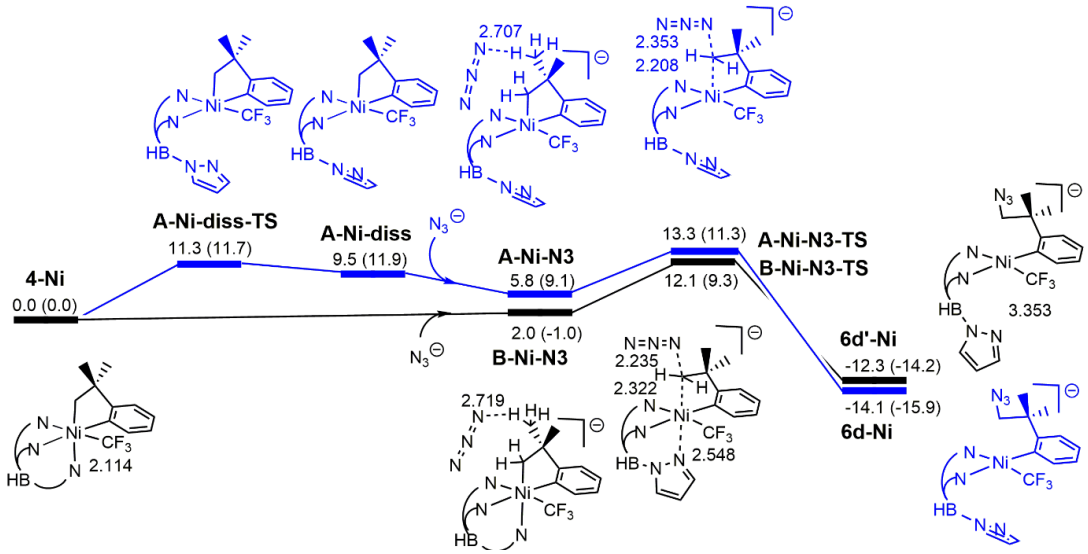

Figure S25. Energy profiles for the reaction of azide with **4-Pd** illustrating alternative pathways involving preliminary dissociation of a pyrazole donor (in blue), or direct interaction of $[N_3]^-$ with octahedral **4-Pd** (in black). Energies ΔG (ΔH) in kcal/mol.

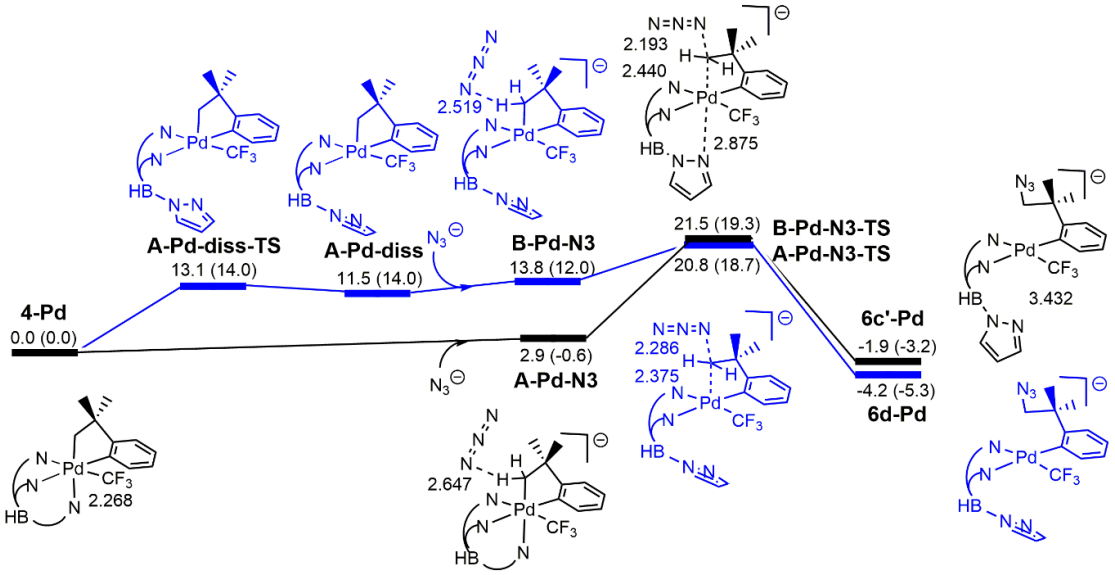

IX. References

[1] Campora, J.; Gutierrez, E.; Monge, Á.; Palma, P.; Poveda, M. L.; Ruiz, C.; Carmona, E. *Organometallics* **1994**, *13*, 1728–1745.

[2] Campora, J.; Lopez, J. A.; Palma, P.; Rio, D.; Carmona, E.; Valerga, P.; Graiff, C.; Tiripicchio, A. *Inorg. Chem.* **2001**, *40*, 4116–4126.

[3] Camasso, N. M.; Sanford, M. S. *Science* **2015**, *347*, 1218–1220.

[4] Camasso, N. M.; Pérez-Temprano, M. H.; Sanford, M. S. *J. Am. Chem. Soc.* **2014**, *136*, 12771–12775.

[5] Bour, J. R.; Camasso, N. M; Sanford, M. S. *J. Am. Chem. Soc.* **2015**, *137*, 8034–8037.

[6] Connelly, N. G.; Geiger, W. E. *Chem. Rev.* **1996**, *96*, 877–910.

[7] Campora, J.; Palma, P.; del Rio, D.; Lopez, J. A.; Alvarez, E.; Connelly, N. G. *Organometallics* **2005**, *24*, 3624–3628.

[8] Bour, J. R.; Camasso, N. M.; Meucci, E. A.; Kampf, J. W.; Canty, A. J.; Sanford, M. S. *J. Am. Chem. Soc.* **2016**, *138*, 16105–16111.

[9] (a) Swain, C. G.; Scott, C. B. *J. Am. Chem. Soc.* **1953**, 75, 141–147. (b) Pearson, R. G.; Sobel, H. R.; Songstad, J. *J. Am. Chem. Soc.* **1968**, *90*, 319–326.

[10] Erdelmeier, I.; Tailhan-Lomont, C.; Yadan, J.-C. *J. Org. Chem.* **2000**, *65*, 8152–8157.

[11] Frisch, M. J.; et al. *Gaussian 09*, revision A.02; Gaussian, Inc.: Wallingford, CT, 2009.

[12] Andrae, H.; Haussermann, U.; Dolg, M.; Stoll, H.; Preuss, H. *Theor. Chim. Acta* **1990**, *77*, 123–141.

[13] (a) Ehrlich, S.; Moellmann, J.; Grimme, S. *Acc. Chem. Res*. **2013**, *46*, 916–926. (b) Antony, J.; Sure, R.; Grimme, S. *Chem. Commun*. **2015**, *51*, 1764–1774.

[14] Weigend, F.; Furche, F.; Aldrichs, R. *J. Chem. Phys*. **2003**, *119*, 12753–12762.

[15] Okuno, Y. *Chem. Eur. J*. **1997**, *3*, 212–218.

[16] Pendleton, I. M.; Pérez-Temprano, M. H.; Sanford, M. S.; Zimmerman, P. M. *J. Am. Chem. Soc*. **2016**, *138*, 6049–6060.

[17] Glendening, E. D.; Read, A. E.; Carpenter, J. E.; Weinhold, F. *NBO*, version 3.1; Gaussian Inc.; Pittsburgh, PA, **2003**.

[18] Yanai. T.; Tew, D. P.; Handy, N. C. *Chem. Phys. Lett*. **2004**, *393*, 51–57. (b) Cramer, C. J.; Truhlar, D. G. *Phys. Chem. Chem. Phys*. **2009**, *11*, 10757–10816.

[19] Poater, A.; Cavallo, L. *Theor. Chem. Acc*. **2013**, *132*, 1353.

X. Spectral Data

^{1}H NMR Spectrum of 1-Ni at 23 ºC (CD_3CN)

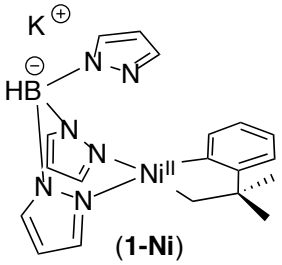

(**1-Ni**)

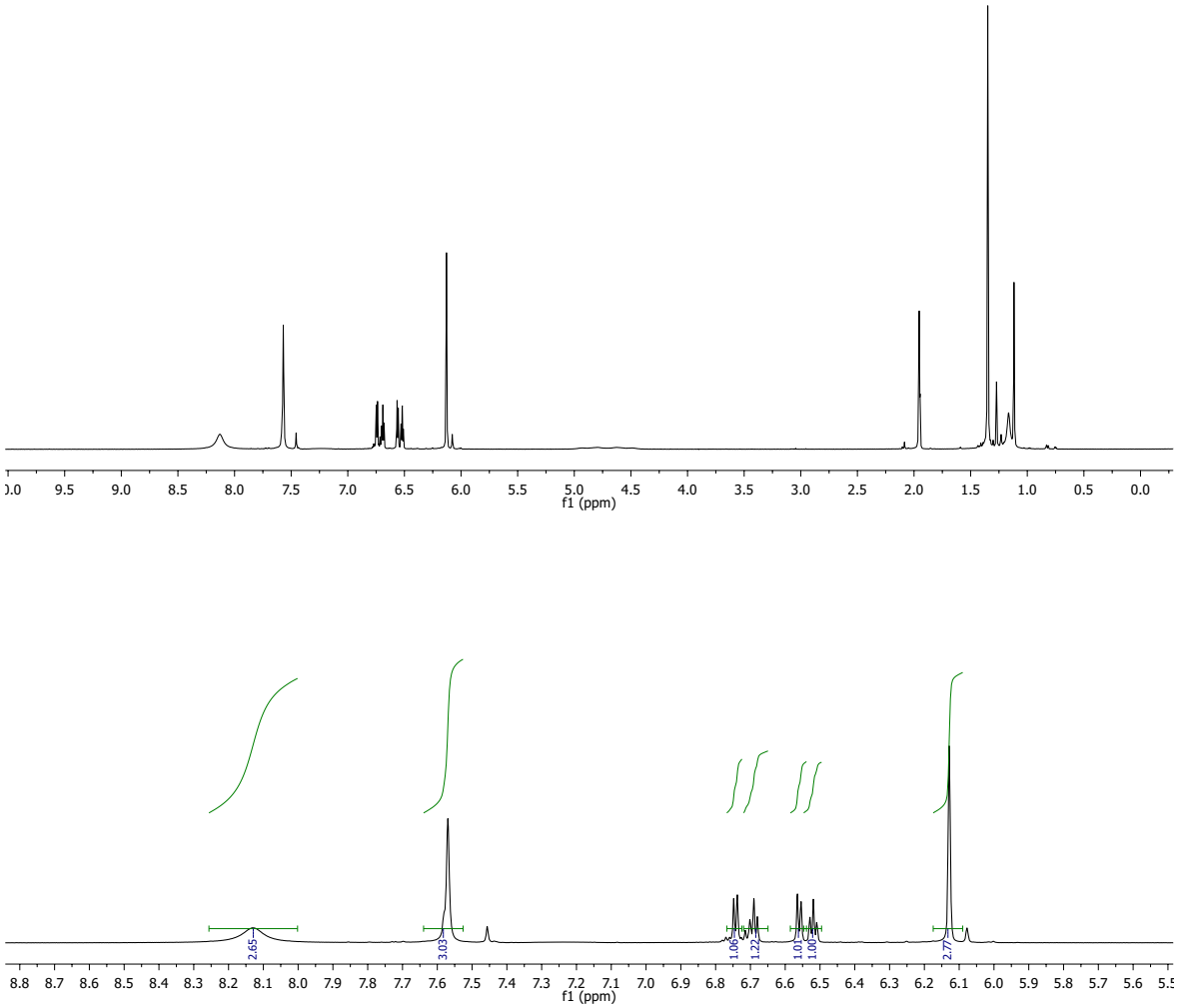

Figure S26. ^{1}H NMR spectra of complex **1-Ni** at 23 ºC in CD_3CN.

^{13}C NMR Spectrum of 1-Ni at 23 ºC (CD_3CN)

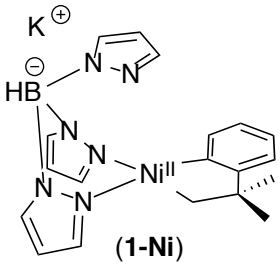

(**1-Ni**)

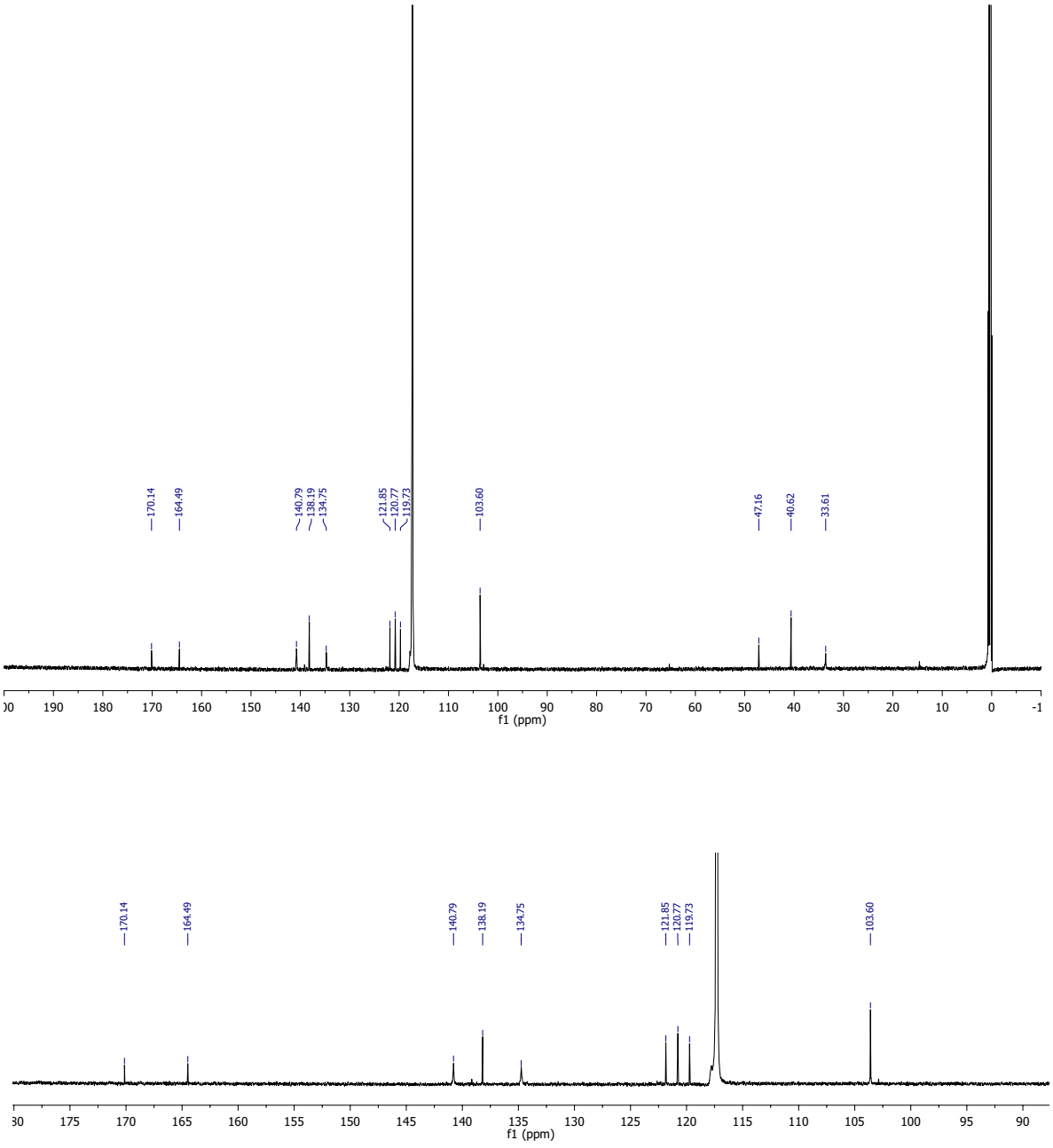

Figure S27. ^{13}C NMR spectra of complex **1-Ni** at 23 ºC in CD_3CN.

^{11}B NMR Spectrum of 1-Ni at 23 ºC (CD_3CN)

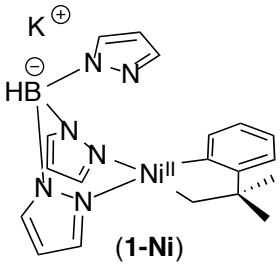

(**1-Ni**)

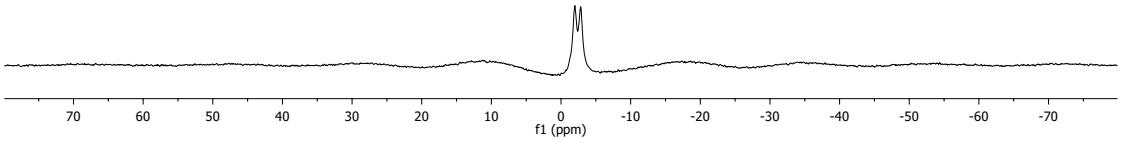

Figure S28. ^{11}B NMR spectrum of complex **1-Ni** at 23 ºC in CD_3CN.

^{1}H NMR Spectrum of 1-Pd at 23 ºC (CD_3CN)

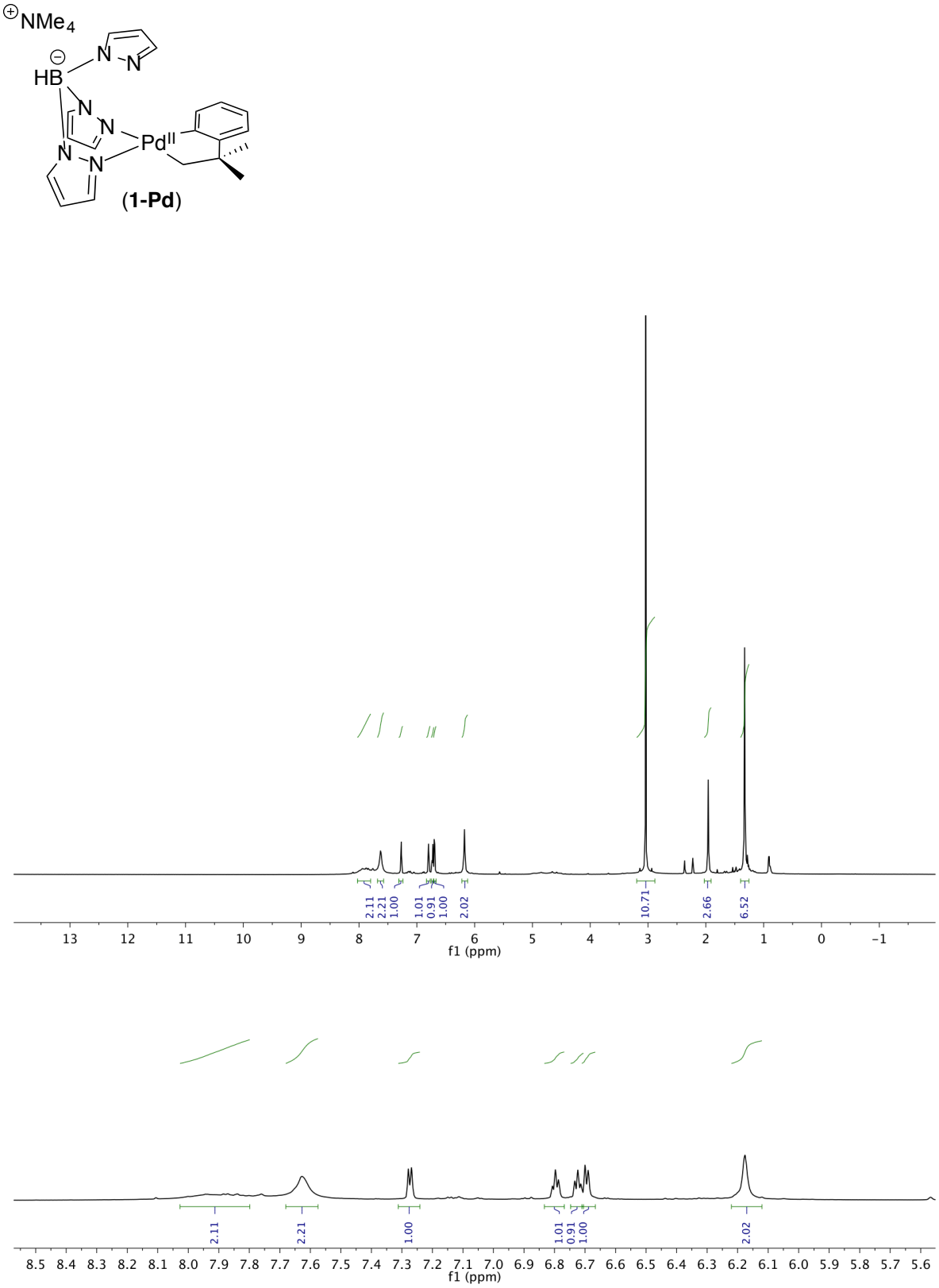

Figure S29. ^{1}H NMR spectra of complex **1-Pd** at 23 ºC in CD_3CN.

^{13}C NMR Spectrum of 1-Pd at 23 ºC (CD_3CN)

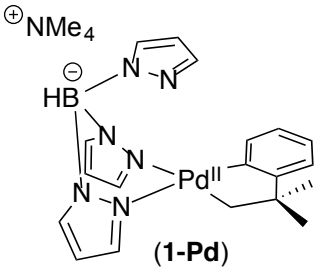

(**1-Pd**)

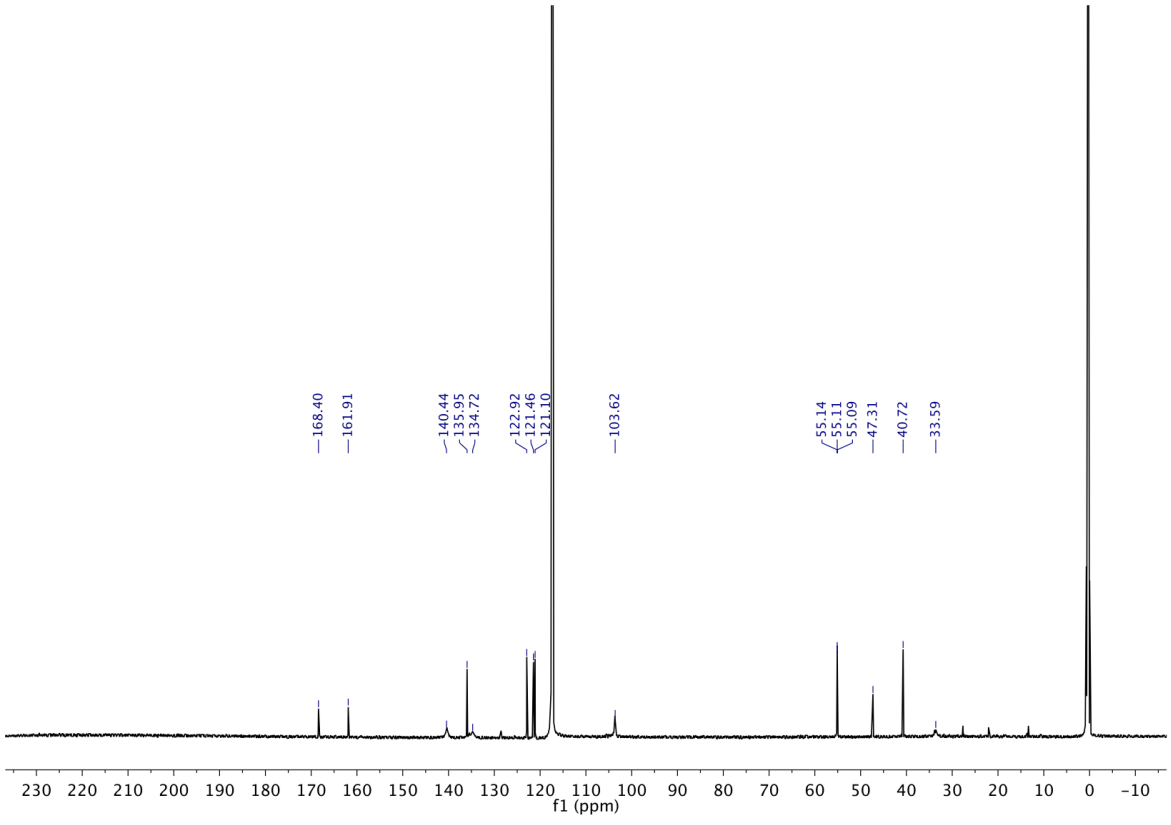

Figure S30. ^{13}C NMR spectrum of complex **1-Pd** at 23 ºC in CD_3CN.

^{11}B NMR Spectrum of 1-Pd at 23 ºC (CD_3CN)

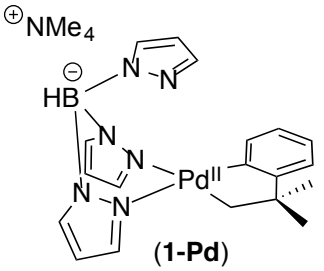

(**1-Pd**)

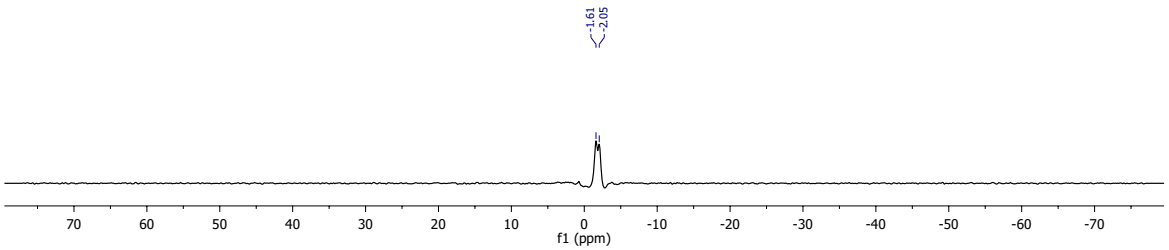

Figure S31. ^{11}B NMR spectrum of complex **1-Pd** at 23 ºC in CD_3CN.

^{1}H NMR Spectrum of 3-Ni at 23 ºC (CD_3CN)

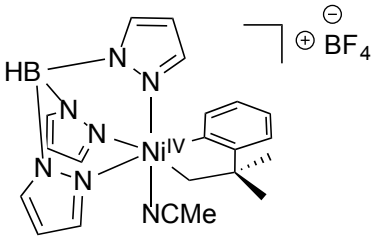

(**3-Ni**)

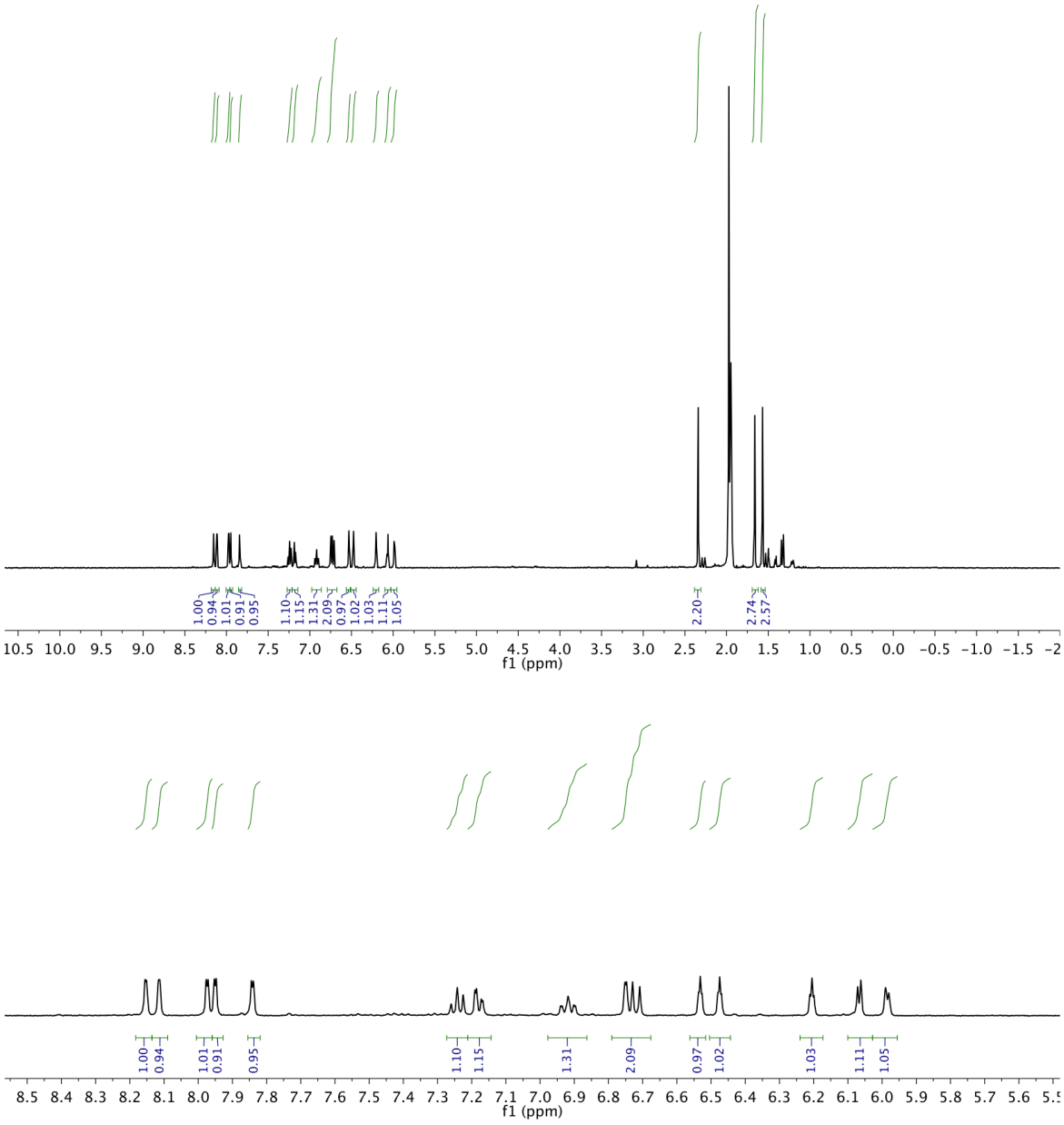

Figure S32. ^{1}H NMR spectra of complex **3-Ni** at 23 ºC in CD_3CN.

^{13}C NMR Spectrum of 3-Ni at 0 ºC (CD_3CN)

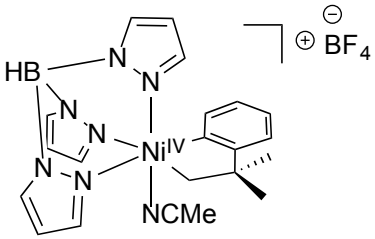

(**3-Ni**)

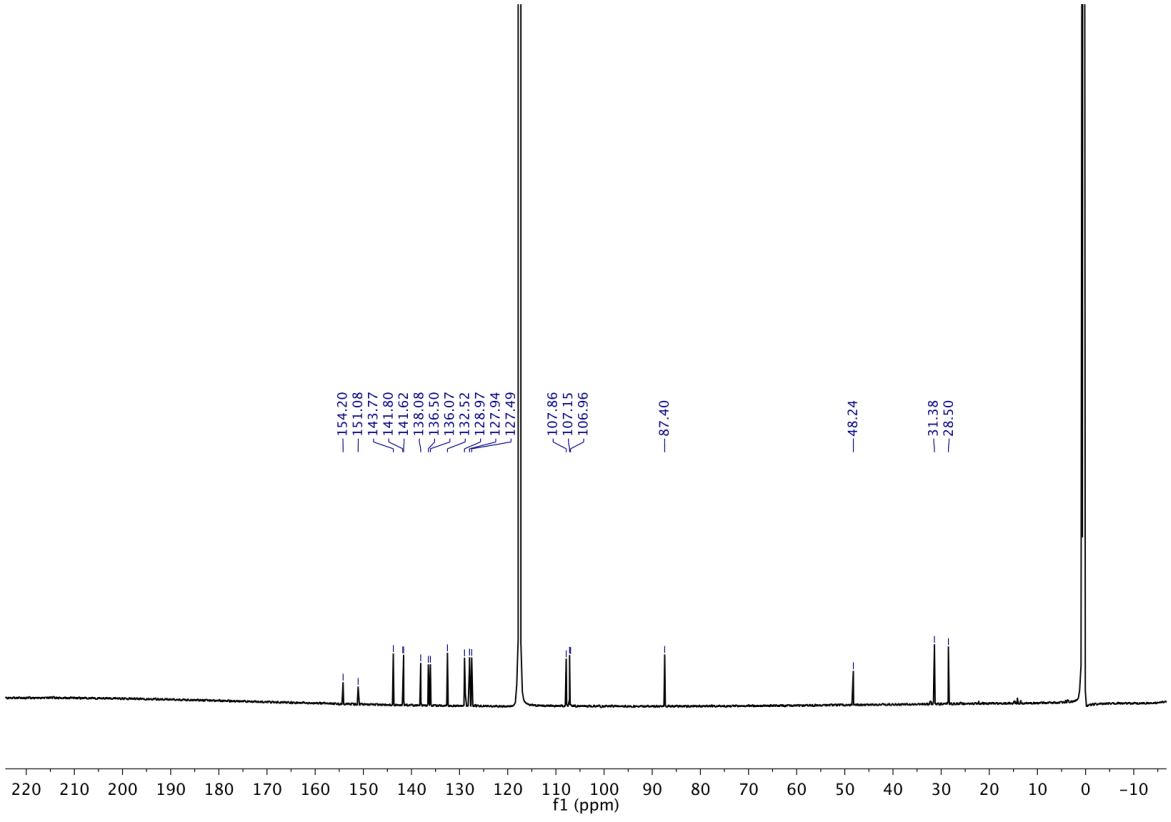

Figure S33. ^{13}C NMR spectrum of complex **3-Ni** at 0 ºC in CD_3CN.

^{11}B NMR Spectrum of 3-Ni at 23 ºC (CD_3CN)

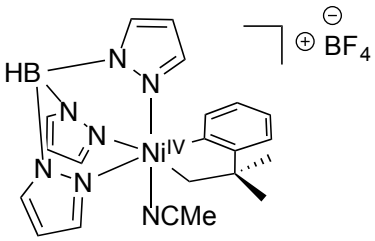

(**3-Ni**)

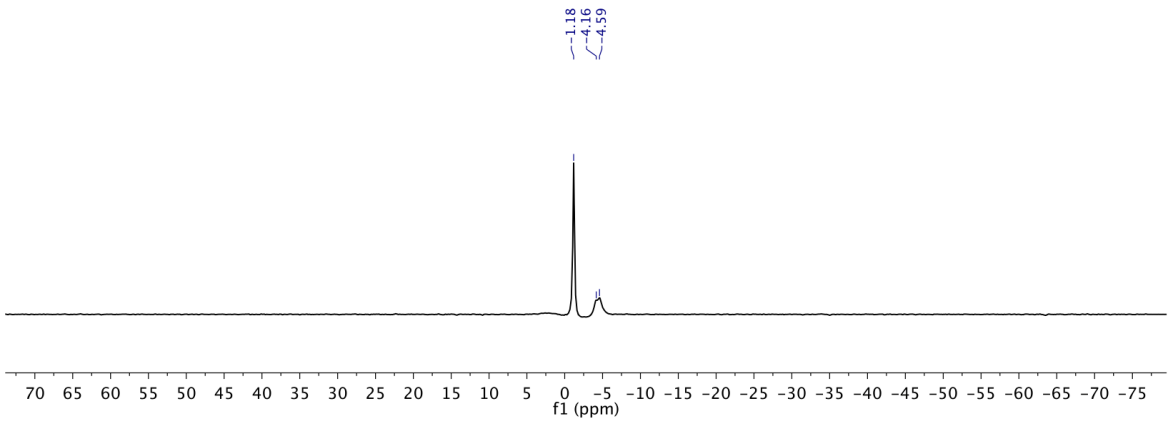

Figure S34. ^{11}B NMR spectrum of complex **3-Ni** at 23 ºC in CD_3CN.

^{19}F NMR Spectrum of 3-Ni at 23 ºC (CD_3CN)

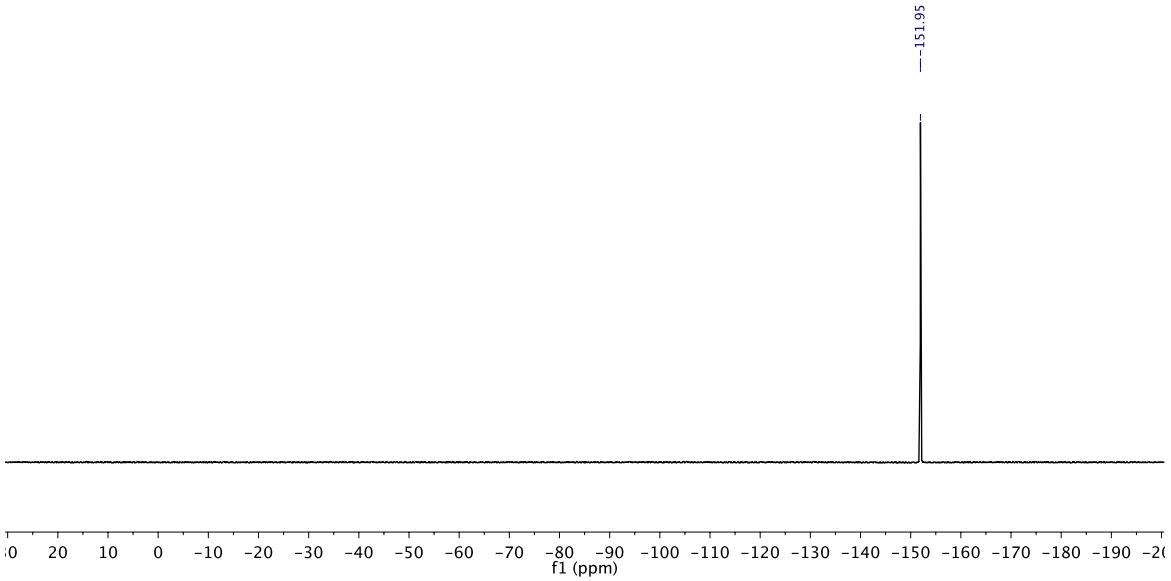

Figure S35. ^{19}F NMR spectrum of complex **3-Ni** at 23 ºC in CD_3CN.

^{1}H NMR Spectrum of 4-Ni at 23 ºC (CD_3CN)

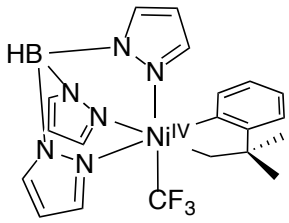

(**4-Ni**)

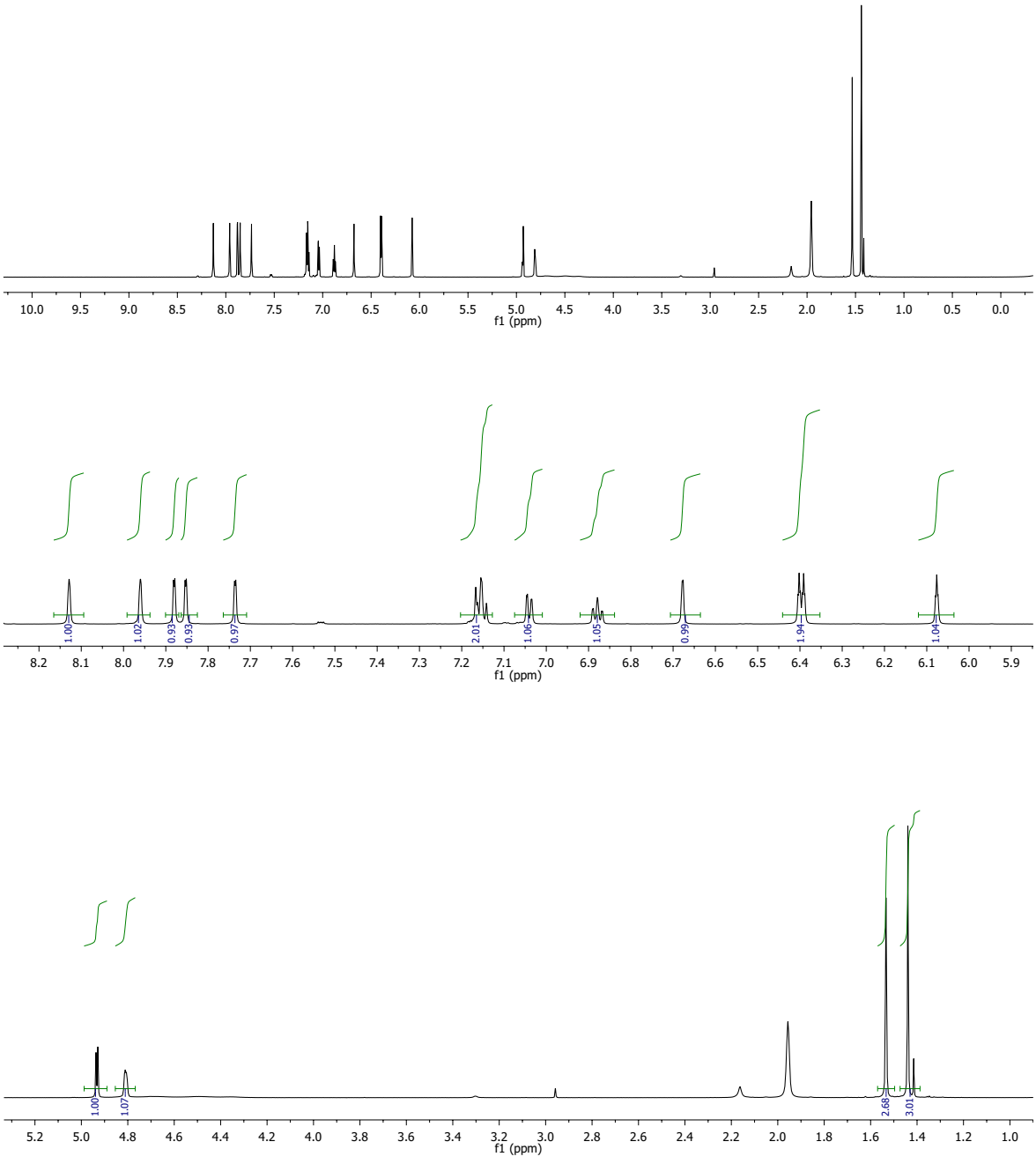

Figure S36. ^{1}H NMR spectra of complex **4-Ni** at 23 ºC in CD_3CN.

^{13}C NMR Spectrum of 4-Ni at 23 ºC (CD_3CN)

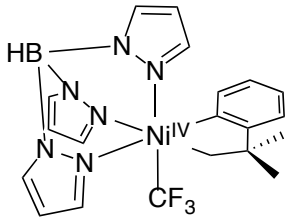

(**4-Ni**)

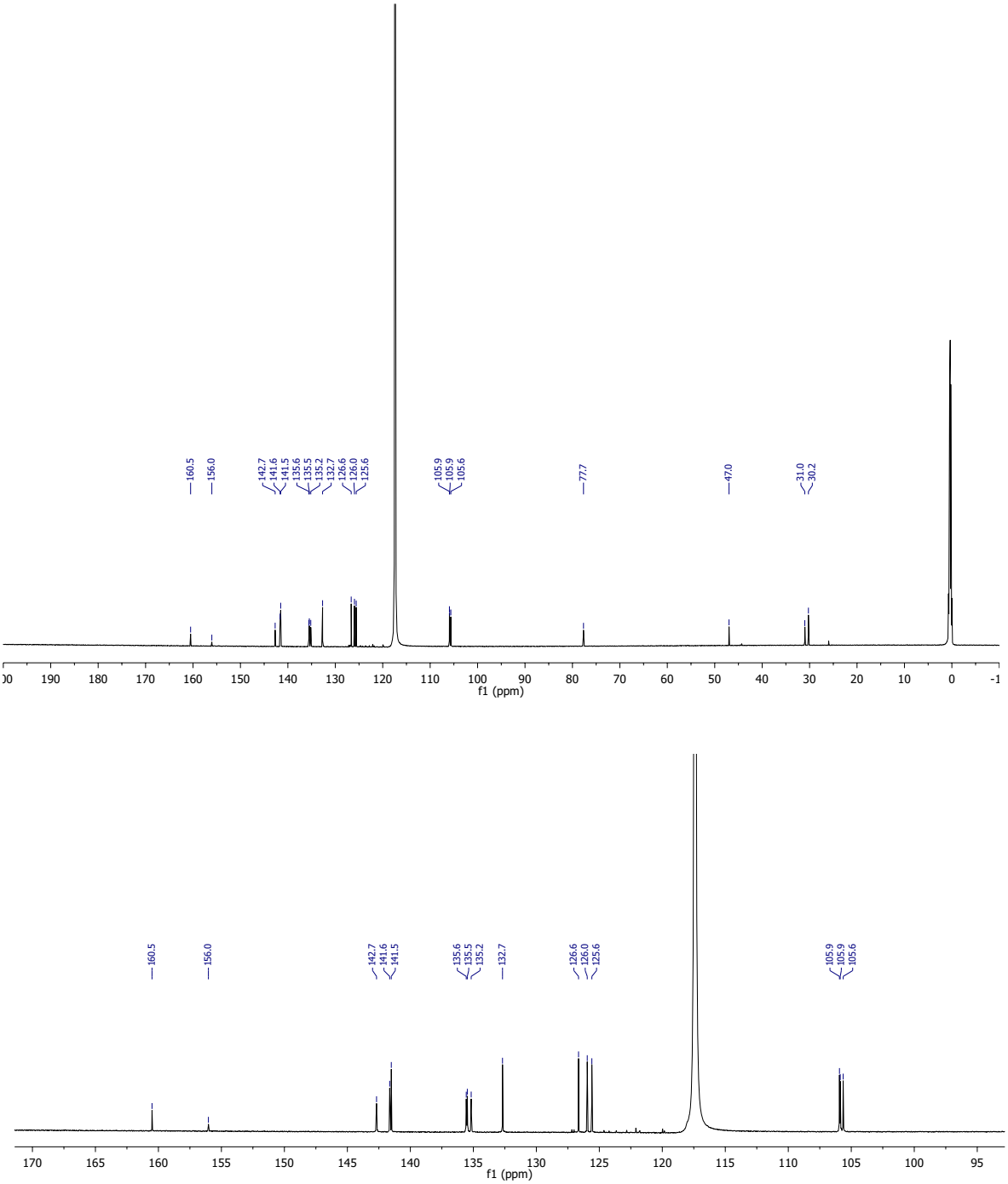

Figure S37. ^{13}C NMR spectrum of complex **4-Ni** at 23 ºC in CD_3CN.

^{19}F NMR Spectrum of 4-Ni at 23 ºC (CD_3CN)

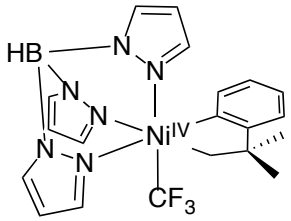

(**4-Ni**)

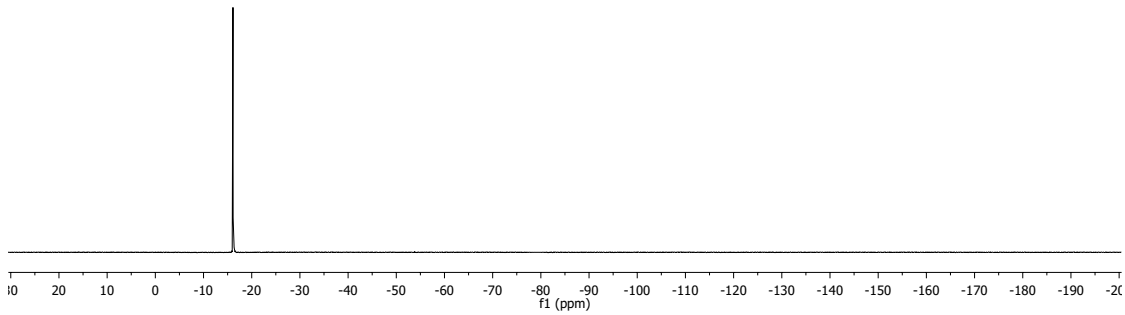

Figure S38. ^{19}F NMR spectrum of complex **4-Ni** at 23 ºC in CD_3CN.

^{11}B NMR Spectrum of 4-Ni at 23 ºC (CD_3CN)

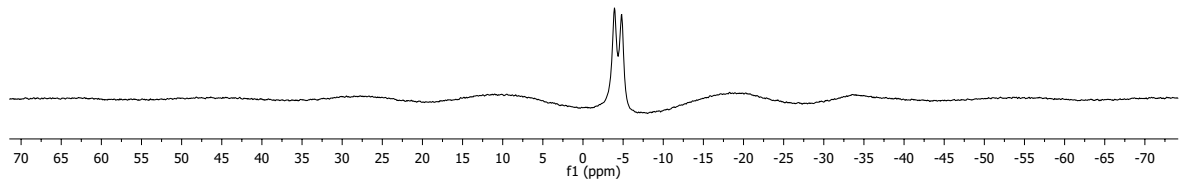

Figure S39. ^{11}B NMR spectrum of complex **4-Ni** at 23 ºC in CD_3CN.

$^{19}F–^{13}C$ HMBC Spectrum of 4-Ni at 23 °C (CD_3CN)

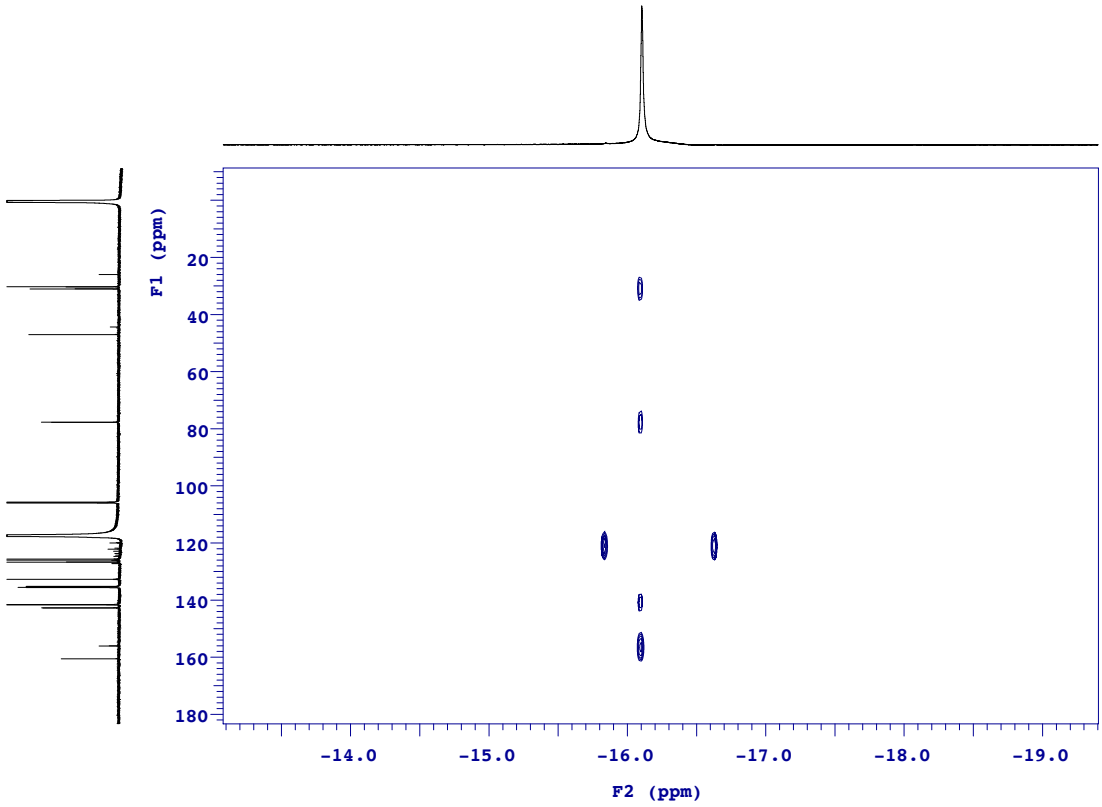

Figure S40. $^{19}F–^{13}C$ HMBC spectrum of complex **4-Ni** at 23 °C in CD_3CN.

^{1}H NMR Spectrum of 4-Pd at 23 ºC (CD_3CN)

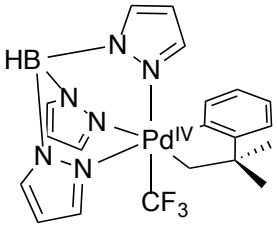

(**4-Pd**)

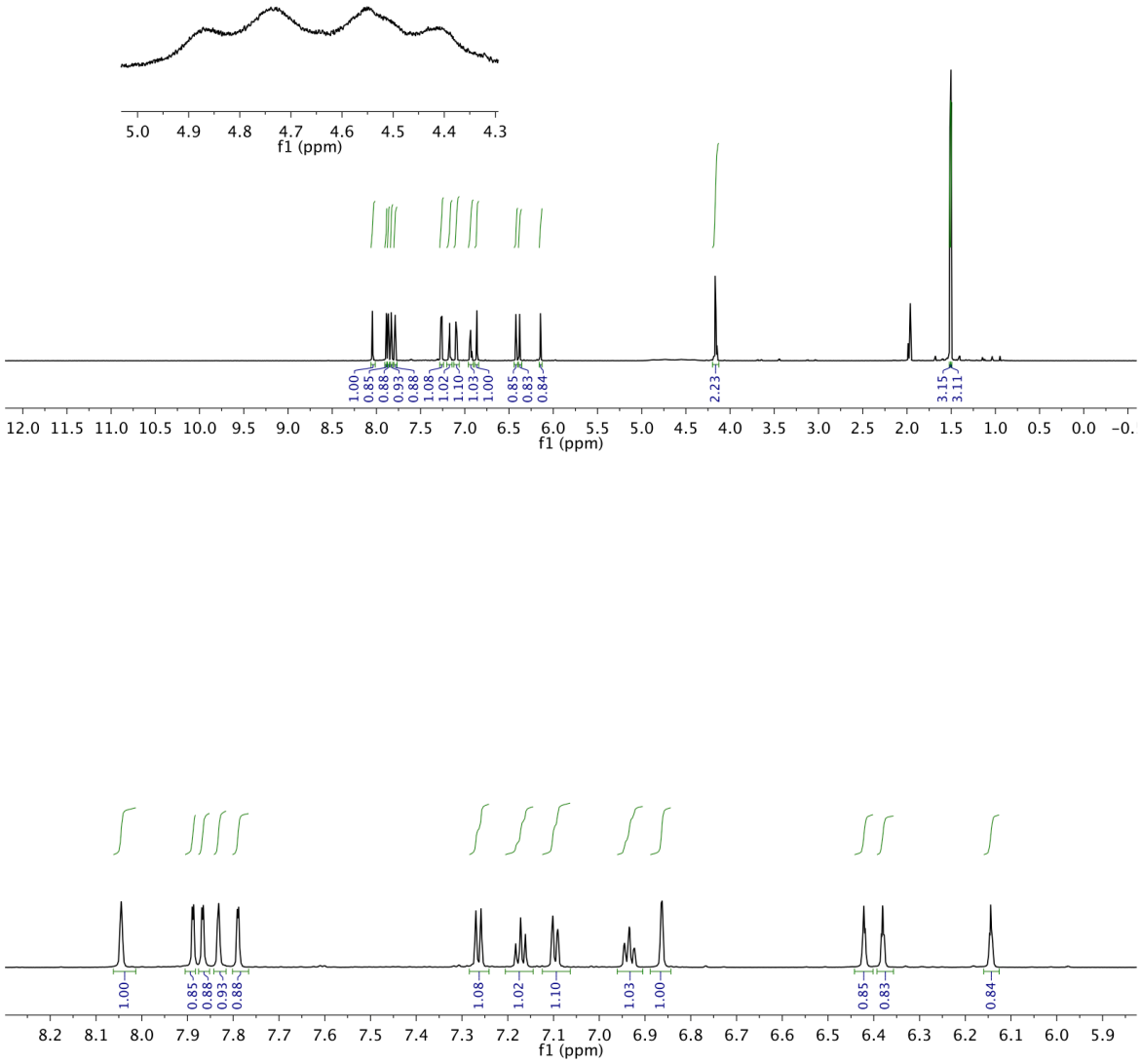

Figure S41. ^{1}H NMR spectra of complex **4-Pd** at 23 ºC in CD_3CN.

^{13}C NMR Spectrum of 4-Pd at 23 ºC (CD_3CN)

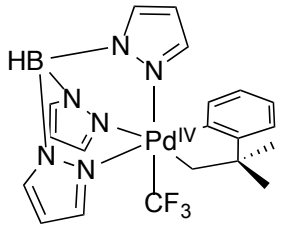

(**4-Pd**)

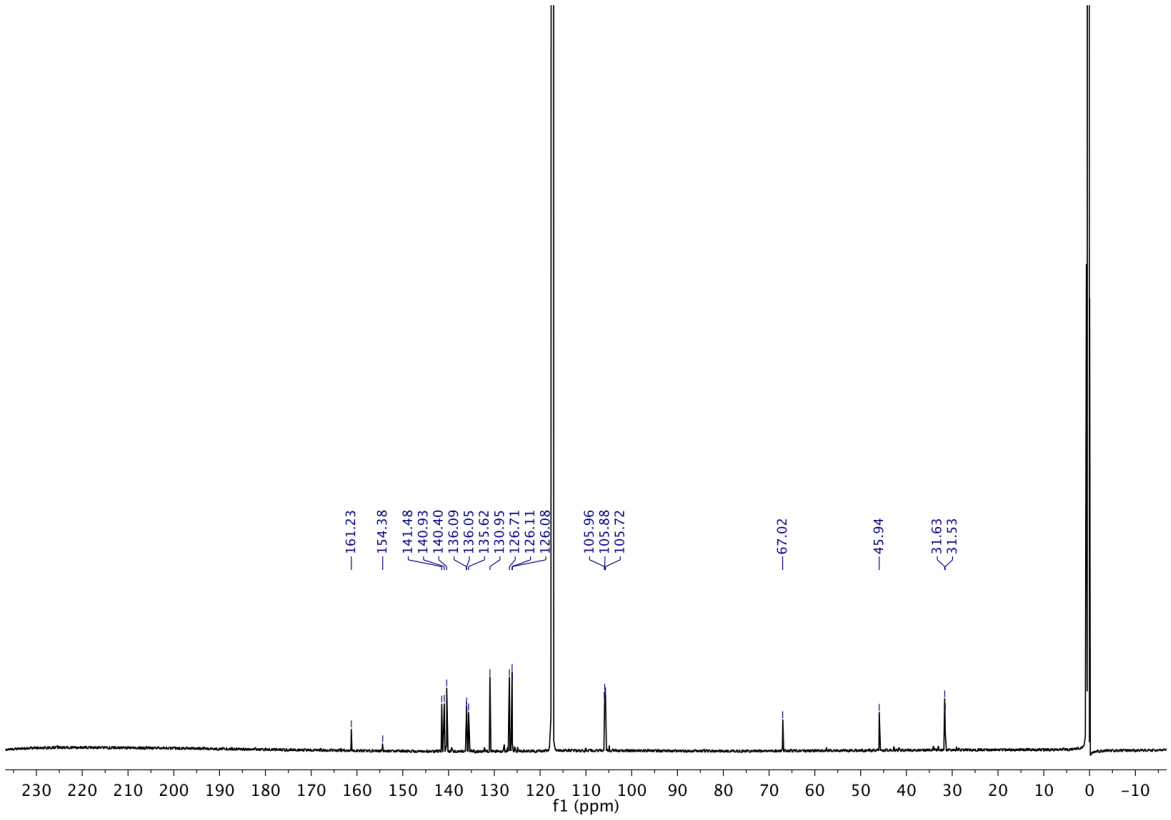

Figure S42. ^{13}C NMR spectrum of complex **4-Pd** at 23 ºC in CD_3CN.

^{11}B NMR Spectrum of 4-Pd at 23 °C (CD_3CN)

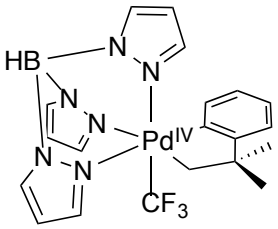

(**4-Pd**)

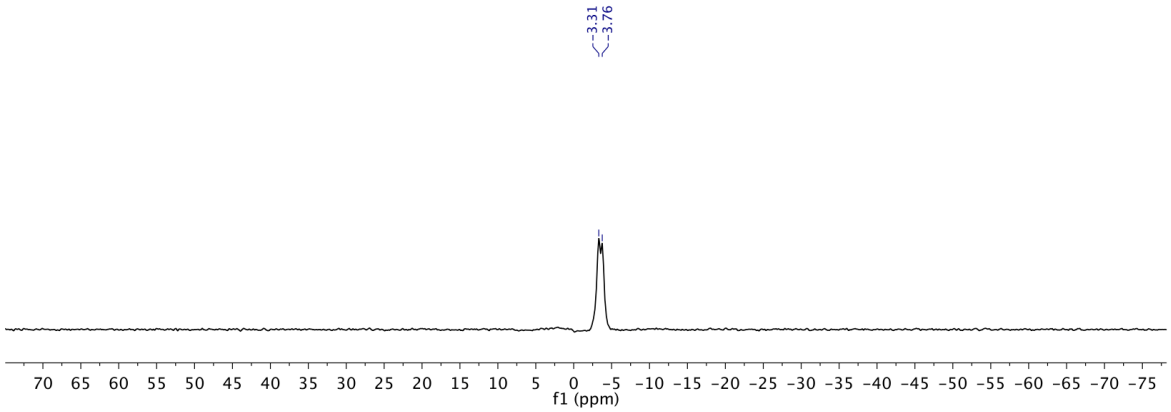

Figure S43. ^{11}B NMR spectrum of complex **4-Pd** at 23 °C in CD_3CN.

^{19}F NMR Spectrum of 4-Pd at 23 °C (CD_3CN)

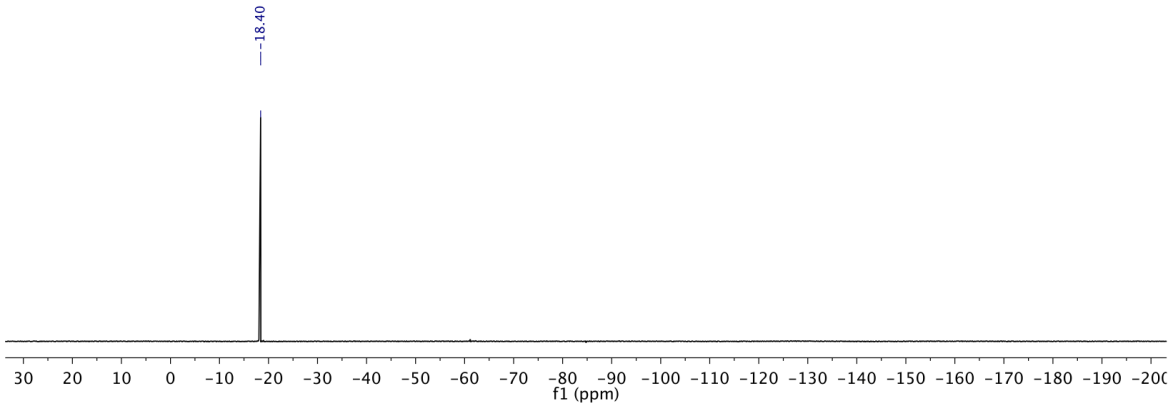

Figure S44. ^{19}F NMR spectrum of complex **4-Pd** at 23 °C in CD_3CN.

$^{19}F–^{13}C$ HMBC Spectrum of 4-Pd at 23 ºC (CD_3CN)

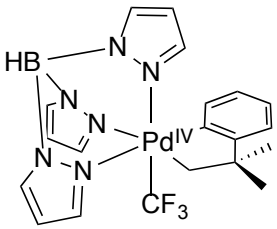

(**4-Pd**)

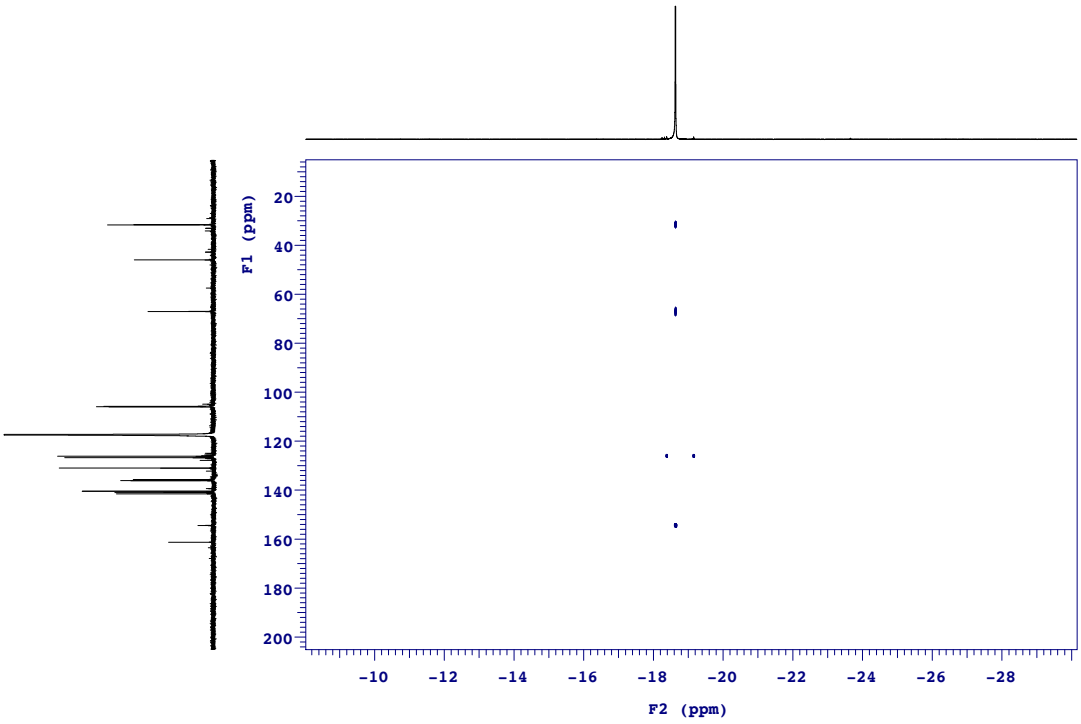

Figure S45. $^{19}F–^{13}C$ HMBC spectrum of complex **4-Pd** at 23 ºC in CD_3CN.

^{1}H NMR Spectrum of 6a-Pd at 23 ºC (CD_3CN)

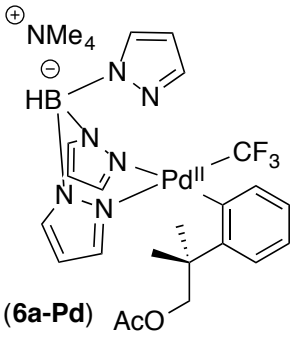

(**6a-Pd**)

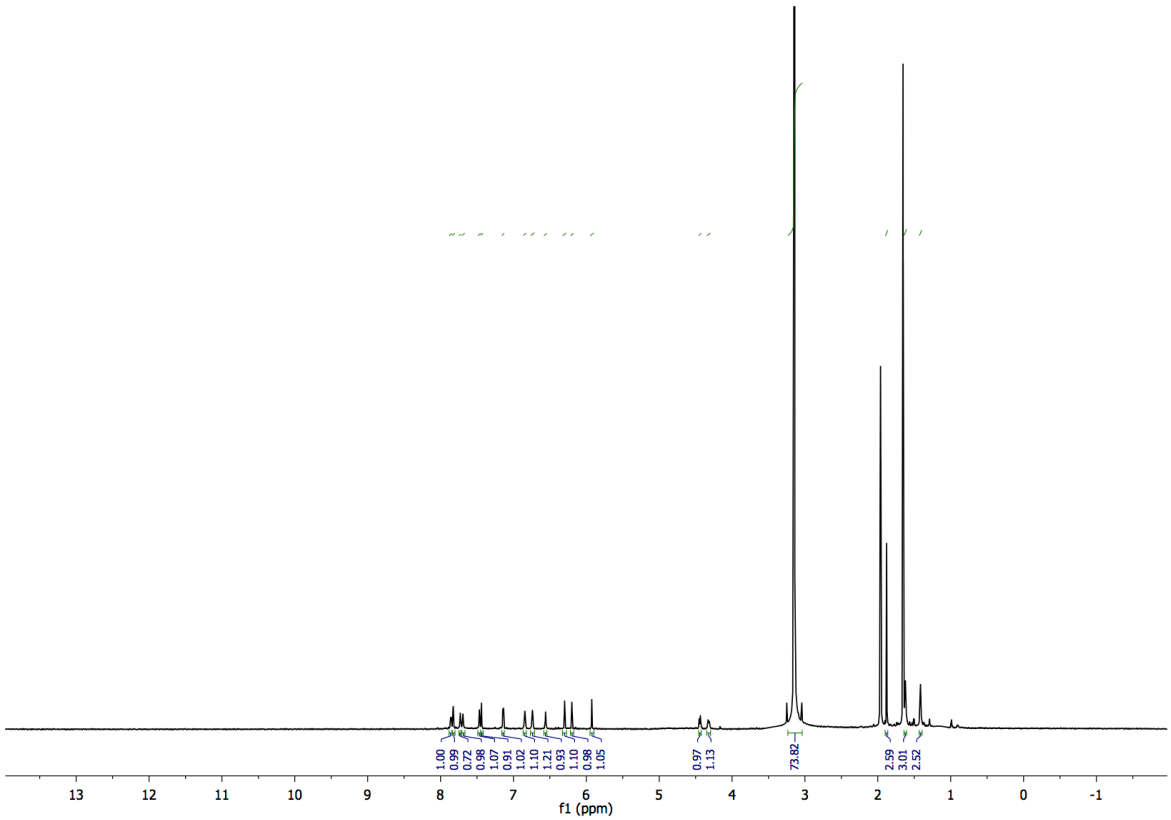

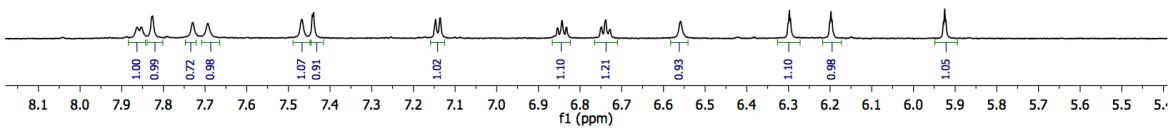

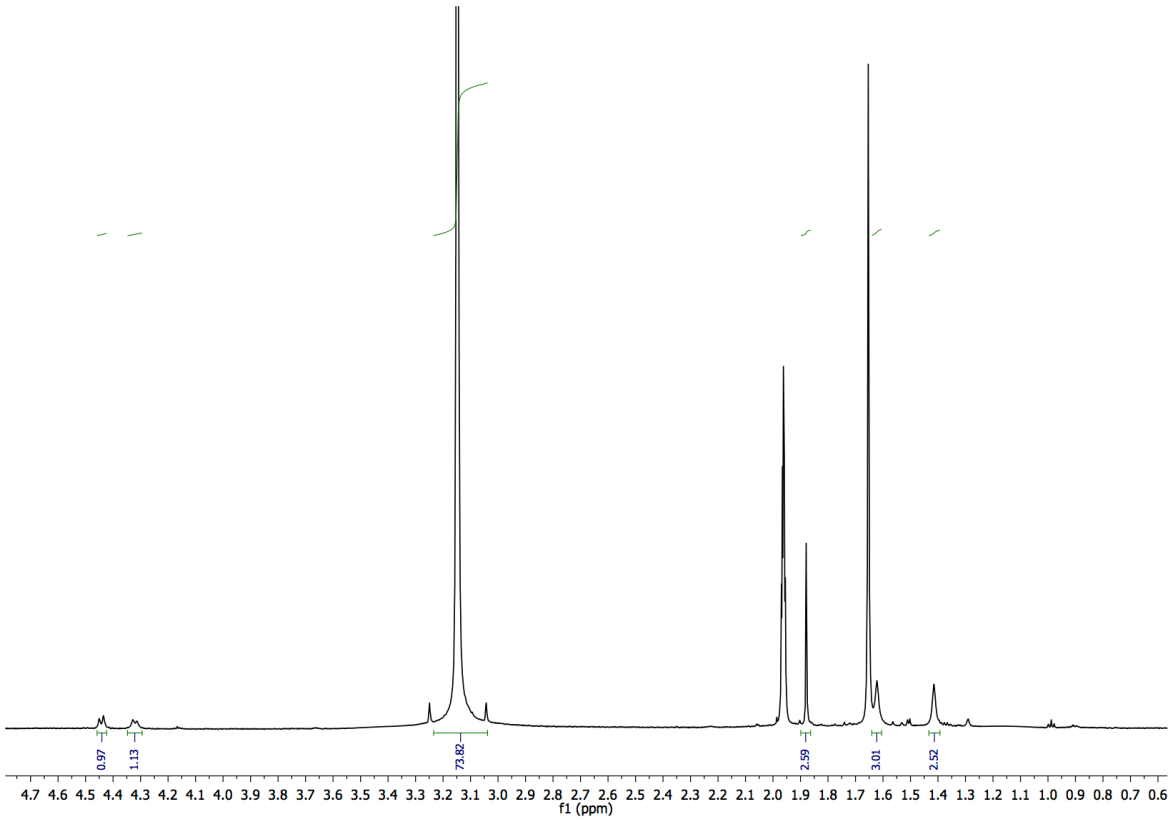

Figure S46. ^{1}H NMR spectra of complex **6a-Pd** at 23 ºC in CD_3CN.

^{13}C NMR Spectrum of 6a-Pd at 23 ºC (CD_3CN)

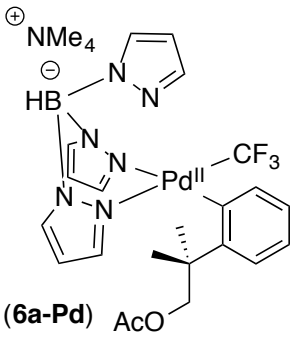

(**6a-Pd**)

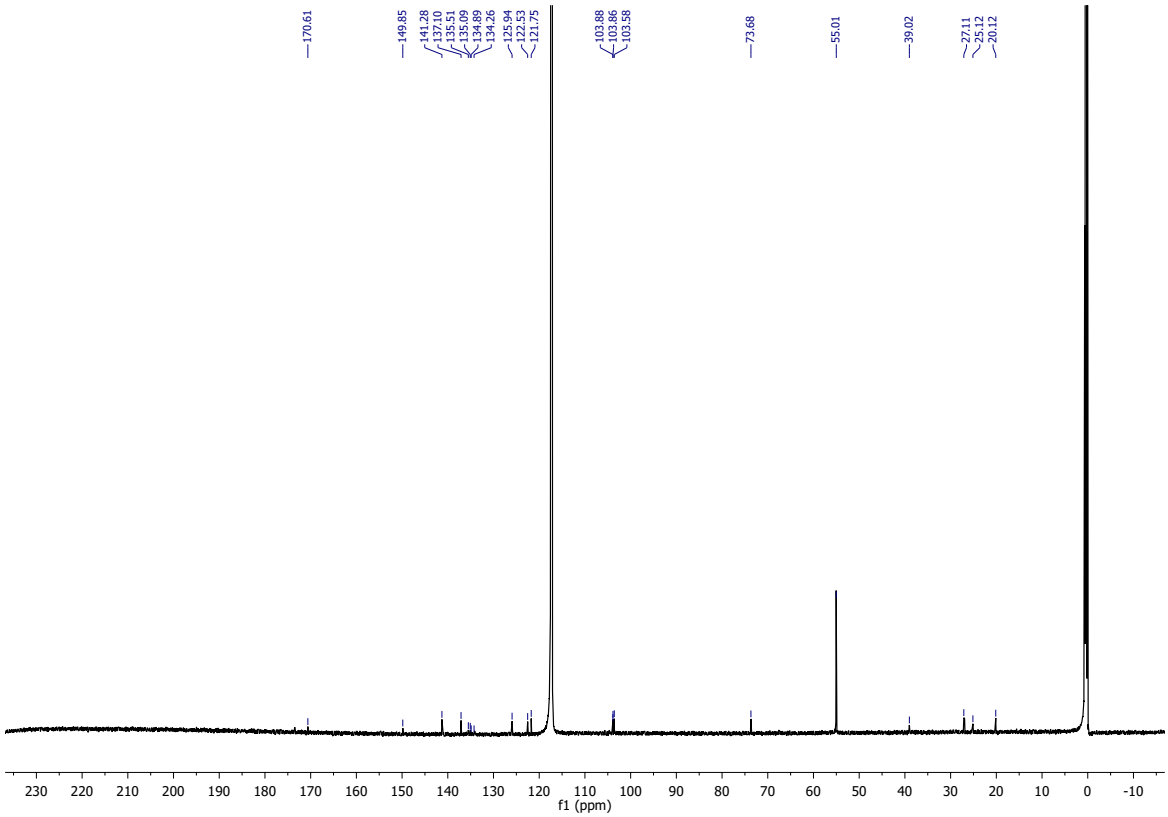

Figure S47. ^{13}C NMR spectrum of complex **6a-Pd** at 23 ºC in CD_3CN.

^{11}B NMR Spectrum of 6a-Pd at 23 ºC (CD_3CN)

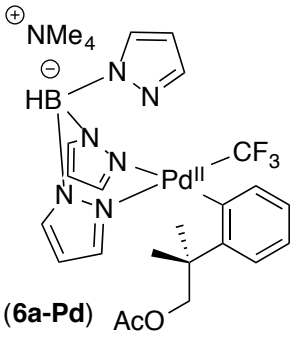

(**6a-Pd**)

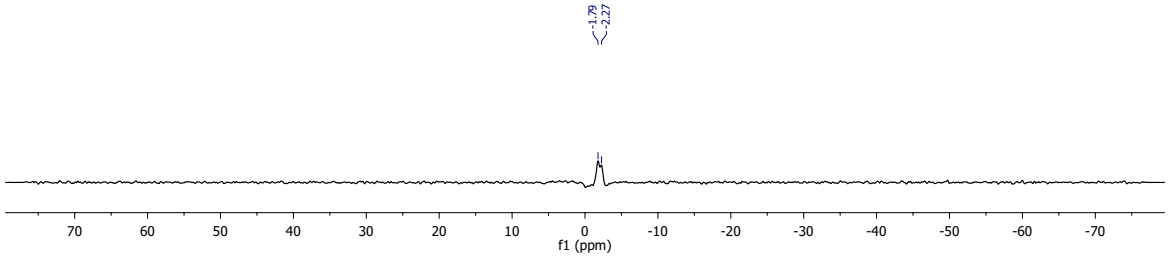

Figure S48. ^{11}B NMR spectrum of complex **6a-Pd** at 23 ºC in CD_3CN.

^{19}F NMR Spectrum of 6a-Pd at 23 ºC (CD_3CN)

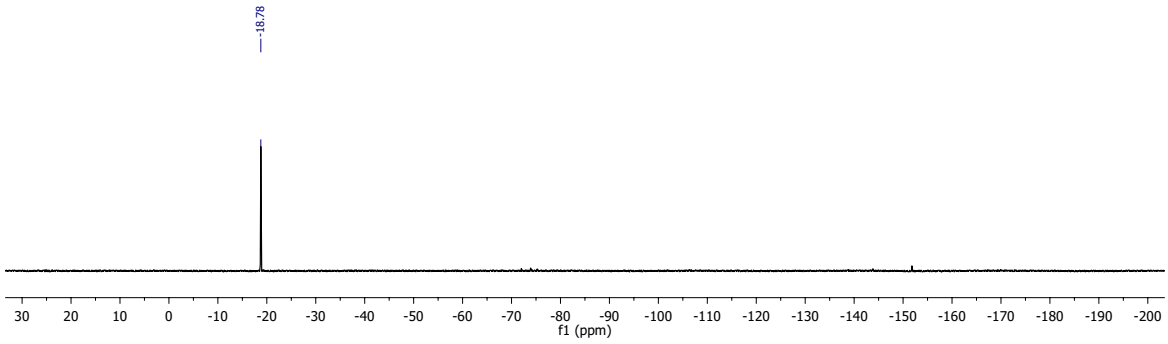

Figure S49. ^{19}F NMR spectrum of complex **6a-Pd** at 23 ºC in CD_3CN.

$^{19}F–^{13}C$ HMBC Spectrum of 6a-Pd at 23 ºC (CD_3CN)

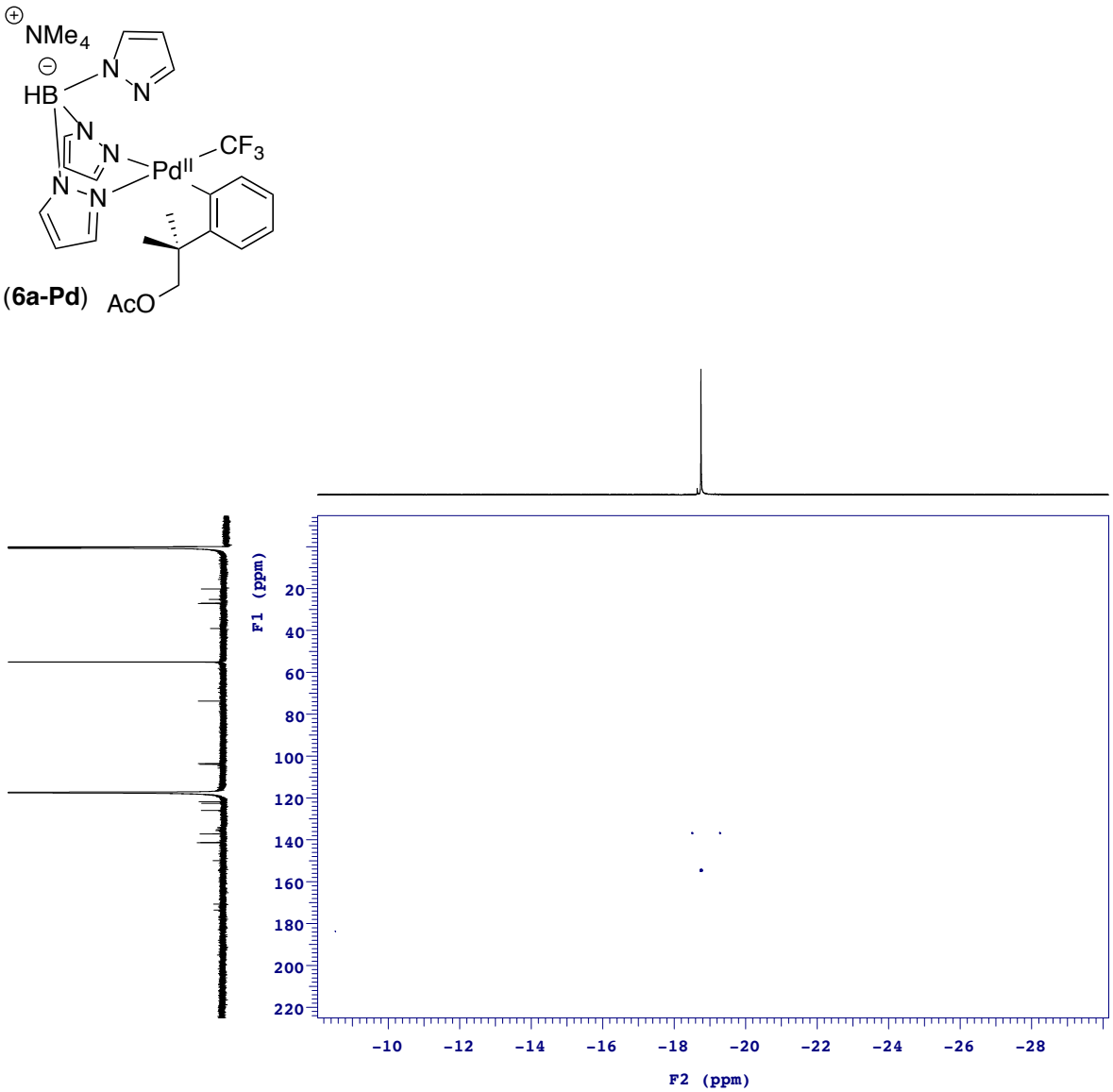

Figure S50. $^{19}F–^{13}C$ HMBC NMR spectrum of complex **6a-Pd** at 23 ºC in CD_3CN.

^{1}H NMR Spectrum of 6b-Pd at 23 ºC (CD_3CN)

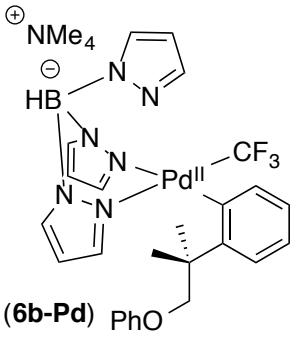

(**6b-Pd**)

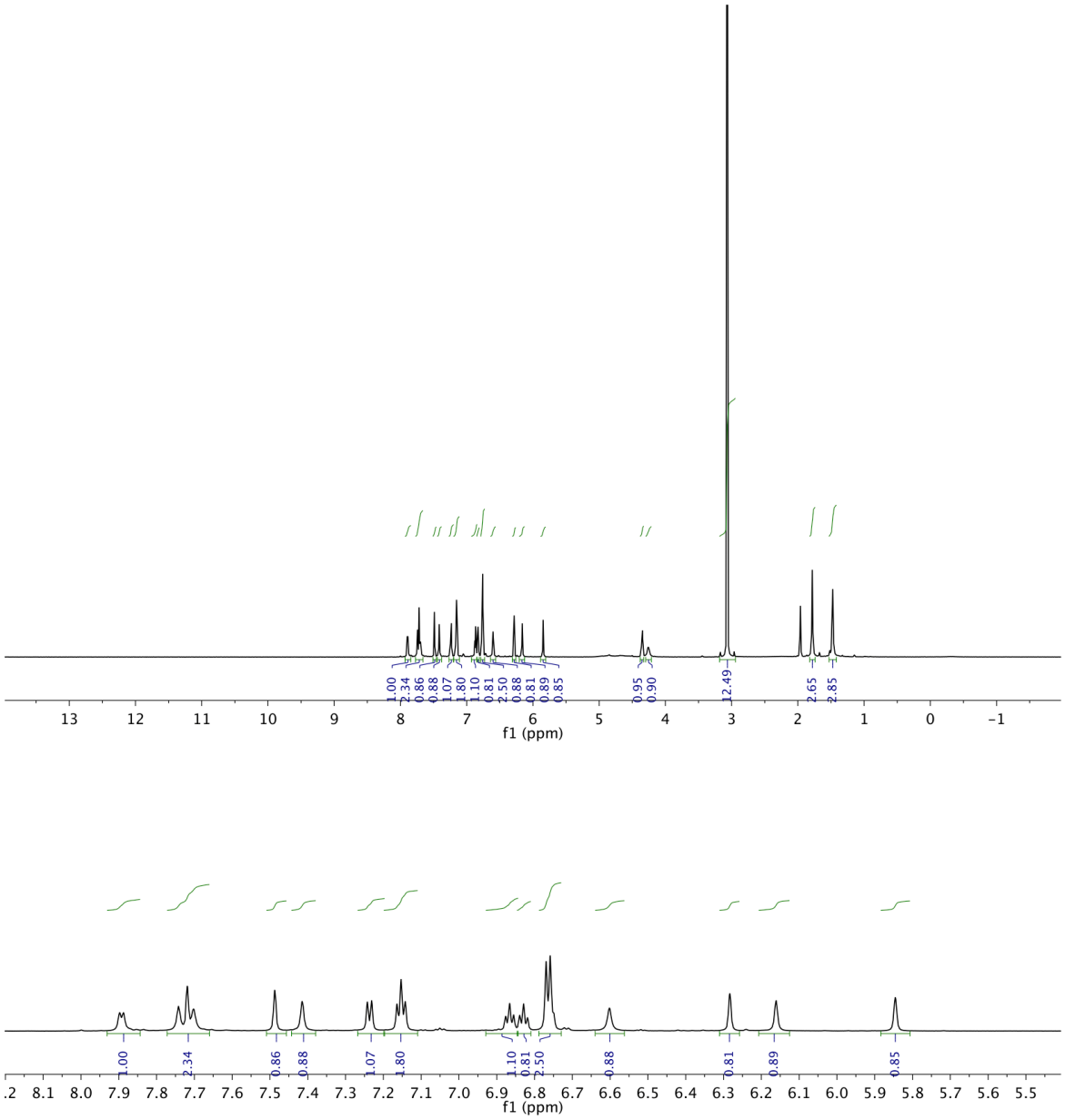

Figure S51. ^{1}H NMR spectra of complex **6b-Pd** at 23 ºC in CD_3CN.

^{13}C NMR Spectrum of 6b-Pd at 23 ºC (CD_3CN)

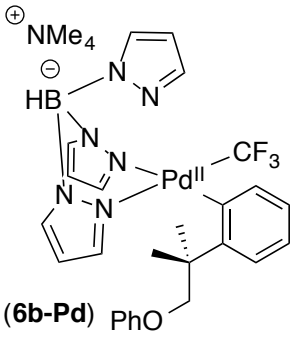

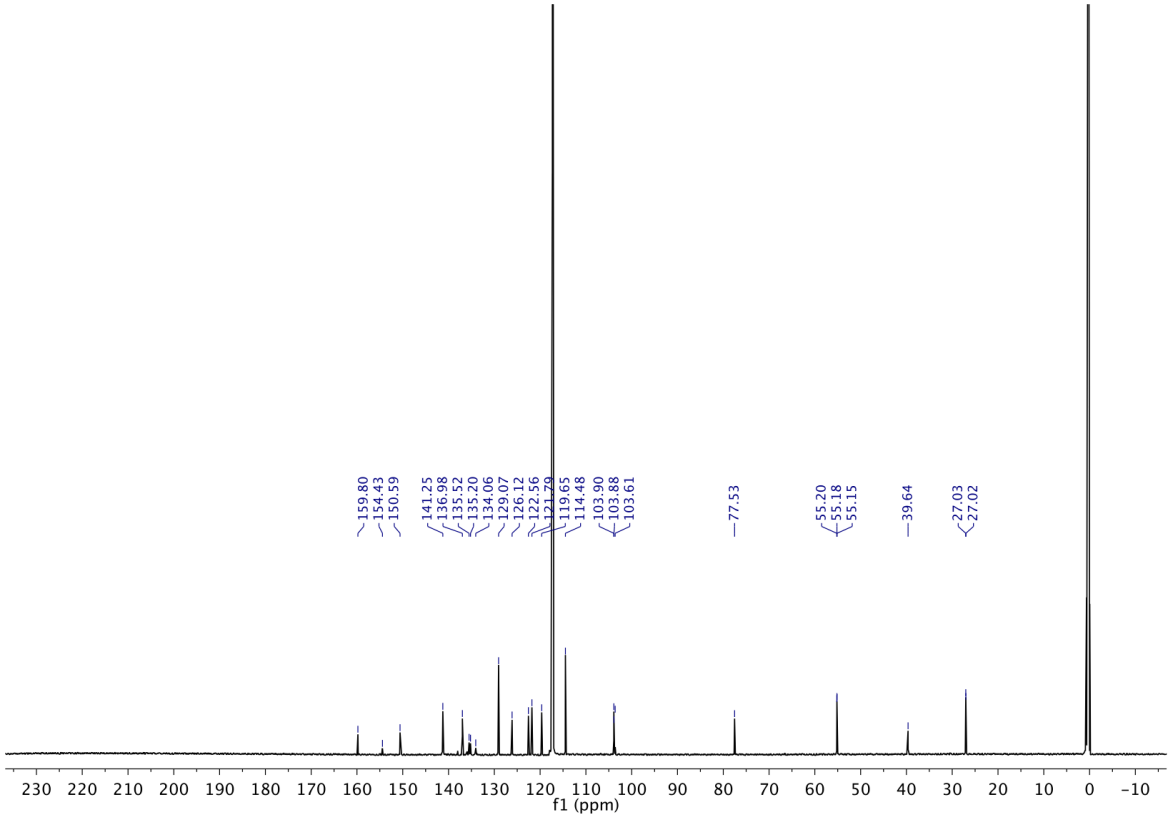

Figure S52. ^{13}C NMR spectra of complex **6b-Pd** at 23 ºC in CD_3CN.

^{11}B NMR Spectrum of 6b-Pd at 23 ºC (CD_3CN)

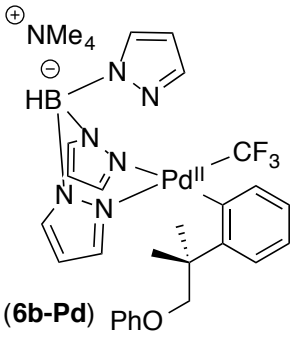

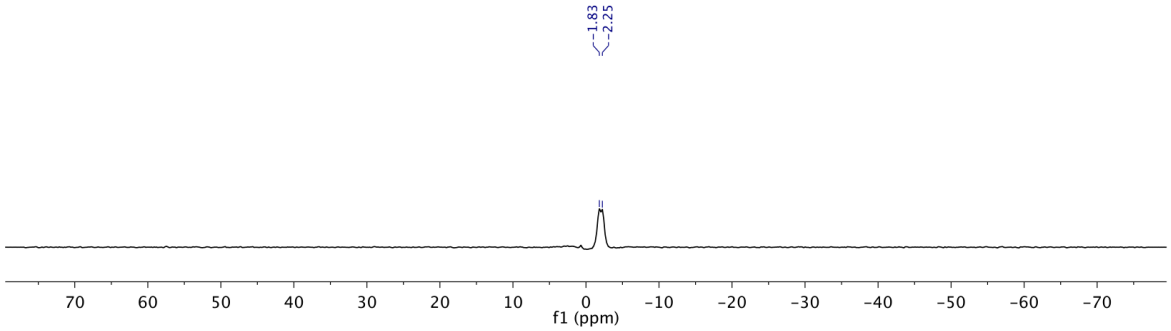

Figure S53. ^{11}B NMR spectrum of complex **6b-Pd** at 23 ºC in CD_3CN.

^{19}F NMR Spectrum of 6b-Pd at 23 ºC (CD_3CN)

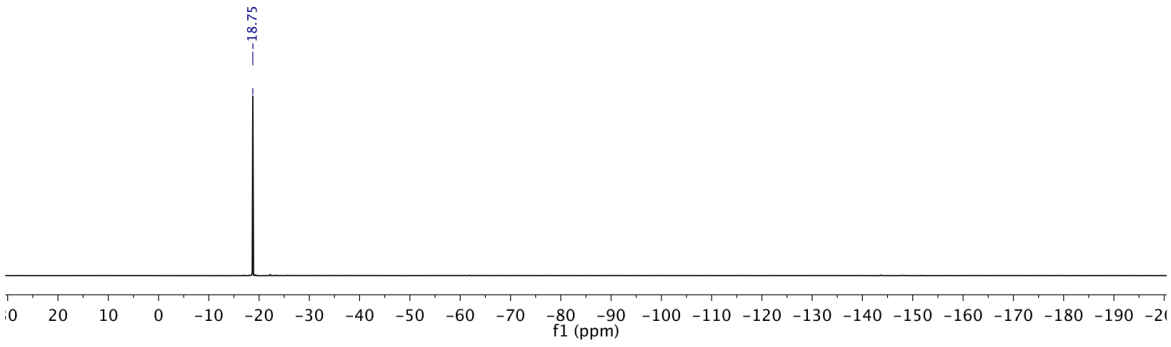

Figure S54. ^{19}F NMR spectrum of complex **6b-Pd** at 23 ºC in CD_3CN.

$^{19}F–^{13}C$ HMBC Spectrum of 6b-Pd at 23 °C (CD_3CN)

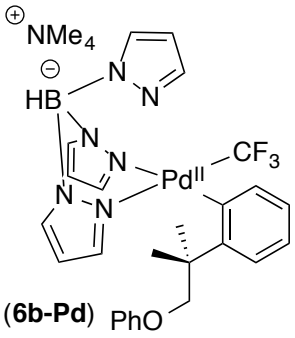

(**6b-Pd**)

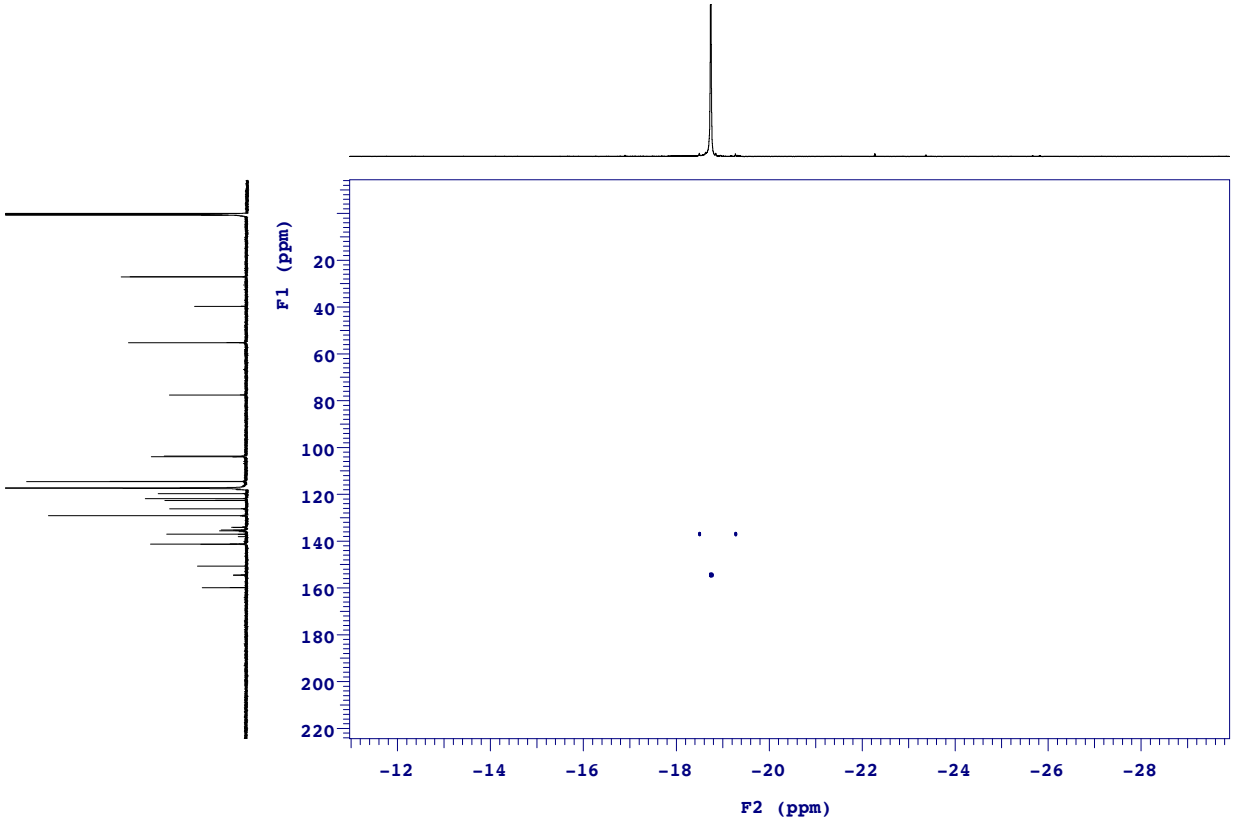

Figure S55. $^{19}F–^{13}C$ HMBC NMR spectrum of complex **6b-Pd** at 23 °C in CD_3CN.

^{1}H NMR Spectrum of 6c-Pd at 23 ºC (CD_3CN)

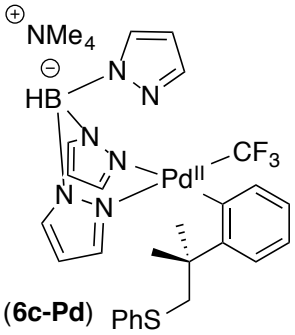

(**6c-Pd**)

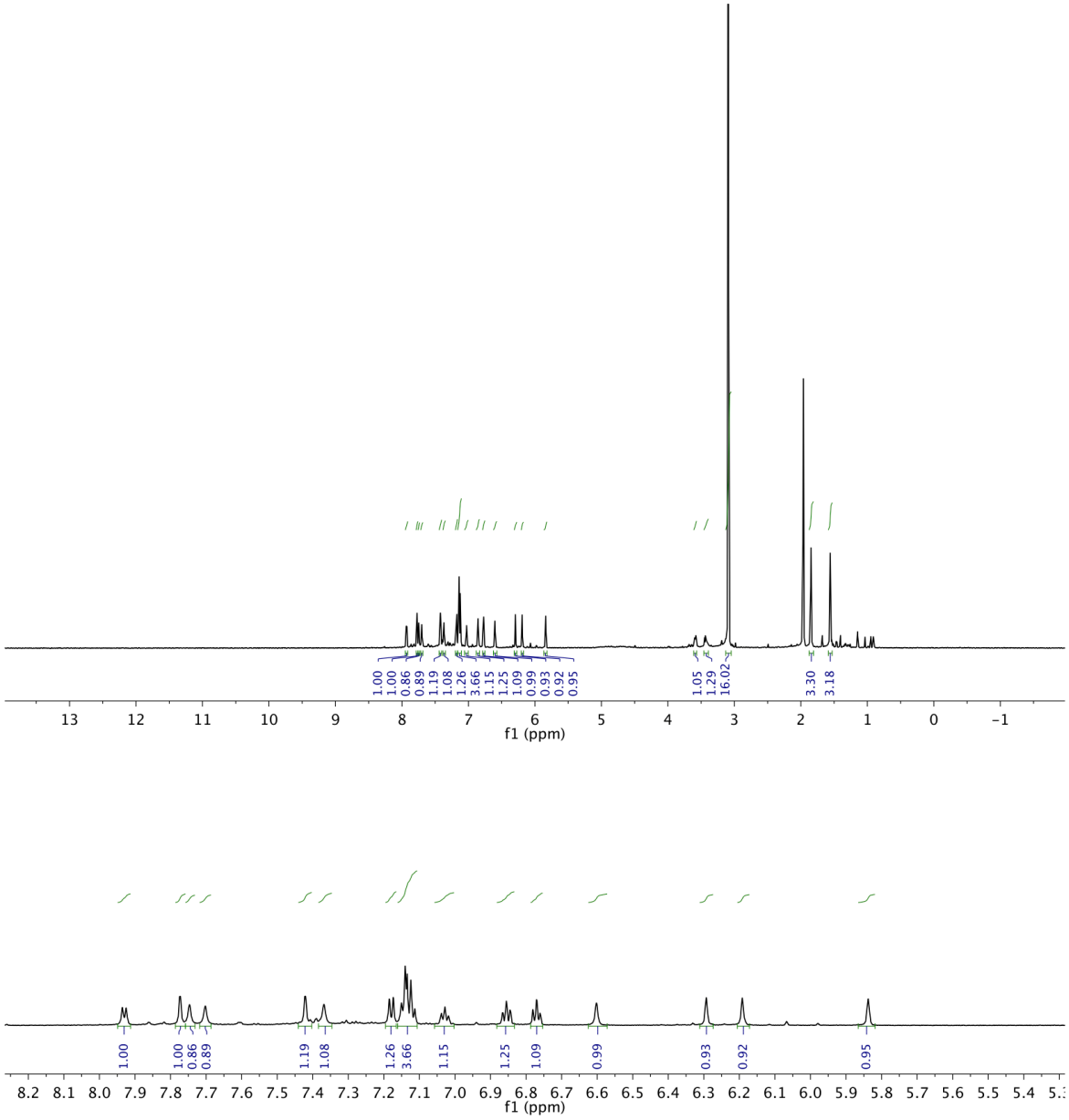

Figure S56. ^{1}H NMR spectra of complex **6c-Pd** at 23 ºC in CD_3CN.

^{13}C NMR Spectrum of 6c-Pd at 23 ºC (CD_3CN)

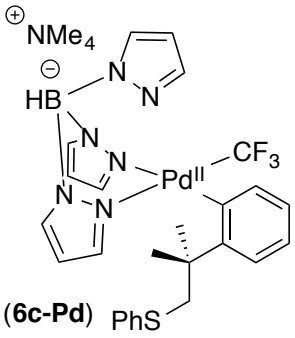

(**6c-Pd**)

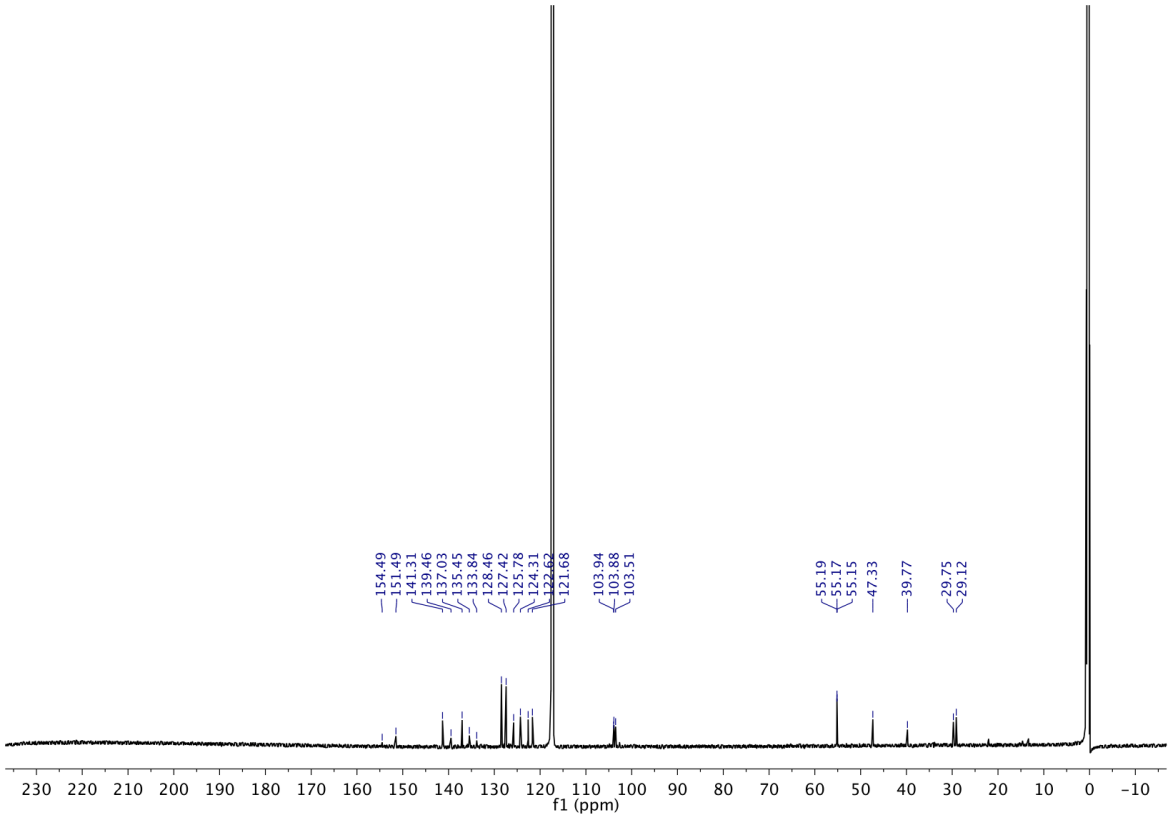

Figure S57. ^{13}C NMR spectra of complex **6c-Pd** at 23 ºC in CD_3CN.

^{11}B NMR Spectrum of 6c-Pd at 23 °C (CD_3CN)

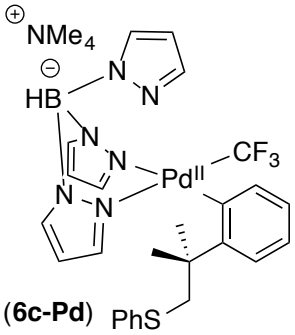

(**6c-Pd**)

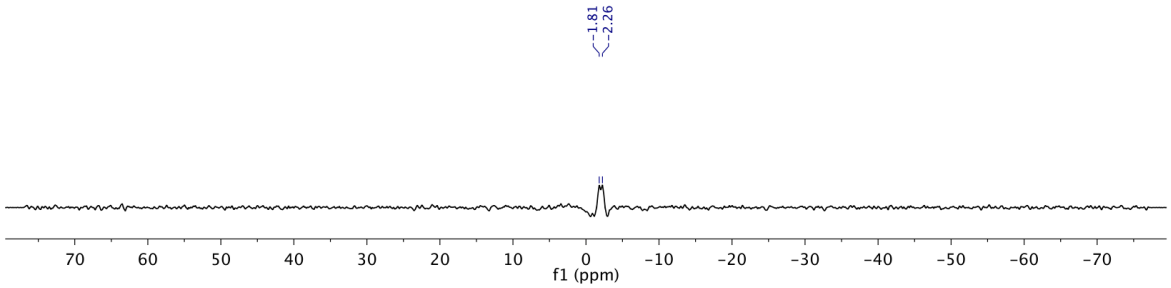

Figure S58. ^{11}B NMR spectrum of complex **6c-Pd** at 23 °C in CD_3CN.

^{19}F NMR Spectrum of 6c-Pd at 23 °C (CD_3CN)

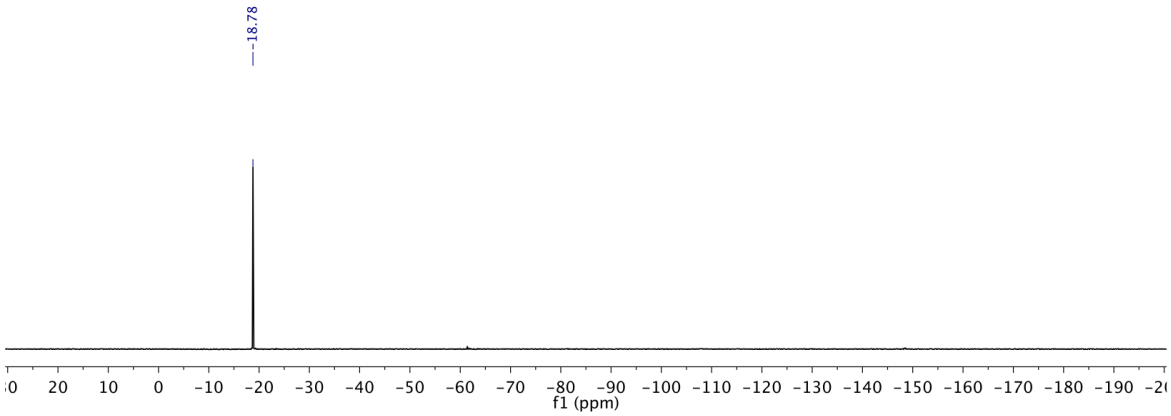

Figure S59. ^{19}F NMR spectrum of complex **6c-Pd** at 23 °C in CD_3CN.

$^{19}F–^{13}C$ HMBC Spectrum of 6c-Pd at 23 ºC (CD_3CN)

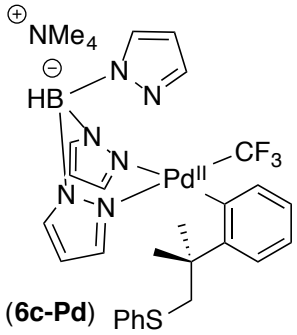

(**6c-Pd**)

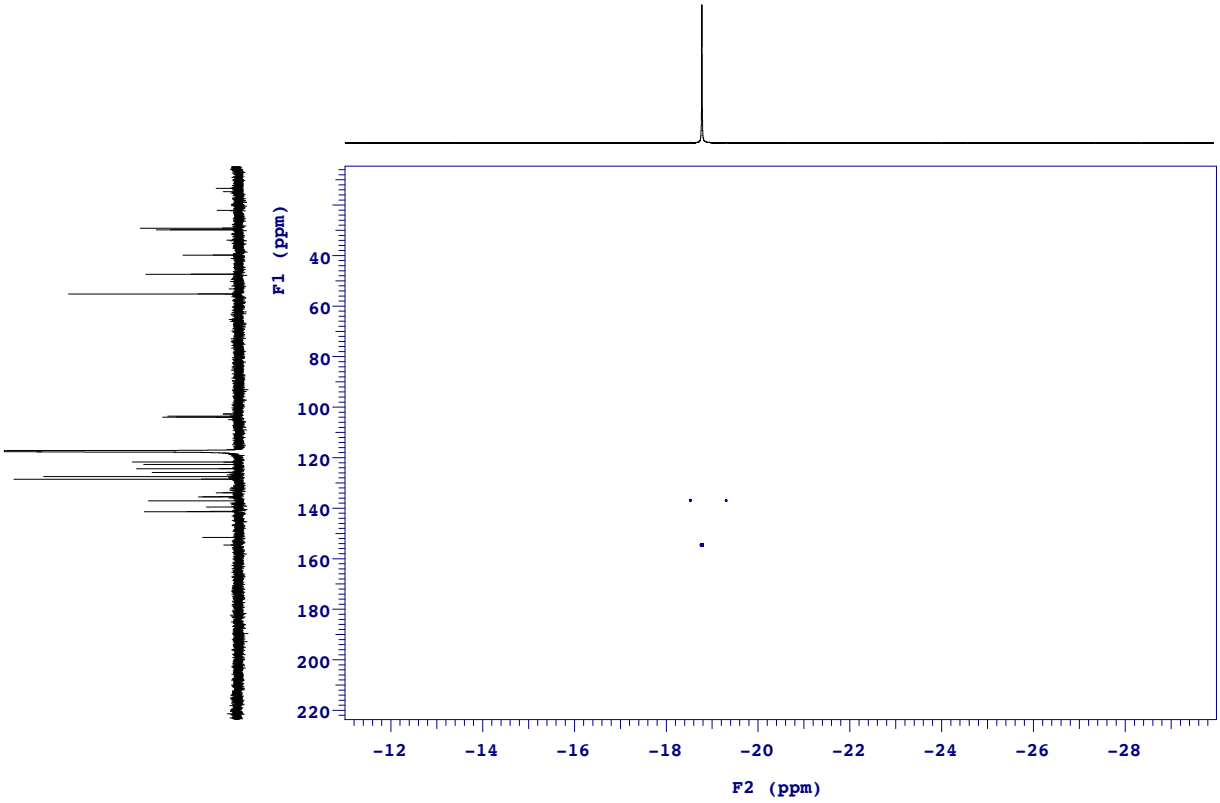

Figure S60. $^{19}F–^{13}C$ HMBC NMR spectrum of complex **6c-Pd** at 23 ºC in CD_3CN.

^{1}H NMR Spectrum of 6d-Pd at 23 ºC (CD_3CN)

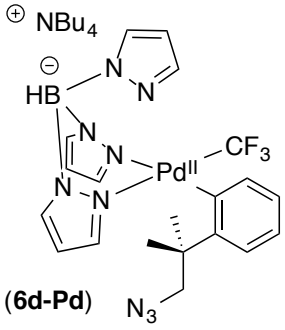

(**6d-Pd**)

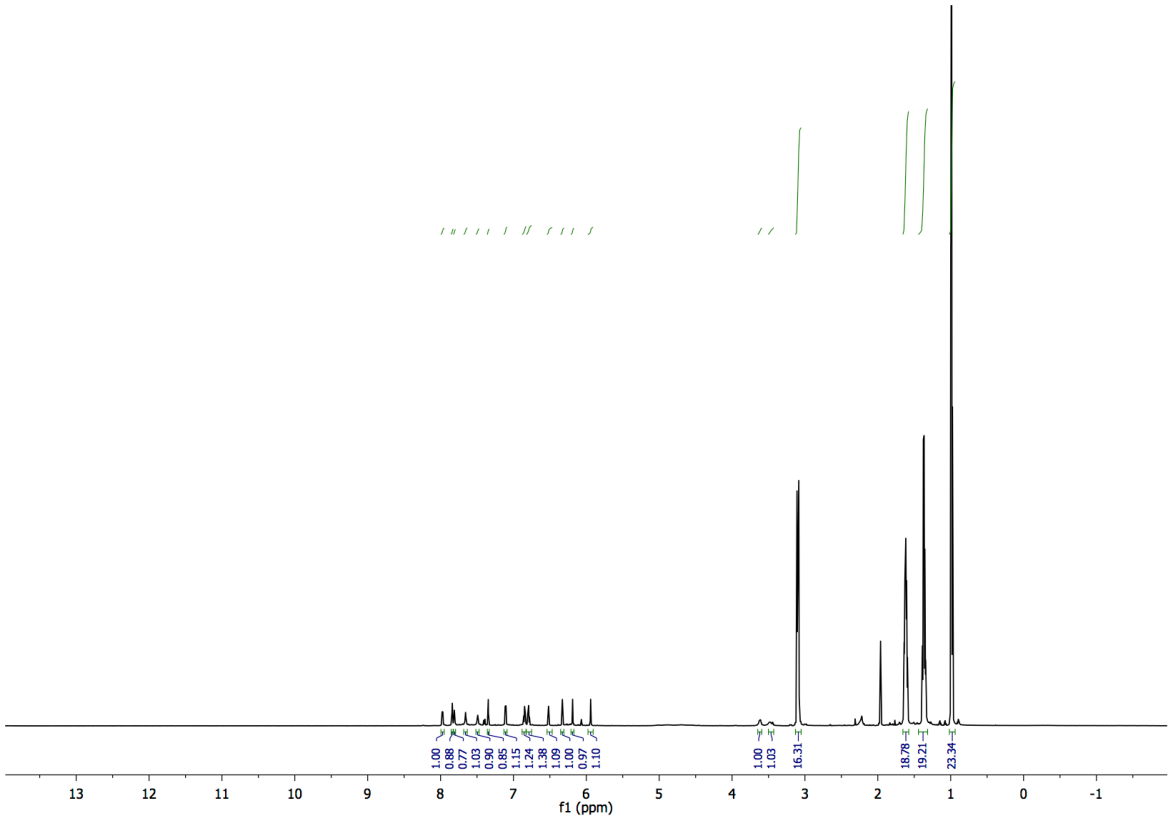

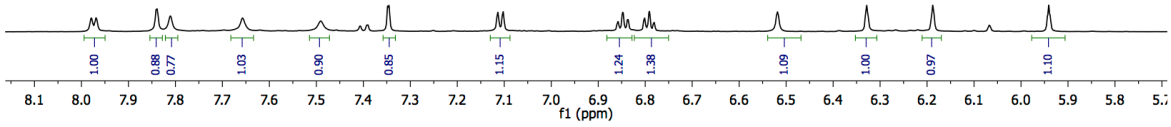

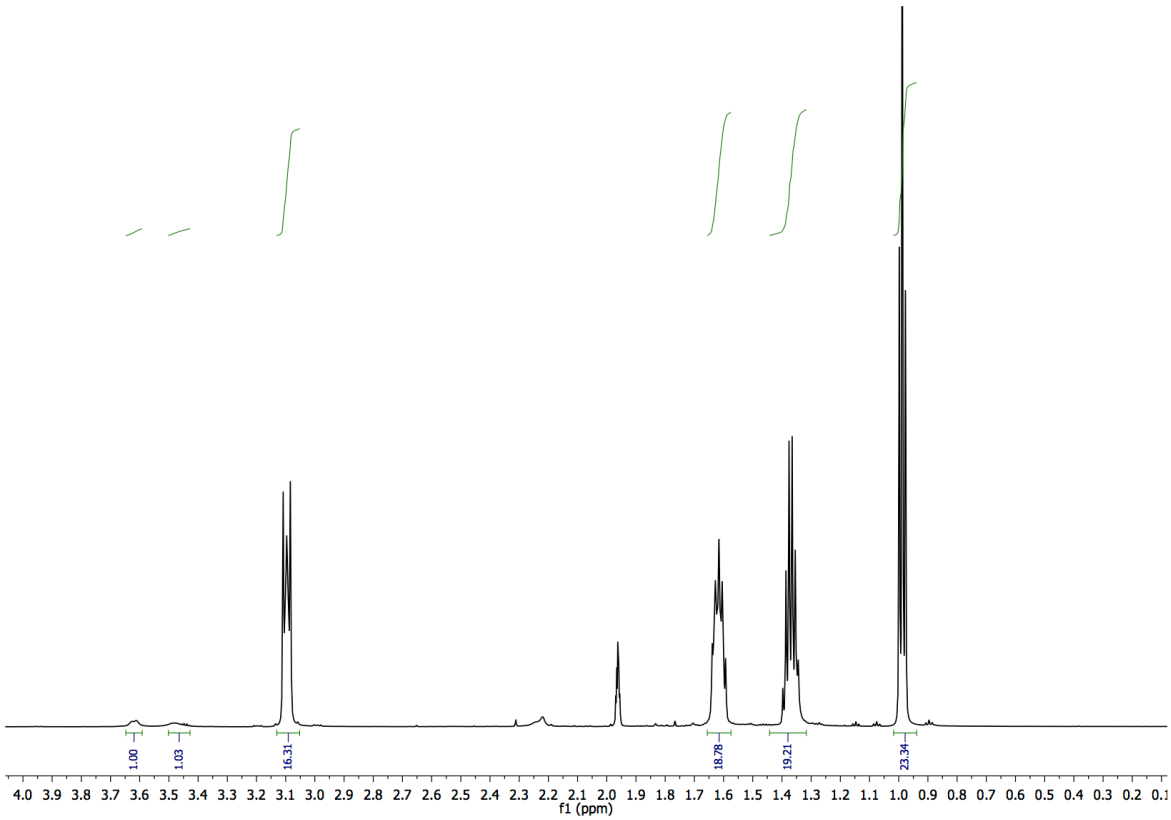

Figure S61. ^{1}H NMR spectra of complex **6d-Pd** at 23 ºC in CD_3CN.

^{13}C NMR Spectrum of 6d-Pd at 23 ºC (CD_3CN)

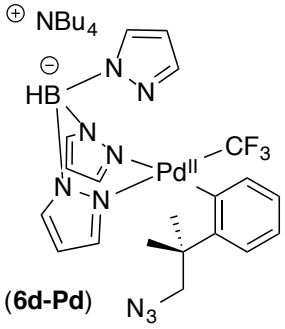

(**6d-Pd**)

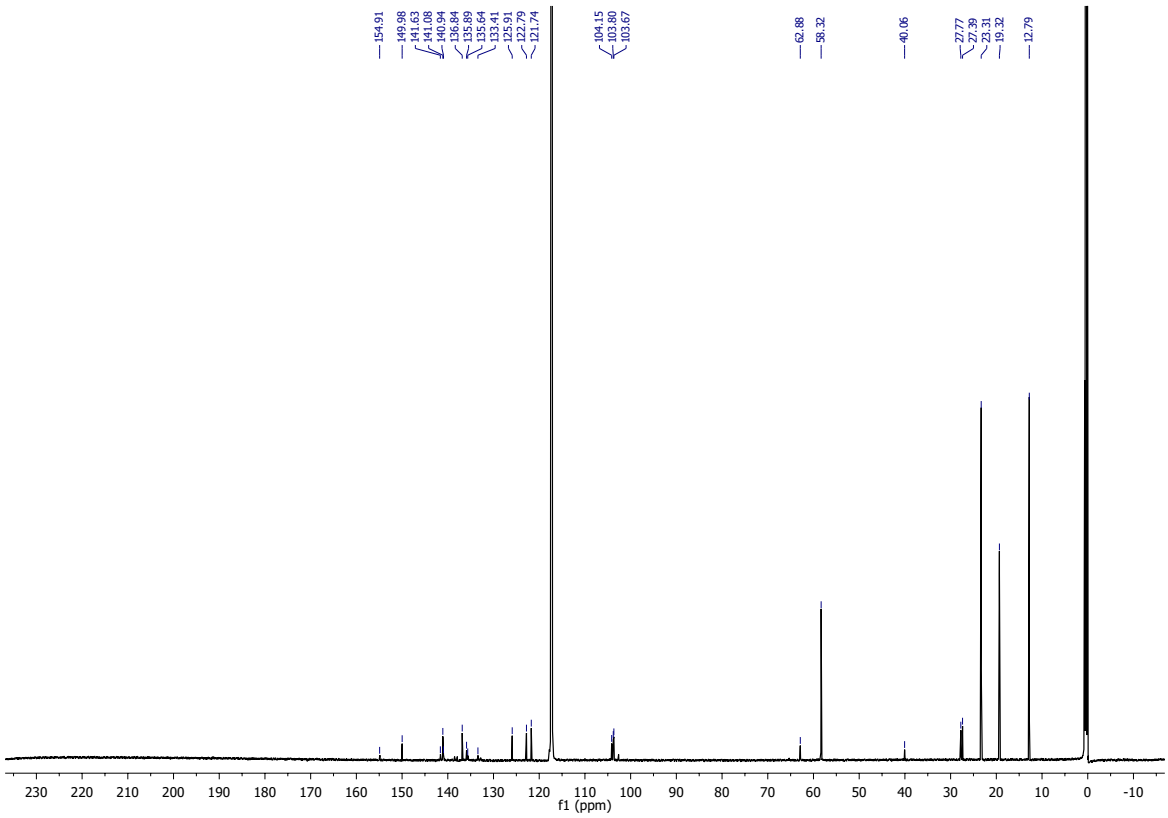

Figure S62. ^{13}C NMR spectrum of complex **6d-Pd** at 23 ºC in CD_3CN.

^{11}B NMR Spectrum of 6d-Pd at 23 ºC (CD_3CN)

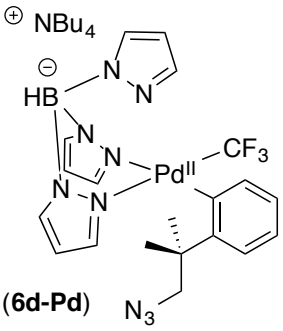

(**6d-Pd**)

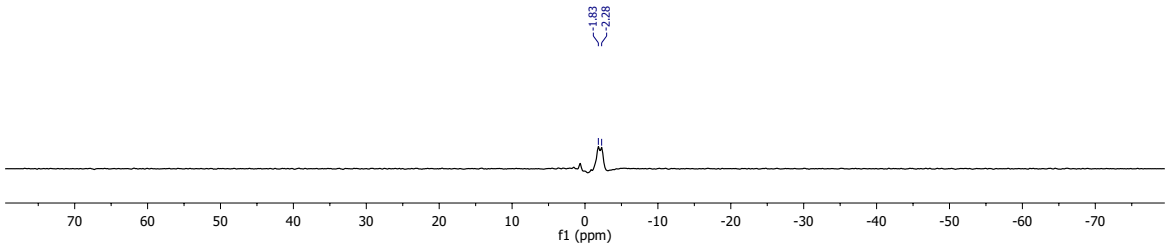

Figure S63. ^{11}B NMR spectrum of complex **6d-Pd** at 23 ºC in CD_3CN.

^{19}F NMR Spectrum of 6d-Pd at 23 ºC (CD_3CN)

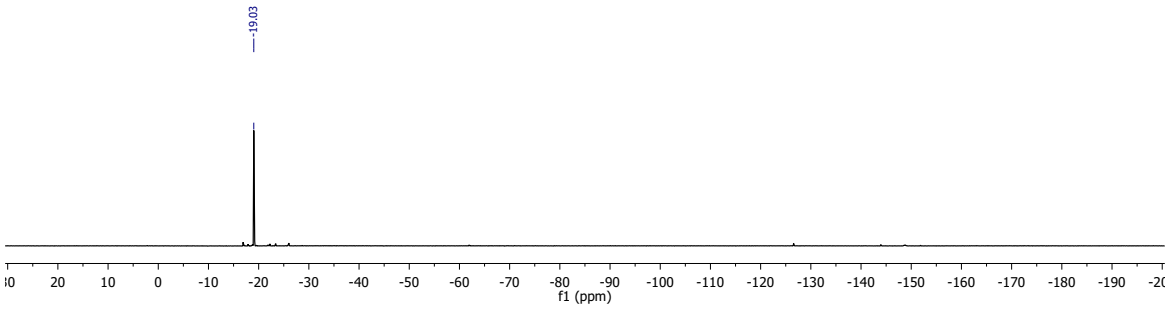

Figure S64. ^{19}F NMR spectrum of complex **6d-Pd** at 23 ºC in CD_3CN.

$^{19}F–^{13}C$ HMBC Spectrum of 6d-Pd at 23 °C (CD_3CN)

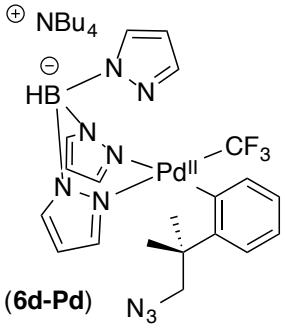

(**6d-Pd**)

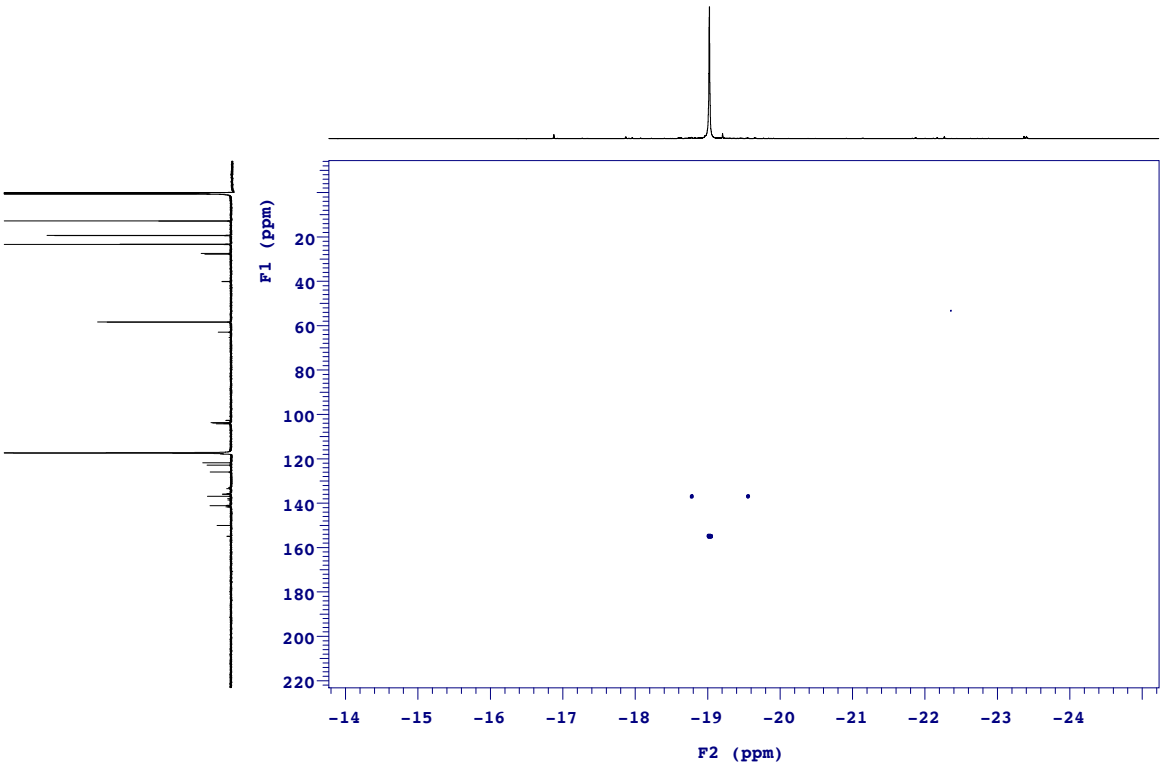

Figure S65. $^{19}F–^{13}C$ HMBC NMR spectrum of complex **6d-Pd** at 23 °C in CD_3CN.

XI. X-Ray Crystallography Experimental Data

X-ray Crystallography Experimental Data of 4-Ni

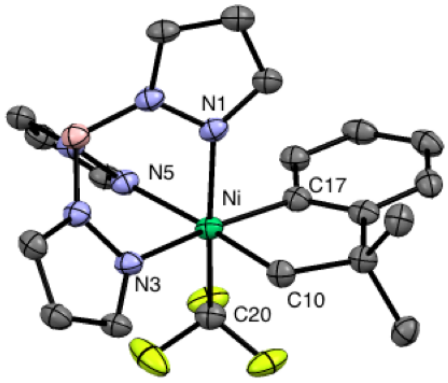

Figure S66. Solid-state structure of **4-Ni**

Yellow block-like crystals of **4-Ni** were grown from a methanol solution of the compound at 22 º C. A crystal of dimensions 0.19 x 0.06 x 0.02 mm was mounted on a Rigaku AFC10K Saturn 944+ CCD-based X-ray diffractometer equipped with a low temperature device and Micromax-007HF Cu-target micro-focus rotating anode (λ = 1.54187 A) operated at 1.2 kW power (40 kV, 30 mA). The X-ray intensities were measured at 85(1) K with the detector placed at a distance 42.00 mm from the crystal. A total of 2028 images were collected with an oscillation width of 1.0° in ω. The exposure times were 1 sec. for the low angle images, 6 sec. for high angle. Rigaku d*trek images were exported to CrysAlisPro for processing and corrected for absorption. The integration of the data yielded a total of 15630 reflections to a maximum 2θ value of 138.58° of which 3185 were independent and 3178 were greater than 2σ(I). The final cell constants were based on the xyz centroids 13366 reflections above 10σ(I). Analysis of the data showed negligible decay during data collection. The structure was solved and refined with the Bruker SHELXTL (version 2014/6) software package, using the space group Cc with Z = 4 for the formula $C_{20}H_{22}BF_3N_6Ni$. All non-hydrogen atoms were refined anisotropically with the hydrogen atoms placed in both idealized and refined positions. Full matrix least-squares refinement based on F^2 converged at R1 = 0.0357 and wR2 = 0.0947 [based on I > 2sigma(I)], R1 = 0.0375 and wR2 = 0.0948 for all data.

Table S5. Crystal Data and Structural Refinement for **4-Ni**.

Empirical formula	$C_{20}H_{22}BF_3N_6Ni$
Formula weight	472.95
Temperature	85(2) K
Wavelength	1.54184 A
Crystal System	Monoclinic
Space group	Cc
Unit Cell Dimensions	a = 10.62710(10) Å, α = 90° b = 14.82650(10) Å, β = 109.5820(10)° c = 14.08920(10) Å, γ = 90°
Volume	2091.54(3) $Å^3$
Z	4
Calculated density	1.502 Mg/m^3
Absorption coefficient	1.749 mm^{-1}
F(000)	976
Crystal Size	0.190 x 0.060 x 0.020 mm
Theta range for data collection	5.331 to 69.292°
Limiting indices	$-12 \leq h \leq 12$, $-17 \leq k \leq 17$, $-14 \leq l \leq 16$
Reflections collected	15630
Independent collections	3185 [R(int) = 0.0501]
Completeness to theta	67.684 (98.8 %)
Absorption correction	Semi-empirical from equivalents
Max. and min. transmission	1.00000 and 0.84728
Refinement method	Full-matrix least-squares on F^2
Data/ restraints/ parameters	3185 / 2 / 287
Goodness-of-fit on F^2	1.071
Final R indices [I>2sigma(I)]	R1 = 0.0376, wR2 = 0.0947
R indices (all data)	R1 = 0.0376, wR2 = 0.0948
Extinction coefficient	0.00079 (19)
Largest diff. peak and hole	0.434 and -0.414 e $Å^{-3}$

X-ray Crystallography Experimental Data of 4-Pd

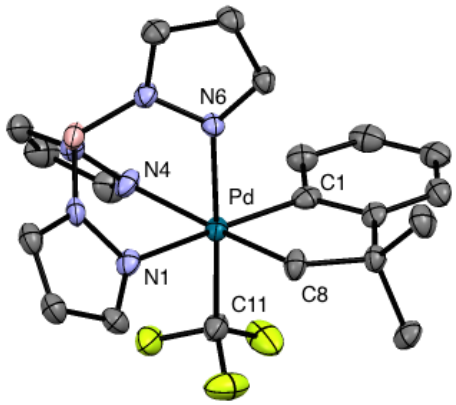

Figure S67. Solid-state structure of **4-Pd**

Colorless needles of **4-Pd** were grown from an acetone solution of the compound at 25 ºC. A crystal of dimensions 0.14 x 0.12 x 0.08 mm was mounted on a Rigaku AFC10K Saturn 944+ CCD-based X-ray diffractometer equipped with a low temperature device and Micromax-007HF Cu-target micro-focus rotating anode (λ = 1.54187 A) operated at 1.2 kW power (40 kV, 30 mA). The X-ray intensities were measured at 85(1) K with the detector placed at a distance 42.00 mm from the crystal. A total of 2028 images were collected with an oscillation width of 1.0° in ω. The exposure times were 1 sec. for the low angle images, 10 sec. for high angle. The integration of the data yielded a total of 32046 reflections to a maximum 2θ value of 136.30° of which 3856 were independent and 3643 were greater than 2σ(I). The final cell constants were based on the xyz centroids 22474 reflections above 10σ(I). Analysis of the data showed negligible decay during data collection; the data were processed with CrystalClear 2.0 and corrected for absorption. The structure was solved and refined with the Bruker SHELXTL (version 2014/6) software package, using the space group P2(1)/c with Z = 4 for the formula $C_{20}H_{22}BN_6F_3Pd$. All non-hydrogen atoms were refined anisotropically with the hydrogen atoms placed in idealized positions. The $–CF_3$ group is rotationally disordered in two orientations. Full matrix least-squares refinement based on F2 converged at R1 = 0.0573 and wR2 = 0.1516 [based on I > 2sigma(I)], R1 = 0.0588 and wR2 = 0.1525 for all data. Acknowledgement is made for funding from NSF grant CHE-0840456 for X-ray instrumentation.

Table S6. Crystal Data and Structural Refinement for **4-Pd**.

Empirical formula	$C_{20}H_{22}BF_3N_6Pd$
Formula weight	520.64
Temperature	85(2) K
Wavelength	1.54178 A
Crystal System	Monoclinic
Space group	P2(1)/c
Unit Cell Dimensions	a = 8.0694(2) Å, α = 90º b = 18.1379(3) Å, β = 101.106(7)º c = 14.7260(10) Å, γ = 90º
Volume	2114.96(16) $Å^3$
Z	4
Calculated density	1.635 Mg/m^3
Absorption coefficient	7.487 mm^{-1}
F(000)	1048
Crystal Size	0.140 x 0.120 x 0.080 mm
Theta range for data collection	3.911 to 68.149º
Limiting indices	$-9\leq h\leq 9$, $-21\leq k\leq 21$, $-17\leq l\leq 17$
Reflections collected	32046
Independent collections	3856 [R(int) = 0.0667]
Completeness to theta	67.679 (99.8 %)
Absorption correction	Semi-empirical from equivalents
Max. and min. transmission	0.550 and 0.375
Refinement method	Full-matrix least-squares on F^2
Data/ restraints/ parameters	3856 / 51 / 311
Goodness-of-fit on F^2	1.142
Final R indices [I>2sigma(I)]	R1 = 0.0573, wR2 = 0.1516
R indices (all data)	R1 = 0.0588, wR2 = 0.1525
Extinction coefficient	0.00075(12)
Largest diff. peak and hole	1.691 and -0.995 e $Å^{-3}$